TRANSPARENT CONDUCTIVE COATINGS BASED ON CARBON NANOTUBES

Index:

TRANSPARENT CONDUCTIVE COATINGS BASED ON CARBON NANOTUBES

Abstract

This research focuses on the use of carbon nanostructures to provide electrical conductivity to films and coatings while maintaining excellent optical transparency. Carbon nanotubes are long cylindrical molecules that can be metallic or semiconducting. Due to this structural characteristic, carbon nanotubes can be considered as one-dimensional conductors that can be used, as well as other materials used throughout this thesis, in transparent and conductive coatings. Examples and data, as well as different applications exhibiting optical transparency for relatively high conductivity, are provided. These relatively new nano-materials are expected to replace the Indium Tin Oxide technology currently in use.

Acknowledgements

First of all I would like to express my gratitude towards Núria Ferrer Anglada from the "Departament de Física Aplicada" of the "Universitat Politècnica de Catalunya", not only for her help and support during the thesis but especially for giving me the opportunity of joining Max Planck Institute in Stuttgart.

Moreover, I would like to thank Dr. Siegmar Roth, head of the Synthetic Nanostructures Group in Max Planck Institute, who accepted me to join his group, as well as the other group members for great support and interest in my progress. Specifically, Viera Skakalova, Serhat Sahakalkan, Dirk Obergfell, Dong Su Lee, Viktor Sielgle and Chen-Wei Liang for teaching me the lab procedures and process techniques and always being open to suggestions and discussions. All of them have been an essential part of this project.

Thanks to my friends from Stuttgart, Miquel, Dorothé, Ana, Raul, Graciela, Serife, Bahar, as well as to my old friends in Barcelona, Maruan, Juan Ramón, Miguel, Cesc, Jordi, Miriam, Marisa, Patrick, Mireia, Angels, Marc, Javi, Victor, Laia, David, Gemma, Laura, Oscar, Yasmin, Neus, among others, since they have contributed in this thesis, not only by sharing the fun, stress and nervousness over all the studies but also for being there during the hard times.

And finally, with all my fondness, my most special thankfulness to my family for the support they provided me throughout my entire life and in particular, I must acknowledge my parents, without whose love, comprehension and help, I would not have finished my studies.

Stuttgart, September 2008

Bernat Terrés i Güerri

Chapter 1

Motivation

1.1 From Indium Tin Oxide technology to carbon nanostructures technology

Conductive coatings are used in applications where it is necessary to dissipate electrical charges while not losing the optical properties of the particular substrate or optical component. Thin film conductive coatings are widely used on aircraft windows, flat panels displays, organic light-emitting diodes, automotive windshields, and solar cell arrays. Indium Tin Oxide (ITO) is nowadays used in the manufacturing process of all these industrial applications. ITO main's feature is the combination of electrical conductivity and optical transparency. Nevertheless, due to the high cost and limited supply of Indium, the fragility and lack of flexibility and the costly deposition method during the manufacturing process, alternatives are being sought. Conductive polymer-based thin films are an efficient alternative currently in use but they degrade when exposed to ultraviolet radiation and have other disadvantages. Conductive coatings based on carbon nanostructures seem to be a promising alternative. Carbon Nanotubes (CNT) and Graphene are two of the most promising materials in the carbon's family.

To make suitable transparent and conductive layers one needs to be able to transmit electrons all over the substrate and, at the same time, allow light to pass through it. Carbon nanotubes are long cylindrical molecules, with a small diameter of around a few nanometres and lengths of up to several hundred micrometers. Carbon nanotubes are a highly stable and nearly an atomically perfect molecule. This high degree of perfection leads to a very low scattering probability along the tube. Randomly distributed all over the substrate, carbon nanotubes allow the current flow over the lattice if the concentration reaches or exceeds the percolation threshold. Once above this limit, the contacts between CNT are enough to ensure the electrical transport within any point of the lattice while the light is able to penetrate through the holes in between the CNTs. Having said that, our main objective during this work was to approach the transparency versus conductivity ratio of ITO material.

1.2 Outline of the Thesis.

In this thesis, comparison between different conductive nanomaterials and several deposition methods will be presented in order to improve the conductivity and transparency of the samples. In addition, an attempt to show promising applications of this technology will be introduced. FM antennas and electromagnetic shielding are two of the current applications for these conductive coatings that we decided to analyse in this work.

In chapter 2, the physical and methodological background of these novel nanomaterials are presented along with the general interpretation of the CNTs structure and their promising properties. Moreover, in this section, there is a brief introduction of the PDDA and PEDOT polymers as they have also been used during this work. PDDA was used as a

surfactant in the dispersion and PEDOT polymer as an active material itself in the antenna application.

In chapter 3, characterisation methods are presented. Atomic Force Microscopy (AFM) and RAMAN spectroscopy are introduced as the needed tools to analyze the characteristics of these nano-structured networks.

In chapter 4, the comparison is made between different CNT materials where the aim of the study is to find out which material better suits our requirements. We look for carbon nanotubes with the best conductivity performance, discerning between single walled and multi walled ones.

In chapter 5, different deposition methods are exposed and analyzed. It is also discussed during this chapter the effects of the CNT orientation over the network and their impact in the conductivity performance. Electric field deposition and air blowing deposition (adsorption method) have been also analyzed. In addition, we firstly introduce the sample preparation and discuss the effects on the surface functionalisation of the substrate (silanisation and PDDA treatment).

In chapter 6, following the study of all different deposition methods, two possible applications of this technology are analyzed. Printed FM transparent antennas for the automotive industry and electromagnetic shielding in mobile phones are presented.

Finally, general conclusions are exposed.

Chapter 2

Physical background of carbon nantoubes

Since their discovery in 1991 by Sumio Lijima [1] carbon nanotubes have given rise to great attraction from both theoretical and experimental points of view. This is due to their remarkable physical, chemical, and electronic properties, which brought an interest in using carbon nanotubes in applications ranging from electronics or materials science. Their electronic properties stem from the electronic properties of a single sheet of graphite, called graphene, and the constrain that the geometrical shape of a nanotube puts on these. If the carbon atoms were simply kept in their two-dimensional array, electrons would be able to move in all directions. But, once this array is wrapped into a tubular shape, quantum confinement will only allow electrons to move along the length of the tube.

In this chapter, we introduce the physical background of this novel material. The structure and properties of carbon nanotubes (CNTs), mainly the semiconducting and metallic features, will be discussed as an introduction. Briefly, the nature of graphene will be as well introduced, as it is necessary to understand the electrical behaviour of our carbon nanotubes.

2.1 History

The history of carbon nanotubes is said to begin in 1991 when Sumio Iijima [1] as a result of fullerene investigation, formed multi wall carbon nanotubes using a kind of arc-discharge method. Some think that he should not get all the credit because Roger Bacon had, 31 years before, grown carbon whiskers made of concentric tubes [2] where each cylinder had the morphology of a rolled up graphite sheet. These whiskers were grown with an arc-discharge method under high pressure [3]. Also, we have to point out the fact that a pair of Russian physicists first discovered carbon nanotubes in 1952. However, little attention was given to their discovery since it was published in the Russian language during the Cold War. It was not until 1991 when these unique structures first gained widespread attention among the world's scientists, when Sumio Iijima of the NEC Lab imaged them with a high-resolution transmission electron microscope.

The discovery of multi-wall nanotubes stimulated theorists to start thinking about the simplest system: the nanotube with a single concentric cylinder, that is, the single wall nanotube. It was not until 1993 when these new carbon structures were observed experimentally by Iijima and Ichihashi [4] and by Bethune [5], both working indepently in the topic. These first attempts of growing single wall carbon nanotubes were produced by arc-discharge method in the presence of a metal catalyst. Even though the carbon soot contained at most a small percentage of single wall nanotubes and the purity was really poor, this was enough to shift the interest from multi wall carbon nanotubes to single wall ones. Therefore, the real break-through came in late 1950's when Smalley discovered a more efficient synthesis route towards nanotubes manufacturing involving the laser ablation method [6]. With this method, rates as high as 70% to 90% could be achieved.

Currently scientists are still researching more economic ways to produce big amounts of these carbon structures. Quite a few new techniques were conceived trying to overcome this scaling-up problem (like ultra fast pulses from a free electron laser method or continuous wave laser-powder method).
Nowadays, there have been many proposals of new devices made of carbon nanotubes but before these can be mass produced some essential problems have to be solved. Besides the scaling up problem there is the difficulty of controlling the growth method, that means to be able to select chirality, diameter and length of the carbon nanotubes. Even thought a lot of research has been done in this area the achievements are limited. The CVD process gives some limited control over the position and the length of the tubes but none of the growth methods allow the selection of either chirality nor diameter. These parameters, as we are going to see below in this chapter, are extremely important and should be controllable if we want to improve the conductivity vs. transparency ratio of the coatings.

2.2 Growth methods

Although there had been many appealing attempts to grow carbon nanotubes by different methods, we are going to restrict our exposition to the three most common techniques: arc discharge, laser vaporisation and chemical vapour deposition (CVD). We will focus on the laser vaporisation method (laser ablation) since we had manly worked with carbon nanotubes grown with this technique. Primarily, the grow mechanism of the nanotubes is going to be introduced as it is almost the same for all three techniques.

The way in which the carbon nanotubes are produced is not exactly known as more than one mechanism might be involved during the process. The raction may start with the formation of a C2 molecule on the surface of the metal catalyst particle. Next, a rodlike carbon grows upwards from this metastable carbide particle and then the graphitisation of its wall takes place. Depending on the size of the catalyst particle, single wall or multi wall carbon nanotube can be produced. This growing behaviour is based on in-situ TEM observations reported in [7]. As we will see later, in spite of the growth of the carbon nanotube, which seems to be equal for all three techniques, the exact atmospheric conditions varies for every specific technique.

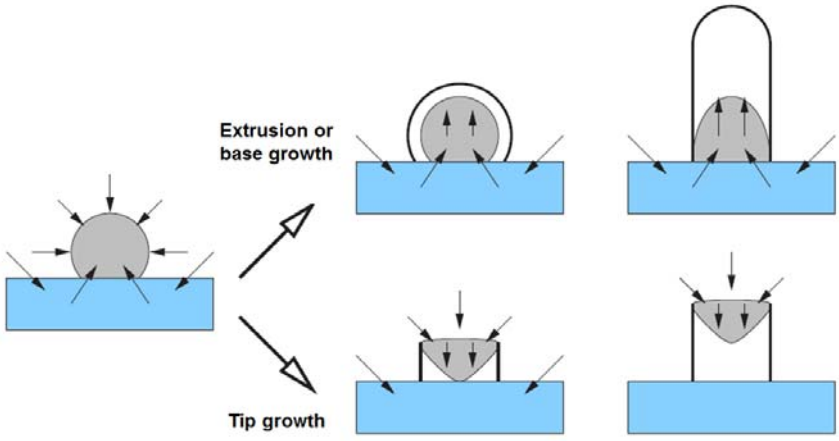

Figure 2.1: Schematics showing one of the possible interpretation of the growth mechanism.

There have been many theoretical attempts made to explain the growing behaviour of the carbon Nanotubes. One theory [8] postulates that metal catalyst particles are floating or are held on graphite or another substrate. This assumes that it is on the spherical or pear-shaped catalyst particles where the deposition of the carbon and post growing of the nanotube takes place. As we can see in **Figure 2.1**, for supported metal particles nanotubes can form either by "extrusion" (also know as base growth) in which the nanotube grows upwards from the metal particle that remain attached to the substrate, or the particles detach and move to the head of the growing nanotube, labelled "tip growth". During the Arc discharge growth method, if no catalyst is used in there, Nanotubes are supposed to grow on the C_2 particles that are formed in the plasma.

Arc discharge

The arc discharge method is probably the most common and easiest way to produce nanotubes as it is rather simple to undertake. However, this technique produces a mixture of catalytic metal particles, amorphous carbon and nanotubes. To get rid of all these unwanted components a separating method is required afterwards and this procedure is not simple to perform. As illustrated in **Figure 2.2**, in the arc discharge method the graphite rods, doped with a transition metal for single wall carbon nantotubes growth, are heated by an electric arc in an enclosure that is usually filled with inert gas (helium or argon). The two carbon electrodes are separated by ~1nm and a voltage difference of 20-25V and is applied, resulting in a current between 50-120 A. The electrons, flowing from the anode to the cathode, hit the gas molecules and ionises them, then positively charged, they find there way back to the cathode. These ions help in the agglomeration of the carbon elements into nanotubes. Consequently the tubes grow in the fume around the negative electrode.

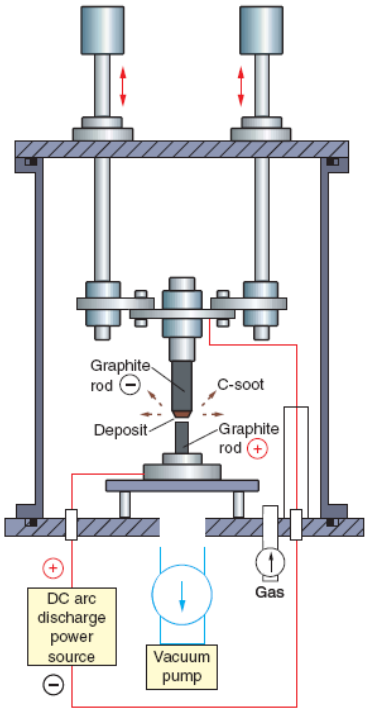

Figure 2.2: Diagram of CNT formation apparatus for the arc discharge method (reprinted from [9]).

Measurements have shown that different diameter distributions of the nanotubes can be found depending on the mixture of helium and argon. Every mixture has his own coefficient and thermal conductivity. These characteristics influence the spreading and cooling speed of carbon and catalyst particles, affecting the diameter of the nanotubes in the process. This means that single wall nanotubes grow on metal particles in different sizes depending on the quenching rate in the plasma and it suggests that temperature, as well as the density of carbon and metal catalyst, affect the diameter distribution of nanotubes [10]. For the production of single wall tubes with the arc-discharge method the growth mechanism is presumably the same as in the laser ablation method.

Chemical vapour deposition (CVD)

Both arc discharge and laser vaporisation methods demand a lot of energy to produce nanotubes. This is due to the fact that graphite vaporises at temperatures over 3.000 ºC, therefore these two methods do not seem adequate for scale up production [11]. Besides this, there is also the problem of placing the tubes in the desired position and due to the nature of these growth processes, this remains a problem not likely to be overcome. In CVD growth, there is some control in the positioning of the nanotube since the growth is taking place on a substrate (usually silicon oxide chip). After depositing a catalyst layer on the SiO_2 (if this is the desired substrate), the silicon chip is placed in a furnace and heated up to 500-1200ºC (depending on the catalyst metal used) in the presence of a carbon source gas. This feedstock gas could be Methane (CH_4) or Ethanol (C_2H_6O) since they are some of the most stable hydrocarbons. We need high stability in order to increase the percentage decomposition of the gas by catalyst opposing its neutral decomposition, taking place at high temperatures and thereby increasing the yield.
General experience prove that low-temperature CVD (600-900°C) gives multi wall nanotubes, whereas high temperatures reactions (900-1200°C) favours single wall growth. This could indicate that single wall nanotubes have a higher energy of creation, apparently owing this to their small diameters, which results in big curvature and high strain energy.

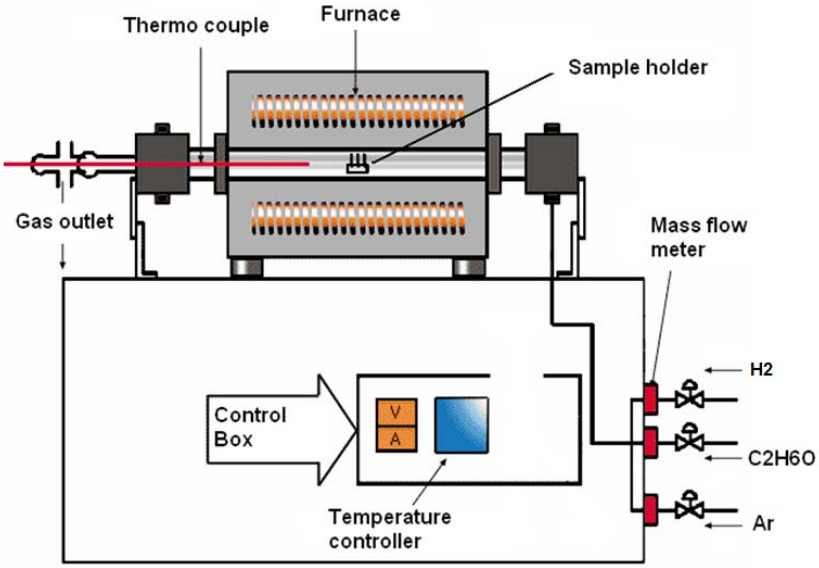

Figure 2.3: Schematic diagram for the CVD growth method.

The schematic setup for this growth method is shown in **Figure 2.3**. The nanotubes start growing directly on the catalyst particles, so, by placing these in predefined spots one can control the position of the nanotubes. Moreover, in quite a number of publications, it has been proved that it is also possible to control the growth direction of the nanotubes by air blowing or by applying an electric field, and more importantly, some claimed to be able to discriminate between semiconducting and metallic tubes during the growing procedure [12] [13].
Both laser ablation and arc discharge methods are mainly used to produce nanotubes in powder form, which can be later followed by a deposition method necessary to place the carbon nanotubes over the desired substrate. This suggests another advantage of the CVD method against the other techniques and it is due to the fact that nanotubes are grown directly on the sample (In-situ growth), consequently there is no need for purification and also avoids the deposition process. Both processes, either purification or deposition, tend to introduce defects on the nanotubes and are even capable of decreasing the length of the nanotubes due to the fracturing effects caused by sonication during the dispersion preparation.

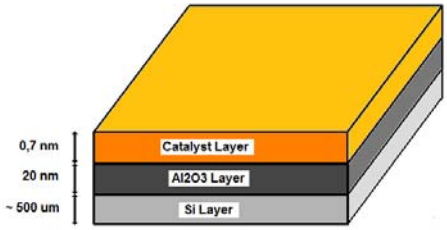

Figure 2.4: Chip sample for SWCNT growth by CVD method.

CVD is an easy and economic way for synthesizing CNT at low temperature and ambient pressure. During this thesis we performed some growth attempts by CVD method just to demonstrate the working principle. The three main parameters for CNT growth are the hydrocarbon used in the process, the catalyst and the growth temperature. **Figure 2.4** shows the substrate used in the experiment. On a silicon oxide chip a very thin layer of about 0,7 nm thick must be deposited onto the surface of the sample by dip-coating or spin-coating. By controlling this thickness one may control the density of nanotubes. Iron (Fe), Nickel (Ni) or Cobalt (Co) are the metal catalyst particles chosen for the test, these particles must be in the order of nanometres (nanoparticles) if one wants to obtain nantotubes. We start placing the samples on the chip holder, then we heated up in the furnace during 5-20 min at 600 °C in the presence of a mixture of Hydrogen (5 vol.%) and argon (95 vol.%). During this time the catalyst is activated and prepared for the growth phase. Later on, we add to the enclosed atmosphere ethanol as a carbon source, the heating temperatures and running time varies depending on the used catalyst, these are summarised in **Table 2.1**.

Catalyst	Heating time	Temperature
Nickel	~30 min	600 – 700 ºC
Iron	~20 min	800 – 950 ºC
Cobalt	~20 min	700 – 800 ºC

Table 2.1: Heating temperatures for the different catalyst metals.

SEM observations, as one can see in **Figure 2.5**, prove the presence of carbon nanotubes on the substrate. Despite the fact there are carbon nanotubes on it, neither the amount nor the quality appears to be sufficient. The concentration of the catalyst, the temperature, the heating time and even the temperature ramp rate should be improved to get rid of these undesired materials and obtain CNT forest like the ones in **Figure 2.6**.

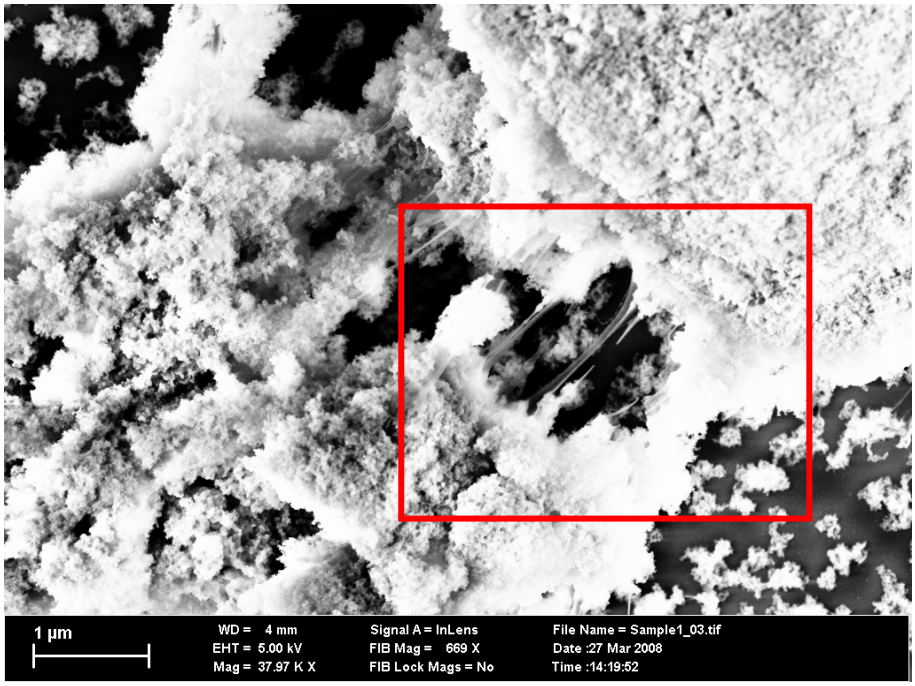

Figure 2.5: SEM image of carbon nanotubes bundles.

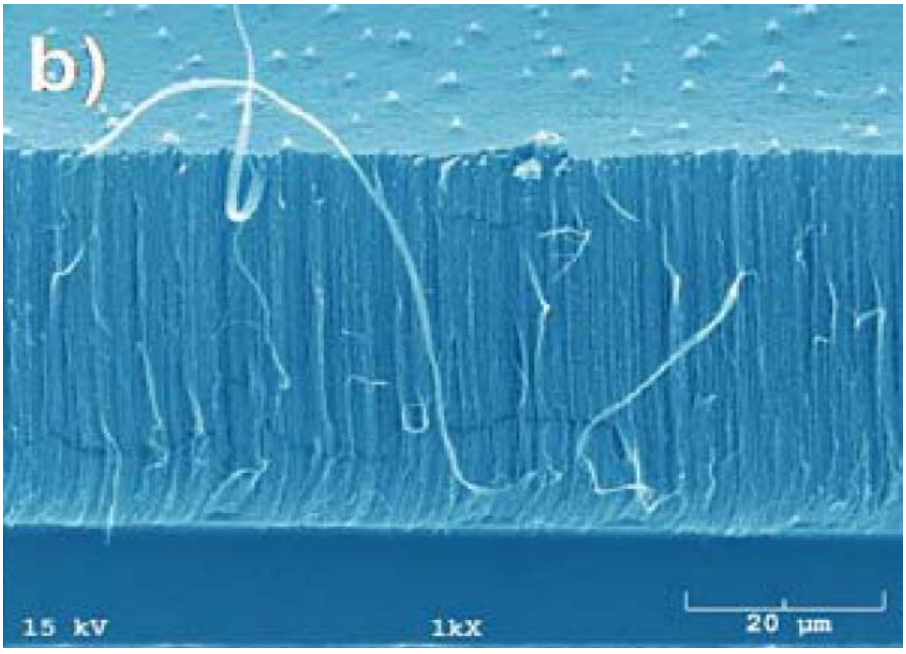

Figure 2.6: CNT forest (picture took from [14]).

Laser vaporisation (Laser Ablation)

It was Smalley´s group in 1995 at Rice University [15] who reported the first successful attempts to synthesise carbon nanotubes by the laser vaporisation method. This technique, also called laser ablation, is almost comparable to arc discharge, since the optimal settings in the gas and catalyst concentration are very similar. This might be due to strong similarities within both growth mechanisms, as the reactions taking place during both processes are almost the same.
As shown in **Figure 2.7**, the laser spot hits the target consisting of a mixture of graphite and the transition metal. Since the energy density of laser is very high, the laser is suitable for vaporising materials with a high boiling temperature such as carbon.

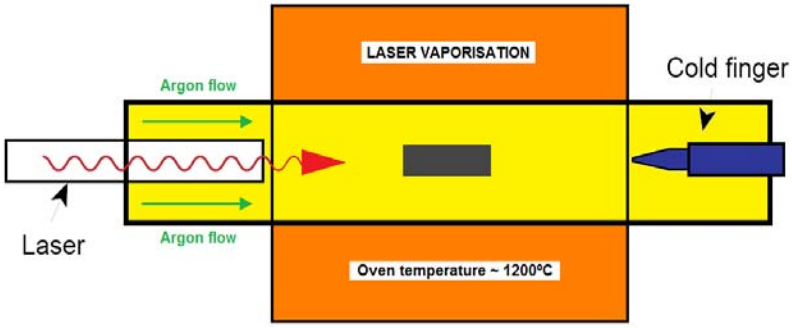

Figure 2.7: Schematic view of the setup for the laser vaporisation method.

The hot vapour cloud expands through the tube to the cold finger by the flow of an inert gas (the oven is filled with Argon or Helium). A furnace heats the pipe to a temperature around 1200°C and the water cooled finger, placed outside the oven, condenses the vaporised material in carbon nanotubes and carbon-catalyst soot. As mentioned before and despite of being close to others growth techniques, the way in which carbon nanotubes are grown during this specific process is still not clear, however, some proposals have been made [16]. The laser pulses heat the target surface with enough energy density not to cleave the target into graphite particles but to vaporize it at the molecular level. The small carbon atoms sweep down to the cold finger and quickly condense to form larger clusters probably including fullerenes. The metal catalyst also start to condense and attach to the carbon cluster, this prevents the carbon structures to close into cage structures like C_{60} fullerenes. The catalyst might even open already closed smaller fullerenes when they attach to them. From these carbon-catalyst molecules the growth takes place. The feedstock material during this procedure is the carbon atoms or molecules that either attaches the catalyst or the tube.

The diameter of the tubes can be controlled by changing the furnace temperature and the flow rate. A higher furnace temperature results in single wall nanotubes with larger diameters [17]. Depending on the metal catalyst one can also modify the diameter of the tubes, i.e. Ni-Y alloy catalyst increases the diameter, whereas a Rh-Pd catalyst reduces it [18] [19]. Flow rate affects the diameter distribution, which means that the growth procedure is quite slow compared with the vaporisation processes.

Compared to the other growth methods laser vaporisation offers some advantages such as the produced nanotubes have high quality, which means minimal defect in the structure and less contaminants such as amorphous carbon and catalyst metals. Furthermore it gives control over the diameter of the tubes and allows for the investigation of the growth dynamics since the parameters involved during the process are stable and permanently controllable.

2.3 Structure and electrical properties

A carbon nanotube, as we can see in **Figure 2.8**, is nothing else than a two dimensional hexagonal sheet of carbon elements rolled up into a hollow thin cylinder. The diameter is several orders of magnitude smaller than the length resulting in a large aspect ratio that allows approximation of the CNT as a 1D system. The high aspect ratio and the extremely high conductivity of the carbon nanotubes make them suitable for transparent and conductive coatings.

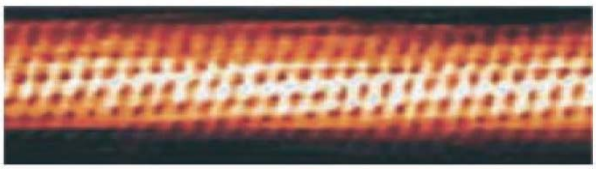

Figure 2.8: Scanning Tunnelling Microscope image of a carbon nanotube.
Image taken from [20].

The cylindrical nanotube usually has at least one end capped with half of a fullerene molecule [21]. This topology distinguishes nanotubes from other carbon structures. There are two main kinds of nanotubes: single wall nanotubes (SWCNT) which are individual cylinders and multi wall nanotubes (MWCNT) which are a collection of several concentric graphene cylinders binded together by the effect of Van der Waals forces [22]. Both SWCNT and MWCNT are interesting materials but for applications requiring high conductivity single wall are more desirable (comparative results between single and multi wall carbon nanotubes are exposed in Chapter 3). The basic structure of the nanotube is defined by the diameter, the length, the number of concentric shells and the chirality of the tube. The diameter of SWCNTs, which is usually 0,6~1,8 nm, and the way the hexagons wind around the tube (helicity) determines its electronic properties. Nanotube helicity can be understood by variations in the way in which grapheme sheets can be rolled to form a nanotube cylinder (see **Figure 2.9**). If the edge of the grapheme sheet is rolled in such a direction that carbon atom O is joined to carbon atom A, then the chiral vector can uniquely define the tube helicity. The chiral vector Ch(n,m) is simply defined by:

$$C_h = n \cdot a_1 + m \cdot a_2$$

Where a_1 and a_2 are units vectors as defined in **Figure 2.9**

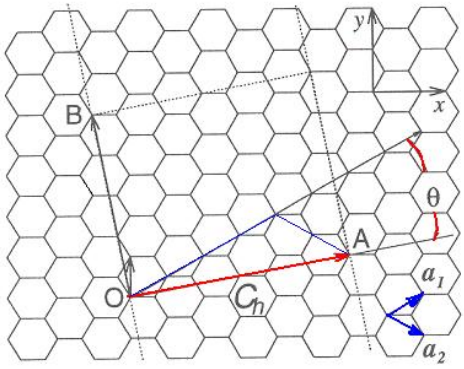

Figure 2.9: Two dimensional hexagonal real lattice of graphene where the unit vectors are indicated by a_1 and a_2. A carbon nanotube with certain chirality C_h is built up by rolling the lattice into a cylinder by joining the points O and A.

Although there exist an infinite number of different nanotubes sorts, all of them can be classified in one of the following groups (**Figure 2.10**):

- Armchair nanotubes → Tubes fulfilling the relation $C_h = (n,n)$
- Zigzag nanotubes → Tubes fulfilling the relation $C_h = (n,0)$
- Chiral nanotubes → Tubes fulfilling the relation $C_h = (n,m)$

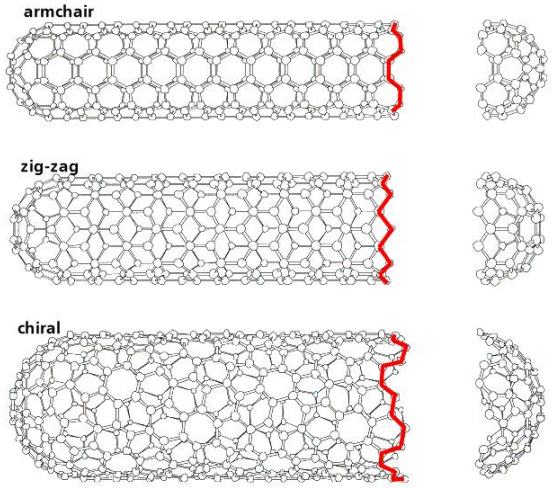

Figure 2.10: Carbon nanotubes family's structures (a) armchair, (b) zigzag and (c) chiral tubes. Image was taken from [23].

All the armchair tubes show metallic behaviour and the other configurations exhibit semiconducting or metallic manner depending on their (n,m) relation. On the average, one of the third of bulk CNT has metallic behaviour and the rest are semiconducting.

It is seen that $|C_h|$ is equal to the circumference length of the nanotube, so, one can extract that the diameter d_t of the tube:

$$d_t = \frac{|C_h|}{\pi}, \text{ where } |C_h| = a\sqrt{n^2 + m^2 + nm}$$

The translation vector T

The translation vector T describes how far one should move along the nanotube before the pattern of carbon atoms repeats itself. T therefore defines the length of the nanotube unit cell and it is defined by:

$$T = t_1 a_1 + t_2 a_2 \text{ where } t_1, t_2 \text{ are the indices}$$

To understand the origin of both semiconducting and metallic behaviour of the CNTs, the two dimensional hexagonal lattice of carbon atoms, which is called graphene, has to be studied. The electronic structure of the carbon nanotube comes from the electronic structure of the graphene and the constraint that the cylindrical shape of the nanotube force on it. Referring to **Figure 2.11** one can see the real space lattice of graphene where the lattice vectors can be written as:

$$\vec{a}_1 = a_0\sqrt{3}\left(1/2; \sqrt{3}/2\right)$$
$$\vec{a}_2 = a_0\sqrt{3}\left(-1/2; \sqrt{3}/2\right)$$

In the Cartesian (X;Y) coordinate system and with $a_0 = 1{,}42$ Å (distance between closer carbon elements). The graphene honeycomb lattice can be formed by translating the unit cell using the real translational vector $\vec{R} = n_1\vec{a}_1 + n_2\vec{a}_2$, where n_1 and $n_2 \in \mathrm{N}$.

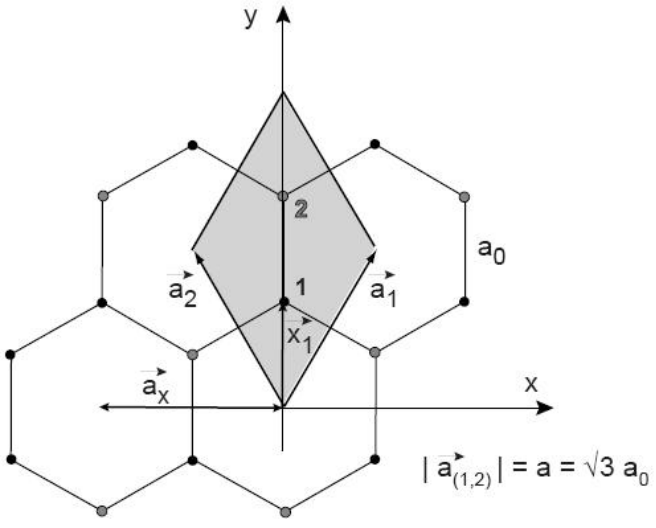

Figure 2.11: Lattice of graphene. Carbon atoms are located in the crossing sections and the lines indicate the chemical bonds between carbon elements. Also shown above, there are the primitive lattice vectors $\vec{a}_1$ and $\vec{a}_2$, as well as the unit cell of the lattice (in shadow). There are two carbons per unit cell, labelled by 1 and 2.

Every periodic structure has two lattices associated with it. The first is the real space lattice (**Figure 2.11**), and this describes the periodic structure of the crystal lattice. The second is the reciprocal lattice (**Figure 2.12**), and this determines how the periodic structure interacts with waves. From the real space lattice one can construct the reciprocal lattice, which also has hexagonal symmetry, using the following relationships:

$$\vec{b}_1 = 2\pi \frac{\vec{a}_2 \times \vec{a}_3}{\vec{a}_1 \cdot (\vec{a}_2 \times \vec{a}_3)}$$

$$\vec{b}_2 = 2\pi \frac{\vec{a}_3 \times \vec{a}_1}{\vec{a}_1 \cdot (\vec{a}_2 \times \vec{a}_3)}$$

Where $\vec{a}_1$ and $\vec{a}_2$ have been defined before, $\vec{a}_3$ is the unit vector in the Z direction and $\vec{b}_1$, $\vec{b}_2$ are the reciprocal lattice basis vectors. Before calculating these two reciprocal basis vectors one should place the two real space basis vectors in point 1 (see **Figure 2.11**). After applying the relation above, one may get the following reciprocal basis vectors:

$$\vec{b}_1 = \frac{4\pi}{\sqrt{3}a}\left(\sqrt{3}/2; 1/2\right)$$

$$\vec{b}_2 = \frac{4\pi}{\sqrt{3}a}\left(-\sqrt{3}/2; 1/2\right)$$

Figure 2.12 shows, due to the basis vectors $\vec{b}_1$ and $\vec{b}_2$, the representation of the reciprocal lattice as well as the first Brillouin zone, this Brillouin zone is a uniquely defined primitive cell of the reciprocal lattice where the description of waves (in our case the dispersion relation of the electrons in graphene) can be completely characterized by their behaviour in a single Brillouin zone.

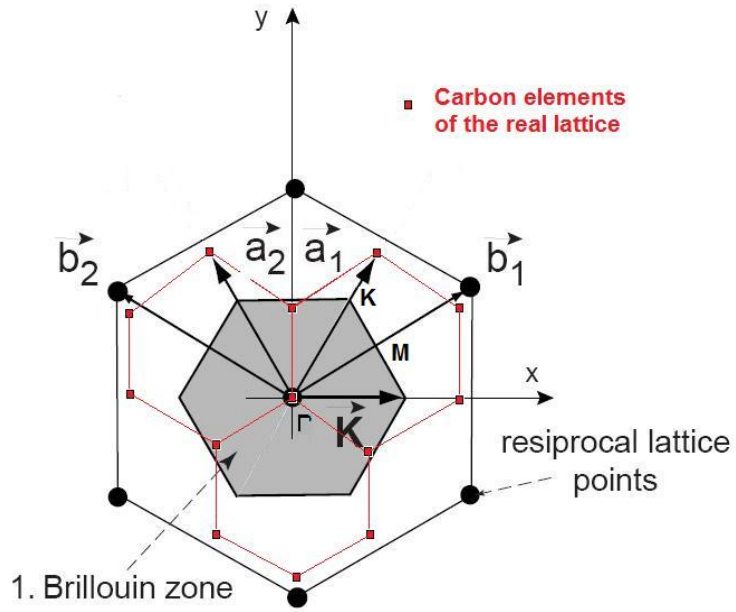

Figure 2.12: Reciprocal lattice of graphene with the first Brillouin zone presented in shadow. Carbon honeycomb structure of graphene is printed in red.

Γ, Μ and Κ points appearing in **Figure 2.12** represent the point of high symmetry of the energy dispersion relation. This dispersion relation can be found after applying LCAO approximations (Linear Combination of Atomic Orbitals). The result is often expressed using the (x,y) components for $\vec{k}$:

$$E(k_x, k_y) = \pm\gamma_1 \sqrt{1 + 4\cos\left(\frac{\sqrt{3}ak_y}{2}\right)\cos\left(\frac{ak_x}{2}\right) + 4\cos^2\left(\frac{ak_x}{2}\right)}$$

a is the lattice constant, i.e. $a = \sqrt{3}a_0$, and γ_1 is the transfer integral. This approximation is called the Slater-Koster scheme and is used as a simple approximation for the structure of graphene. In **Figure 2.13**, the energy dispersion relation of graphene is drawn with the help of the equation above where $\gamma_1 = -3{,}033eV$ [7].

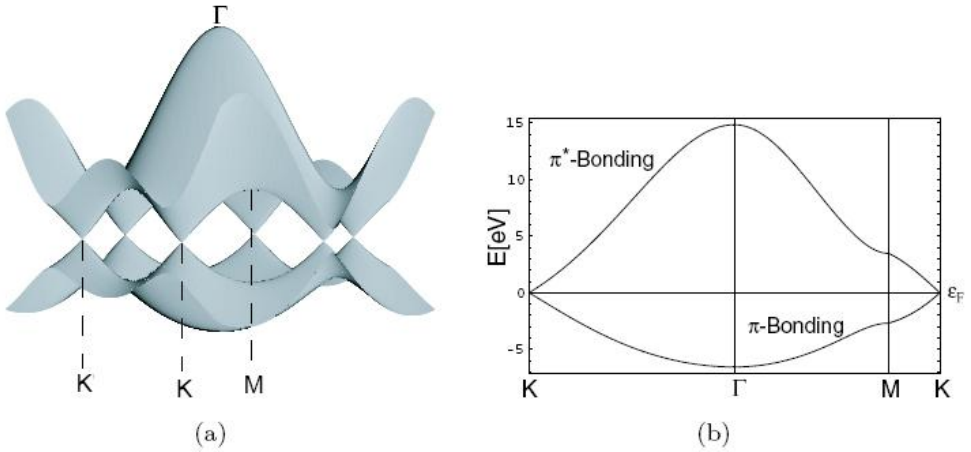

Figure 2.13: (a) shows the dispersion relation of graphene, called tent dispersion. Note this dispersion relation is plotted just inside the Brillouin zone. Points Γ,Μ and Κ are high symmetry points and their placement in the Brillouin zone can be seen in **Figure 2.12**. Plot (b) appeared by cutting (a) in straight lines between the high symmetry points.

Graphene has the peculiar property in that the conduction and valence band only touch each other in six points. Such behaviour makes graphene a so-called semi-metal. The band structure of the single wall carbon nanotubes is found by imposing the following periodic boundary conditions around the circumference of the tube:

$$k \cdot C_h = 2\pi \cdot N$$

Where N is an integer. In others words, the K-vector projected onto the chiral vector, named $k_\perp$ (vector along the circumference), becomes quantized, whereas the K-vector along the tube axis, named kll, is continuous for an infinite nanotube. The 1D dispersion relation or band structure of a carbon nanotube is thus made of the energy bands related to different quantized values N as a function of kll. Whether or not these quantization lines cross a K-point makes the single wall carbon nanotubes a metal or a semiconductor. Based on the three main kinds of nanotubes (armchair, zig-zag or chiral) one can specify the

electronic properties of the CNTs in a more complete way than was mentioned before in this chapter.

The first group contains the armchair tubes, these kinds of nanotubes are truly metallic and have two bands crossing at the Fermi level. In **Figure 2.14 a** one can find the band structure of a (5,5) armchair nanotube. The corners of the hexagons in the reciprocal lattice are the so called K-points and this is where the conduction and the valence band of graphene touch each other. If one of the quantization lines passes through two K-points the nanotube is considered metallic. As well, **Figure 2.14 b** shows the band structure of a (9,0) zigzag tube which can be considered metallic judging from the band crossing the Fermi level. The bands of the zigzag tube stem from the quantization lines drawn in **Figure 2.14 d**. As well, **Figure 2.14 e** shows a (8,0) zigzag SWCNT. For these kind of nanotubes the quantization lines do not cross the K-points in the reciprocal space (not shown). So, this nanotubes are semiconducting with a band gap in the order of 1eV. As one can see, zig-zag tubes can be metallic or semiconducting depending on the chirality.

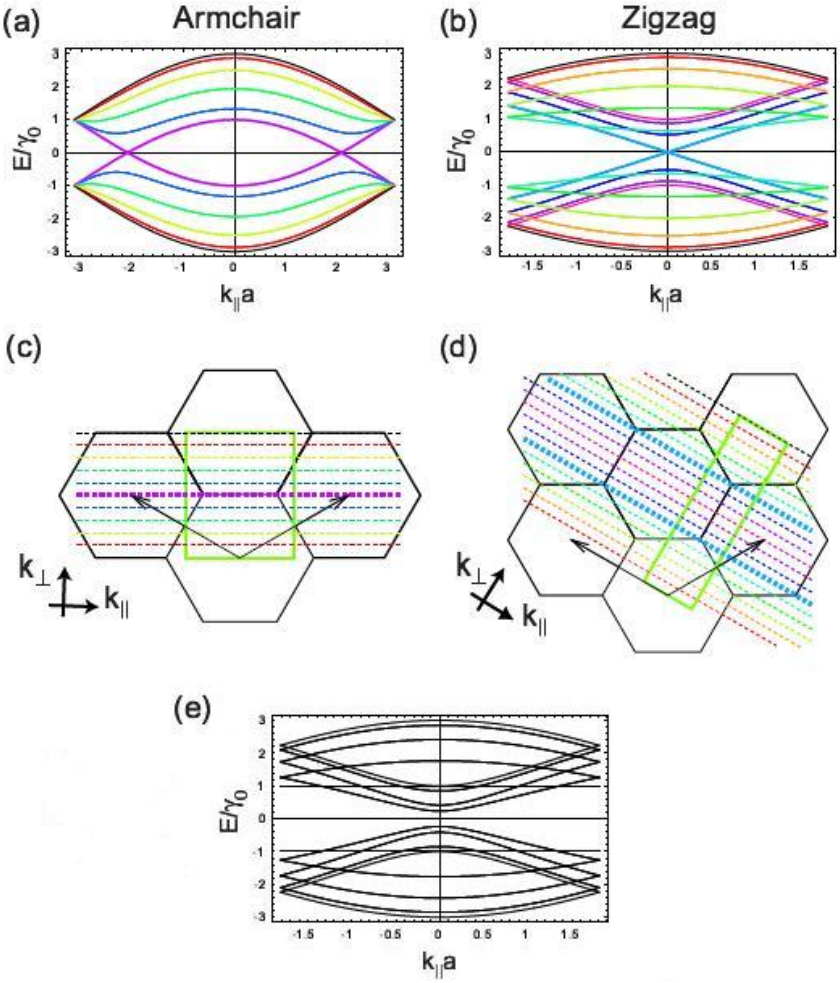

Figure 2.14: (a) Band structure of a (5,5) armchair nanotube. The purple band stem from the quantization line in (c) which crosses the K-points and makes this SWCNT metallic. (b) Band structure of a (9,0) zigzag nanotube. It has a double band crossing the Fermi level stemming from the two blue thick lines in (d). (e) Some tubes are semiconducting with a bigger band gap as the (8,0) zigzag tube. Note that either in (c) and (d) the unit cell of the nanotube appears in green.

All armchair tubes are considered metallic conductors whereas zigzag and chiral behave as metallic when their chiral vector fulfils the following relation: $n - m = 3k$ where $k \in Z$. When the (n-m) relation is not a multiple of 3 the nanotubes can be seen as semiconducting tubes with a band gap in the order of 1 eV [24][25].

2.4 Conclusions

The history and the way that carbon nanotubes are manufactured were treated in detail during this chapter but, more importantly, this chapter attempted to analyze their electronic band structure to understand the basis of their unique electronic properties. The geometry-dependent nature of their electronic structure has been explained through an analysis of the electronic structure of graphene using the (n,m) indices.

Chapter 3

Characterisation methods

3.1 Raman spectroscopy

Transport measurement as in the example of gate voltage dependence measurements, are direct observations of the electronic structure of a single carbon nanotube. However, it is not so easy, or impossible at this point, to strictly characterize a bulk material only with electrical measurements. That is why, optical measurements are more convenient to study the electronic structure of carbon nanotube bulk samples.

Raman spectroscopy has been widely used for characterise carbon nanotubes. With this optical technique one can determine not only the purity of the nanotubes but also the diameter of the nanotubes and even the assignment of the (n,m) indices [26] [27] which determines the electronic structure of the samples (see Chapter 2). When incident light interacts with a sample, as in **Figure 3.1**, photons are scattered with a certain frequency and it is by observing this scattered light that one can resolve the characteristics of the carbon nanotubes.

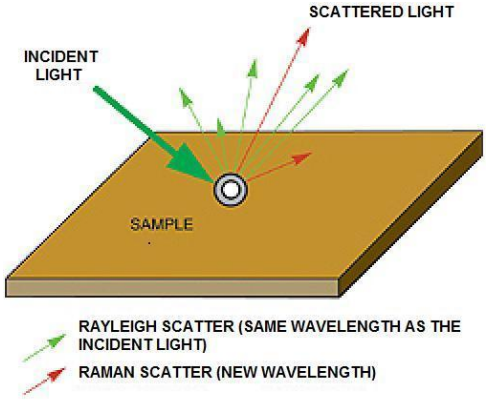

Figure 3.1: Principle of Raman scattering.

Most of the electrons which are excited come back to the initial energy level, emitting light with the same frequency as the incident light. This phenomenon is called Rayleigh scattering. In addition, a very small fraction of the photons ($\sim 10^{-7}$ of the incident light) are scattered showing a frequency difference between incident and emitted light. The shift of the frequency (w) is attributed to the relative vibrational energy level spacings of the target material (molecules). The shift of $V_f - V_i$, where V_f and V_i are the final and initial vibrational states respectively, can be detected positively and negatively which are called Stokes and anti-Stokes scattering, respectively. The situation is schematically shown in **Figure 3.2**.

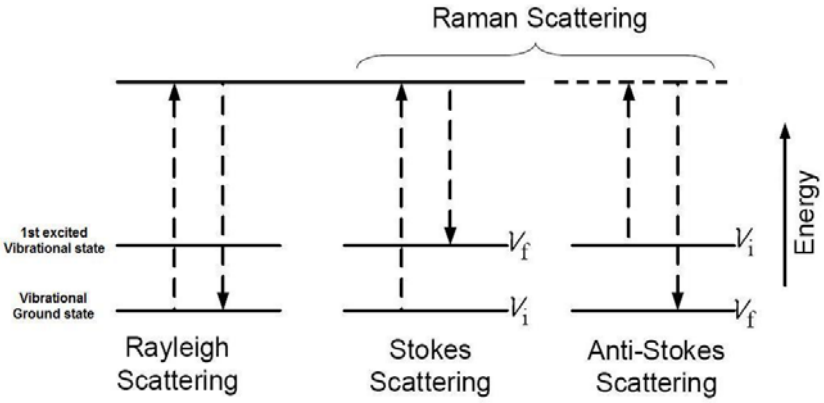

Figure 3.2: Schematic energy diagram of Raman scattering.

The energy of the incident laser can be adjusted to coincide with an electronic transition of the molecule. This is called Resonant Raman Spectroscopy. When the frequency of the laser beam is tuned to be near an electronic transition (resonance), the vibrational modes associated with that particular transition exhibit a greatly increased Raman scattering intensity. An example of resonant Raman data for carbon nanotubes is shown in **Figure 3.3**. The spectra are obtained from a bulk sample of HiPco material using an incident light source of 514 nm Ar+ laser. We can distinguish several peaks which correspond to vibrational modes of the nanotubes. The modes which are observed in the region of $w \leq 350 cm^{-1}$ are called Radial Breathing Modes (RBM), from which one can determine the vibrations of the nanotubes in radial direction. The "D mode" peak around $w \approx 1350 cm^{-1}$ gives us information about the concentration of defects and it is used to determine the quality of the bulk material. Within the range going from 1550 to $1600 cm^{-1}$, there are several peaks, known as "G-mode", induced by the modes of the tangential vibrations.

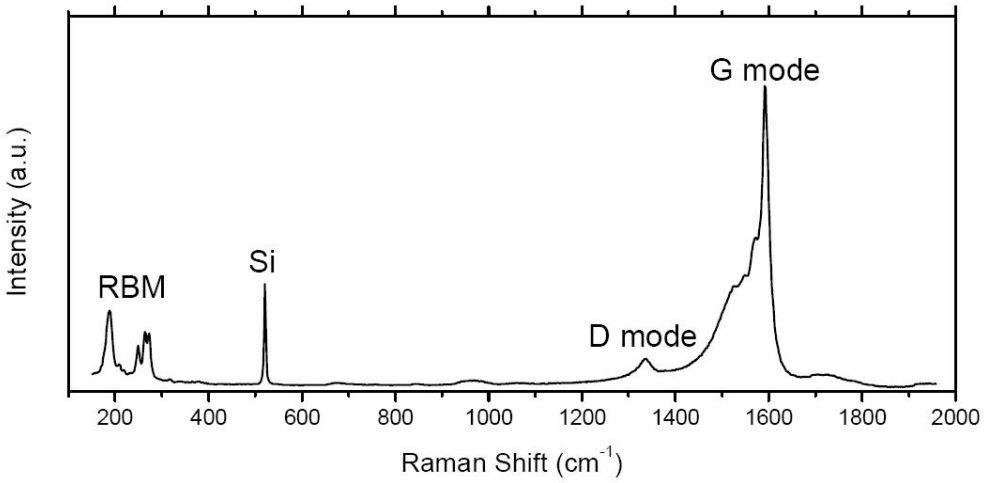

Figure 3.3: Example of Raman spectra. The data was obtained from a bulk sample of HiPco material. Note that the bulk CNT material was deposited over a Silicon Oxide substrate.

The RBM signal is strongly dependent on the tube diameter, thus, one can determine the diameters of individual tubes from the RBM Raman data without using any observation tools such as scanning electron microscope (SEM) and atomic force microscope (AFM). Also from the RBM data, some information on the electronic properties of the nanotubes can be extracted and even the (n,m) indices can be precisely assigned.
This makes Raman observation an extremely important tool for the study of the carbon nanotubes since it is a really simple and quick test to perform.

Figure 3.4 a) shows the qualitative pattern of Van Hove singularities points predicted for the electronic density of states of a semiconducting single wall carbon nanotube. As shown in this figure, the absorption of photons with E22 energy is followed by fluorescence emission near E11. The values of E11 and E22 will vary depending on the tube structure. The excitation energy on a nanotube is limited to a certain energy boundary, where strong Raman RBM signals occur (resonant Raman), known as allowed optical transition (AOT).

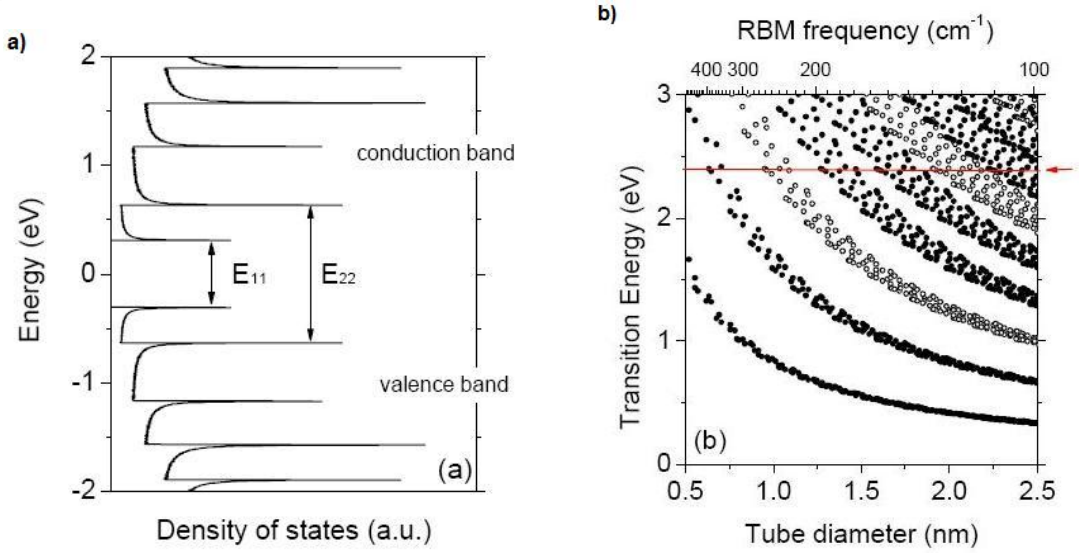

Figure 3.4: a) Density of states of a semiconducting single wall carbon nanotube. E_{11} and E_{22} show the transition energy of this molecule. b) Kataura plot showing the relation between the diameter of the tube and the transition energy. Each data point corresponds to a (n,m) species of nanotube. Metallic nanotubes (open circles) are separated from semiconducting (filled circles).

As we can see in **Figure 3.4 b)**, each type of nanotube has its own transition energy. The relation between the AOT (or transition energy) and tube diameter (or RBM frequency) for each (n,m) tube is also figured in the "Kataura plot" [26]. A 514 nm laser light means an energy of 2,41 eV as indicated in **Figure 3.4 b)** with a red line. Only the tubes with an AOT near this energy line can contribute to the Raman RBM signal. The RBM frequency $(w_{RBM}\,[cm^{-1}])$ is reciprocally dependent on the tube diameter $(d_t[nm])$ as $w_{RBM} = 223.5/d_t + 12{,}5$ when the carbon nanotubes are dispersed in solution. These relations are also considered in **Figure 3.4 b)**.

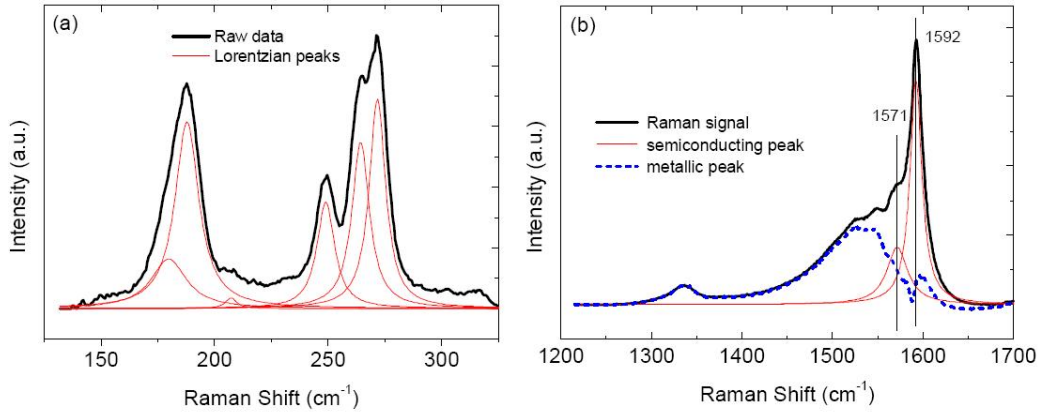

Figure 3.5: a) Raman spectra of the RBM region for HiPco CNT material. The picture shows that the Raman data is decomposed in Lorentzian peaks.b) G-mode frequency range. Contribution of the semiconducting and the metallic Lorentzian peaks.

In the low frequency range, $130\,cm^{-1} < w < 350\,cm^{-1}$, one can observe differences between metallic and semiconducting tubes, both peaks are visibly separated from each other. Semiconducting peaks usually emerge within 130 and $200\,cm^{-1}$, although metallic peaks appear from 220 to $280\,cm^{-1}$. In the G-band region, the lineshapes for semiconducting and metallic nanotubes are also slightly different. This difference is also used to distinguish semiconducting nanotubes from metallic. **Figure 3.5** shows a Raman data set of RBM and G-mode obtained from a HiPco material. The RBM peaks can be regarded as a superposition of Lorentzian peaks (**Figure 3.5 a**). The G-mode Raman signal from single wall carbon nanotubes is also a superposition of the profiles generated by semiconducting and metallic tubes (**Figure 3.5 b**). Semiconducting CNTs show two sharp peaks at ~1560 and ~$1593\,cm^{-1}$ while metallic CNTs generate a broad and asymmetric peak at ~$1540\,cm^{-1}$ [27,28].

3.1.1 Polarized Raman for orientation characterisation

In order to understand the electrical behaviour of the oriented conductive networks studied in Chapter 5, it is necessary to know the distribution of the orientation of its structural unit, the carbon nanotube. The high aspect ratio of the carbon nanotube results in an anisotropy in the electrical, magnetic and electrical properties. By the use of polarized Raman one can study these electric properties along parallel and perpendicular directions to the nanotube axis. Specifically, polarized Raman spectroscopy is used to compare the observed G-band polarisation intensities and their angular dependence (90º). Whatsmore, it is possible to observe differences in the relative intensities of the Raman D-band (1320 to $1400\,cm^{-1}$) as they are also sensitive to the orientation of the optical electrical field with respect to the nanotube axis.

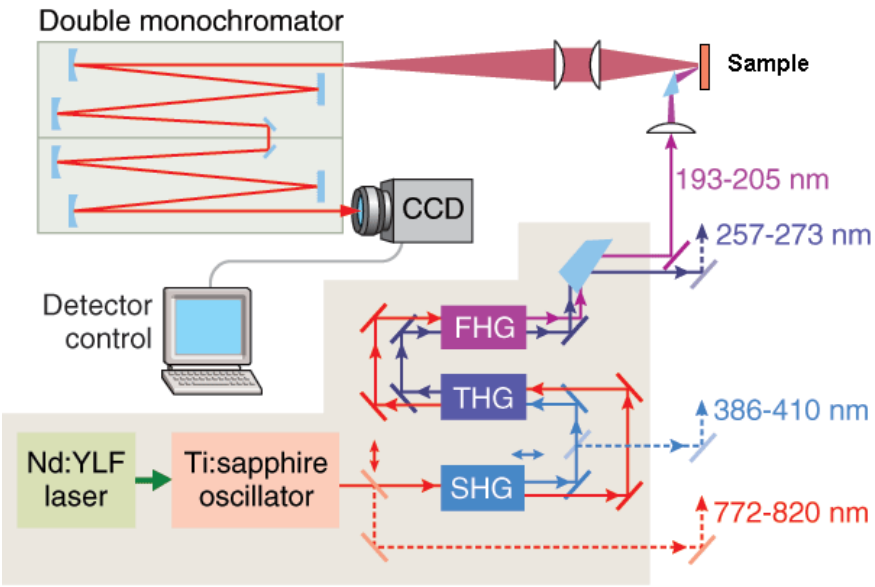

Figure 3.6: Overview of polarised Raman spectroscope.

In polarised Raman analysis, the information obtained from the measurements of the intensity of orthogonal linearly polarized components of a Raman band is very useful. Normally polarised laser illumination of the sample induces inelastic scattering (Raman scattering). The polarized components of the scattered light are discriminated by selecting each component with a linear polarization analyser. Afterwards, the data are recorded using a spectrograph. Normally the polarisation of the laser beam is made by an electro-optic modulator to alternate between the two orthogonal directions and the received orthogonal scattered components are measured by rotating the polarization analyzer by 90º. Subsequently, the two recorded spectra can be used to determine the depolarisation ratio of a Raman band like G-band or the D-band. There are also simpler techniques to polarise the light, it is possible to rotate two quartz plates through the laser beam to produce the alternation of polarisation. Figure 3.6 shows the schematics of the configuration used to measure both directions simultaneously. In this case and in order to get the instantaneous output of the depolarisation ratio, a phase sensitive detector is used. If a charge coupled device (CCD) is installed as a detector, one can record alternate spectra from the two different polarisations. This enables the recording of the two polarised beams simultaneously but this was not implemented in our Raman spectrophotometer device. During our analysis, a single polarized Raman spectrum is recorded one after the other and there was not linear polarisation analyzer to detect the scattered light. In our case, all the scattered light is recorded which is accurately enough to discern between both orthogonal orientations.

3.2 Atomic Force Microscopy

Atomic Force Microscopy is a member of the Scanning Probe Microscopy (SPM) family. In 1981 the first member of that family, the Scanning Tunnelling Microscopy (STM), was developed. Binnig and Rohrer were the first to provide a real space

representation of a Si surface using STM. They brought a sharp tip so close to the Si substrate that a tunnelling current started to flow by applying a voltage between the tip and the surface. From these results emerges the most important disadvantage of STM, this microscopy technique is limited to conductive materials. It was not until 1985 when the invention of the Atomic Force Microscope AFM was able to overcome this limitation. Nowadays, AFM has become an essential tool for imaging and characterise surfaces in many applications. With this technique it is possible to create three-dimensional micrographs with resolutions down to the nanometre and angstrom scales.
The measurements can be performed in air, gases or liquids, independently of the pressure and temperature conditions. The applications range from roughness analysis to surface characterisation but it is also used to evaluate the nanomechanical properties of many materials. During the surface exploration the piezoelectric motors are in charge of combing the square surface taking approximately (depending on the scale and the resolution) 5 minutes to image a complete area (5 μm x 5 μm). This is somewhat problematic when biological in-situ exploration has to be performed as they usually require a faster imaging procedure.

3.2.1 AFM working principle

An extremely sharp pyramidal tip, several microns in length and with a 10 nm radius, is situated at the free end of a reflective cantilever (~200 μm long). This cantilever is then brought closely to the sample surface by a very low force in the order of typical intermolecular forces. This working principle is pictured in **Figure 3.7**.

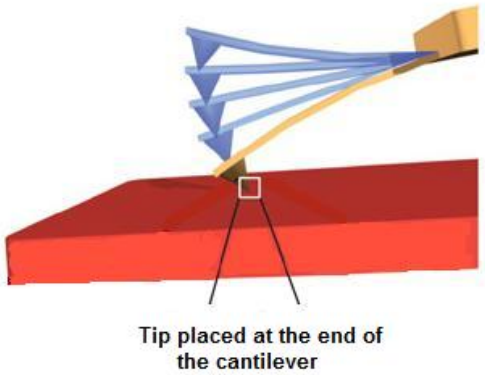

Figure 3.7: A sharp pyramidal tip at the free end of a reflective cantilever is brought into close proximity of the sample surface. The laser beam is focused opposite to the tip on the other side of the cantilever.

A piezo-electric tube scanner provides the movement to the cantilever, due to this movement the tip can scan the surface area. The tip is then moving along the surface and feeling the surface by vertical movements accordingly to the roughness of the sample. This vertical movement of the cantilever is detected by a laser deflection technique. The laser beam is focused on the rear side of the cantilever as closely as possible to the final edge and the reflected beam is received by a position-sensitive detector (PSD). The measured differential PSD voltage provides the AFM signal, which represents a very sensitive representation of the vertical cantilever deflections.

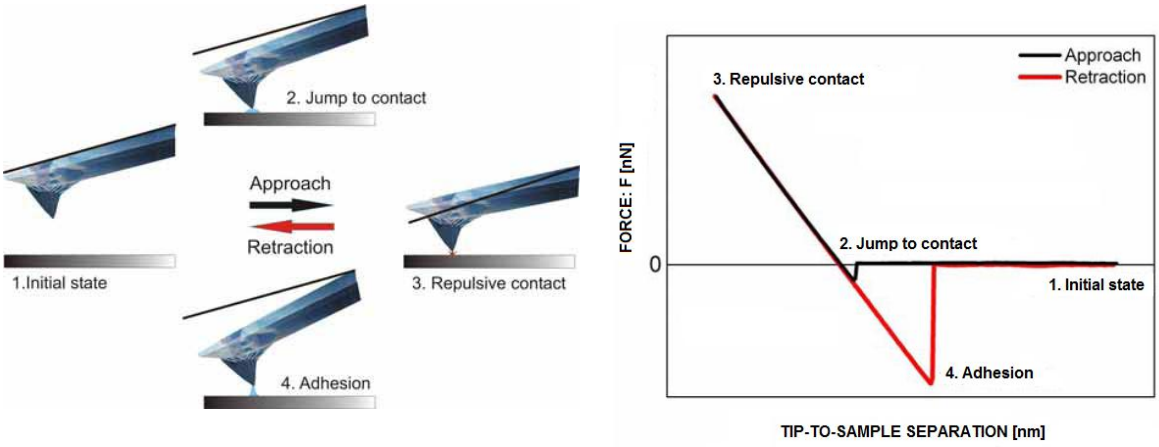

Figure 3.8: Cantilever deflections during approach and retraction to the sample.

As showed in **Figure 3.8**, at the initial state, the distance between tip and substrate is high (step 1). Gradually the cantilever is pushed closer to the surface and forces an increasing attraction of the tip until finally, at a very small separation distance, the cantilever suddenly jumps into contact (step 2) and a new equilibrium between the forces is then reached. Attractive (van der Waals and capillary forces) and repulsive forces (Pauli repulsion) are now acting with equal strength on the probe tip. At this point the distance between tip and surface atoms is comparable with a typical chemical bond length (several angstroms). Pushing the cantilever further towards the sample surface results in an increasing repulsive force as more atoms are getting closer to the tip and their electron clouds start to repel each other electrostatically. These forces cause the cantilever to bend rather than forcing the tip closer towards the sample (step 3). This phenomena is also present when the tip hits upon high particles on the surface where the cantilever has then to retract from the surface. Once these peaks are surpassed the tip remains in contact with the surface due to adhesion forces causing the cantilever to bend downwards (step 4). Eventually the piezoelectric tube scanner overcomes the maximum adhesion force, the probe tip breaks free and the cantilever returns to its initial state (step1).

3.2.2 Operating modes

In AFM there are several operating modes to image and characterize the samples, contact, non-contact, intermittent-contact and pulsed force mode. All of them are based on the same working principle: a sharp tip scans the surface and a map is composed afterwards by the point-by-point measurements of the interaction between tip and sample. Different modes operate in distinct force regimes, which can be associated with specific ranges of the Lennard-Jones potential. This potential is only dependent on the distance d between the molecules or atoms and is described as:

$$P(d) = 4u \cdot \left[\left(\frac{j}{d} \right)^{12} - \left(\frac{j}{d} \right)^{6} \right]$$

Where u and j are the empirical Lennard-Jones parameters and have the units [J] and [m] respectively. A schematics of the potential as a function of the distance d with the corresponding operating mode is pictured in **Figure 3.9**.

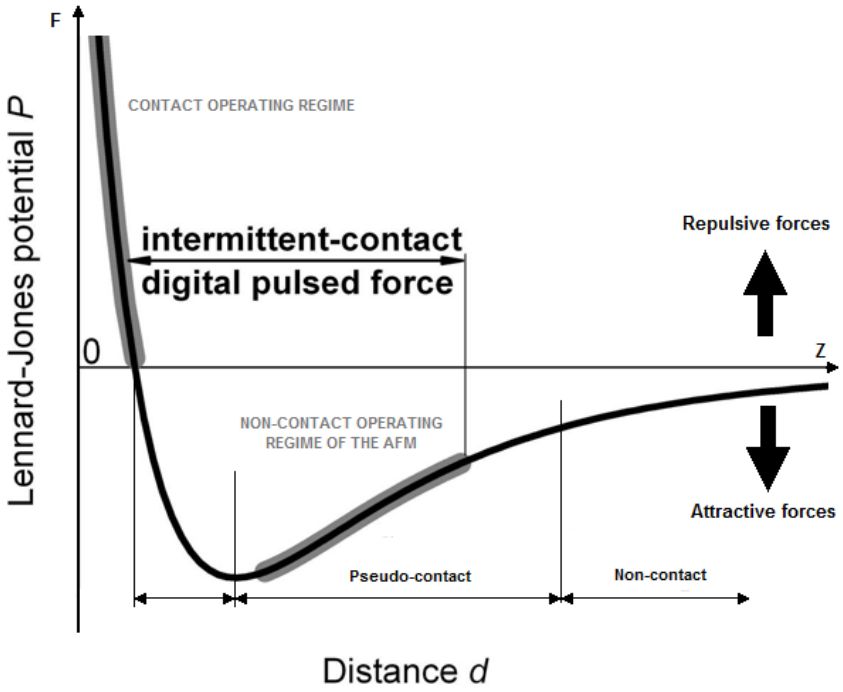

Figure 3.9: Lennard-Jones potential P as a function of distance d. The operating modes regions for the AFM are displayed along the curve.

The Lennard-Jones force is the negative derivative of the potential. It is mildly attractive as two uncharged molecules or atoms approach each another from a distance, but strongly repulsive when they get too close.

Contact mode

In this running mode the cantilever deflection is directly proportional to the force between tip and sample. This mode is called contact mode as the tip is constantly touching the surface. This is why contact mode is not always suitable for soft samples, where their weak bond to the surface could damage them. This technique requires a re-adjustment of the cantilever position above the surface during the scanning procedure. There is a detection and feedback system to solve this problem. For the vertical deflection a set point has to be selected which is proportionate to the force pushing the cantilever to the surface. This system-loop measures the cantilever response and adjusts its height by the use of the piezo-electric tube scanner to keep the vertical deflection constantly on the set point (see **Figure 3.10**). This re-adjustment provides the signal for the topography.
In contact mode, stiff cantilevers can be used to increase the signal response, but on the other hand they could be too weak to resist strong attractive forces resulting in the so called “snap-in” instability close to the surface [29]. Thus, this operating mode is commonly used to explore samples where the dragging effects could be negligible. This limitation had been overcome by the further development of the non-contact mode.

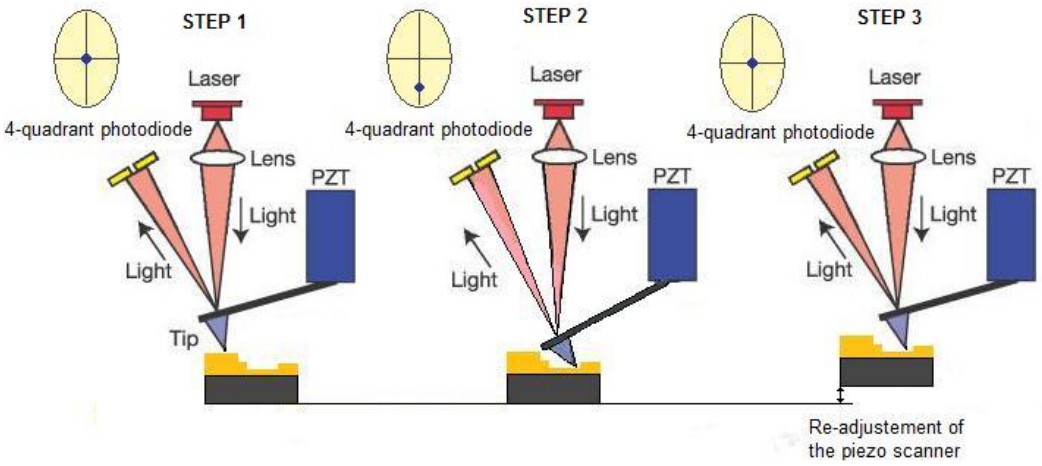

Figure 3.10: AFM running in Amplitude Modulation Mode.
Step 1: Contact surface. Vertical deflection corresponds to the set-point.
Step 2: Scanner moves laterally, tip deflection changes.
Step 3: Piezo-scanner moves vertically to maintain deflection.

Non-contact mode

This running mode uses the vibration of the cantilever by applying a voltage to a piezoelectric in contact with it. The non-contact mode is based on a frequency modulation technique (FM) where the cantilever oscillates at amplitudes around 150 nm. The cantilever, while scanning over the surface, feels the force gradient (in the range of pN) between tip and sample. Therefore, a variation in these interaction forces affects the cantilever and modify the resonance frequency. This frequency shift would be used as feedback signal. In this mode, the total force between tip and samples is much smaller compared with contact mode, thus, providing the necessary protection to operate with soft or elastic samples but does not allow the measurement of mechanical properties. Furthermore, the non-contact mode is not suitable for performing measurements in ambient conditions as under these circumstances the tip can jump spontaneously into contact and damage the surface of the sample. Therefore, automatically resolved non-contact mode images are most often obtained under ultra high vacuum conditions. **Figure 3.11** shows the operating mode of the feedback loop in order to maintain the resonance frequency of the cantilever

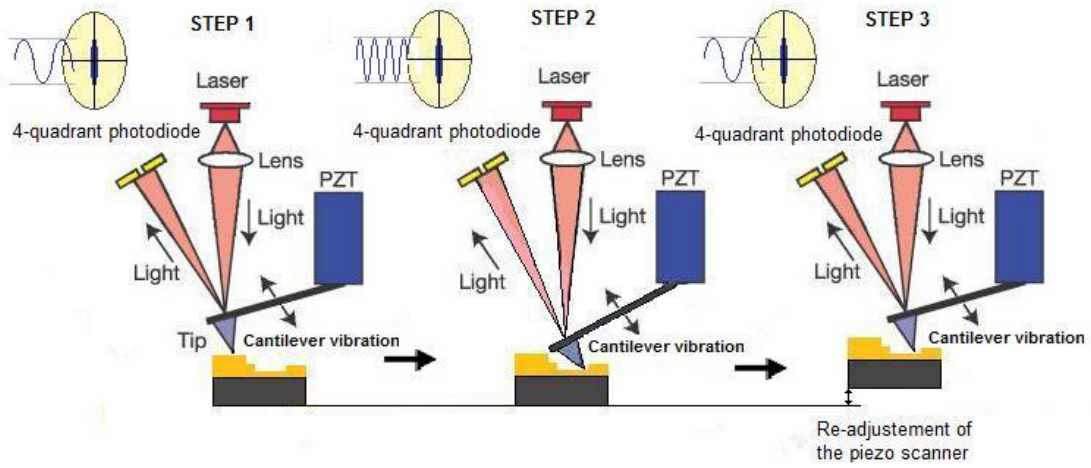

Figure 3.11: AFM running in non-contact mode (Frequency modulation)
Step 1: Contact surface
Step 2: Scanner moves laterally, the cantilever frequency changes
Step 3: Piezo-scanner moves vertically to maintain the frequency

Intermittent-contact mode or tapping mode

The tapping mode is generally used for analyzing soft samples that could get damaged. The snap-in instability is resolved by the use of a high cantilever spring constant of about 40N/m. Tapping mode uses modulated amplitude to drive the cantilever, this amplitude must be large enough to avoid the tip to get stuck on the sample. The frequency of the cantilever is placed close to its resonance, typically in the range of 100-400 kHz, leading to an intermittent repulsive contact with the sample surface. The amplitude of the oscillations starts to decrease as soon as the cantilever cyclically contacts the surface. These losses are taken as a measure of the surface topography. The feedback loop system tries to keep constant the amplitude of the oscillation while the tapping tip is scanning across the sample. Due to this re-adjustment process the detection sensitivity is quite high and is even able to provide sub-angstrom vertical resolution. **Figure 3.12** shows the re-adjustment procedure for this operating mode.

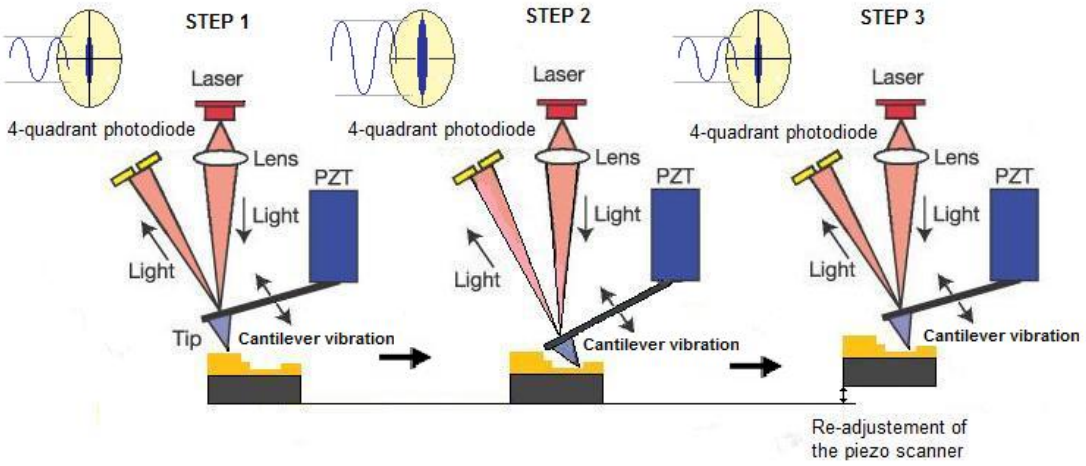

Figure 3.12: AFM running in intermittent-contact mode (Amplitude modulation)
Step 1: Contact surface
Step 2: Scanner moves laterally, the amplitude of the reflected signal is been modified.
Step 3: Piezo-scanner moves vertically to maintain the amplitude.

Pulsed force mode

This operation mode makes it possible to study the full tip-to-sample interaction during the AMF imaging process. Along with the topography it is also possible to record the mechanical and the energetic properties of the sample. Nevertheless, it is often difficult to obtain physical properties from AFM measurements, because of uncontrollable parameters: the environment is continuously modified and the cantilever tip shape is changing while measuring.
During this operating mode the piezo scanner is modulated by the use of a sinusoidal voltage signal of 10-500 nm of amplitude and a frequency from 100 Hz to 2 kHz, far below the resonance frequency of the cantilever. **Figure 3.13** shows the force-distance diagram of an oscillation cycle. At the starting point, the tip is situated well above the surface of the sample. Moving the cantilever closer to the surface, the tip snaps into contact due to the attractive force. The piezo, guided by the sinusoidal excitation, pushes the tip further to the sample. Then, the repulsive force acting between the tip and the sample reaches a maximum. As the piezo scanner pulls back the cantilever the repulsive force becomes smaller and the forces change from repulsive to attractive again. Finally, the tip loses contact and a subsequent free oscillation of the cantilever is damped towards the baseline. This sequence is repeated cyclically.

After the data acquisition process, the baseline and the maximum force (Fmax) are extracted and sent back to the control loop circuit to keep the force constant. This gives information about the topography. The information about forces and baseline, are used to find out not only the topography but also the adhesion image or the stiffness of the sample as well.

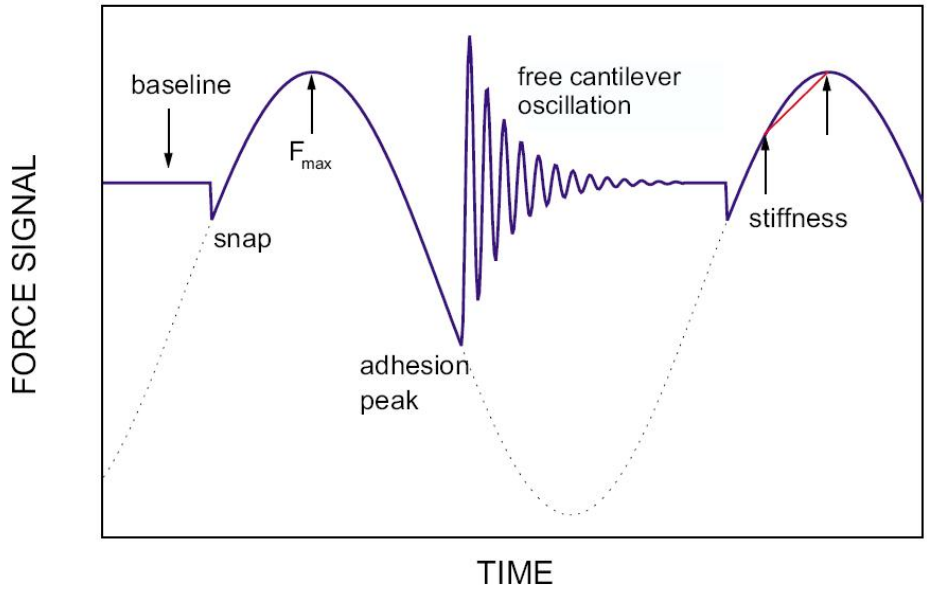

Figure 3.13: Plot showing the modulation voltage signal of the cantilever (dotted line) and the resulting response from it (solid line) over a complete modulation period.

3.2.3 Feedback control loop

The implementation of a feedback control loop is one of the differences between AFM and older topographic measurement devices. As explained before, for all different operating modes the AFM apparatus not only measures the force or the response of the tip interaction, but also regulates it, allowing acquisition of images at very low forces. This feedback control loop (pictured in **Figure 3.14)** is based in a piezo scanner and a compensation network for monitoring the cantilever response and keeps it constant by adjusting the tip-to-sample distance. One point of interest: the faster the feedback loop can correct deviations of the cantilever deflection, the faster the AFM can acquire images; therefore, a well-constructed feedback loop is essential to the microscope performance. AFM feedback loops tend to have a bandwidth of about 10 kHz, resulting in image acquisition times of about one minute.

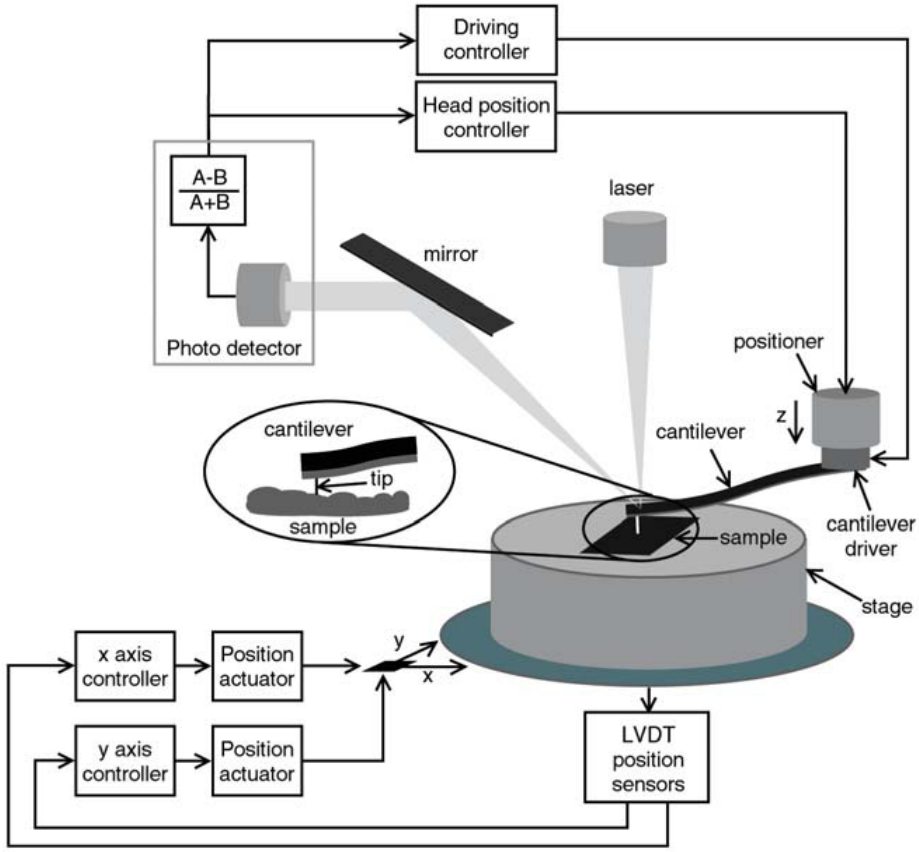

Figure 3.14: Schematics of the AFM microscope. The positioning is controlled by the two loops displayed in the lower part. The adjustment of the cantilever for the different operating modes is performed by the loops displayed on top.

3.3 Conclusions

Both Raman spectroscopy and AFM microscopy were very useful tools during this work. Due to Raman spectroscopy it was possible not only to characterise the carbon nanotubes material but also to determine the orientation of the nanotubes along the substrate. Besides its technical complexity Raman measurements are fast and easy to handle, thus makes this technique the preferred one for the study of carbon nanotubes and its based applications.

With AFM it was possible not only to image the networks over the substrate but also to have a visual interpretation about the percolation and the orientation of the networks. The AFM device used along with this research was from Digital instruments Inc and it is displayed in **Figure 3.15** with a brief description of its components. The software used was version 5.12 rev. B of Nanoscope System software from Digital Veeco Metrology Group. AFM has proved to be an excellent tool and was chosen to be used as the main image technique for the study of our conductive networks. Its simplicity and versatility together with a true atomic resolution made it a very suitable tool for our purposes.

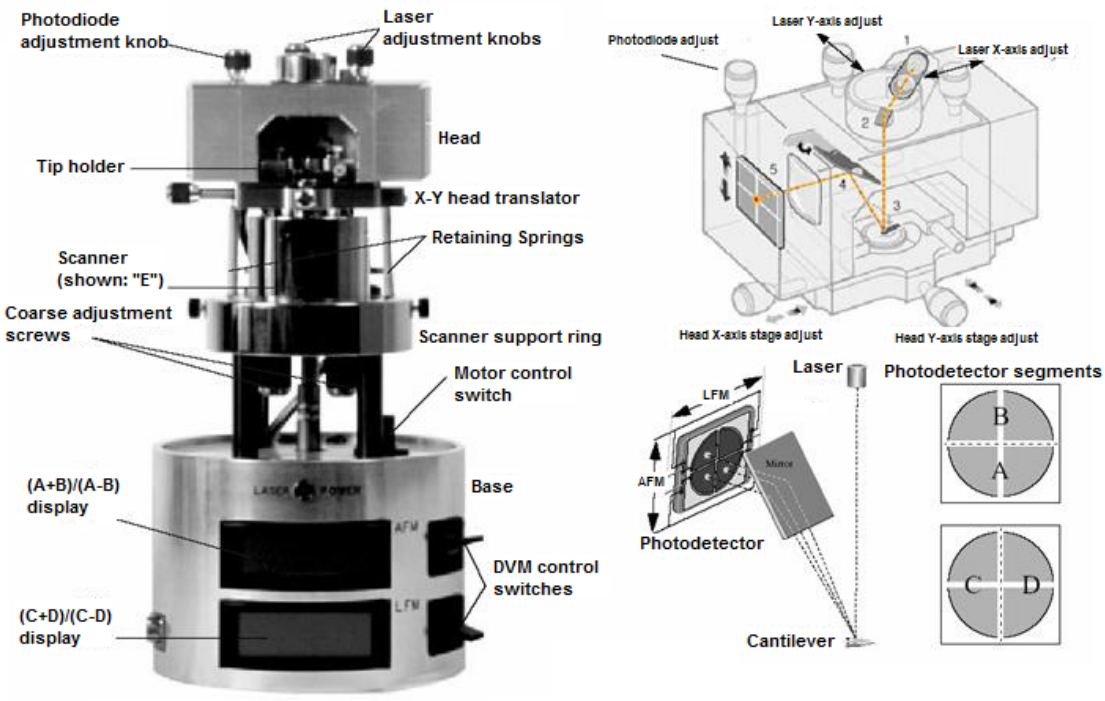

Figure 3.15: Picture and description of the AFM microscope used along with this research.

Chapter 4

CNT comparison and procedures

4.1 Introduction

In this chapter a comparison between different carbon nanotubes sources will be analyzed. Multi wall carbon nanotubes from Ahwahnee, Nanocyl, Baytubes, Elicarb and C-tubes are presented and compared together. As well, we provide comparative data between single wall and multi wall nanotubes from the same manufacturer (Elicarb). The main goal is to find out which carbon nanotube material provides better conductivity values and to prove if this benefits in a highest transparency vs. conductivity ratio. All the procedures for comparison as well as the measurement methods are introduced in the following sections.

When placed together, and because of the Atomic forces or Vander Waals interactions, carbon nanotubes tend to arrange themselves into nanotubes ropes or bundles. Inside these bundles, the tubes are regularly packed with pores between the tubes and within the tubes. In turn, these nanotube ropes can be assembled to form an entangled network called "buckypaper". This agglomeration of pure material might be appropriate for conductivity measurements. After obtaining the buckypaper material and measuring its dimensions, one can perform the conductivity measurements with a four probe technique. This will give an idea about how conductive every carbon nanotube source is.

4.2 Dispersion preparation

The main step during the fabrication of the buckypapers is to get a homogenous and stable dispersion of the nanotubes. Carbon nanotubes are molecules insoluble in water and organic solvants. However, if a surfactant is added to the dispersion, and with the use of sonication, an homogeneous and stable suspension can be obtained. In order to prevent the bundelling effect mentioned in the introduction, Sodium-Dodecyl-sulfate (SDS) was used as surfactant. As we can see in **figure 4.1**, SDS molecule has a tail of 12 carbon atoms, attached to a sulfate group, giving the molecule the amphiphilic properties required for a detergent. The polar end is attracted to the water molecules, while the non-polar end is repelled. By the presence of carbon nanotubes this product attaches to the wall of the tube (hydrophobic molecule) thus avoiding the contact between them and allowing a free standing suspension of the nanotubes in the solution.

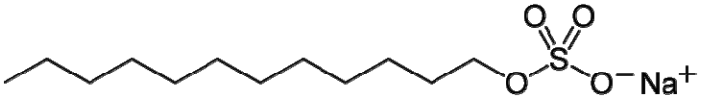

Figure 4.1: Molecular structure of the SDS.

The sonication process is necessary as a source of external mechanical energy which helps the particles to overcome the attractive Van Der Waals forces. When placed together SDS and carbon nanotubes molecules form micelles as showed in **Figure 4.2**. This reaction is

extensively explained in Chapter 5 in the section about the "electric field deposition method". The concentration of the SDS and the concentration of the nanotubes play a large role in whether a uniform suspension is obtained. We carry out the dispersion preparation with a concentration of 1% of SDS in de-ionised water and a concentration of approximately 0,25 mg/mL of carbon nanotubes source.

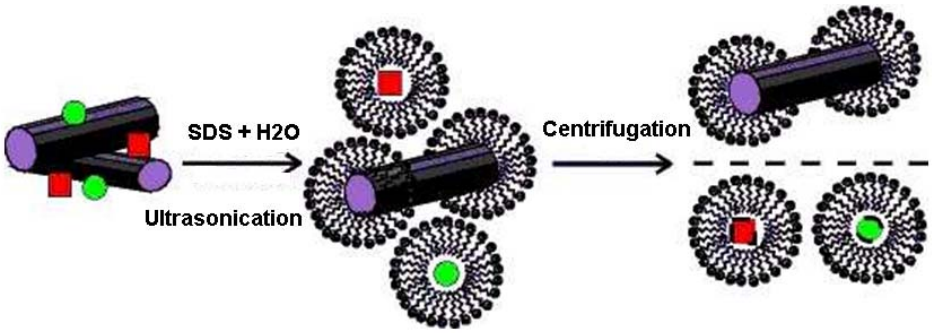

Figure 4.2: Micelle formation during the dispersion preparation.

Another reason for using SDS as a surfactant is because it is especially easy to remove from the buckypapers once the filtration process finishes. For that, the buckypapers were repeatedly rinsed with de-ionised water by the use of the same filter and vacuum pump as for the filtration process.

4.2.1 Purification processes

As already discussed in chapter 2, depending on the method used for the growth of the carbon nanotubes, one can find different impurities within the carbon soot. Graphite, amorphous carbon, catalytic residues or fullerenes are the most common substances which have to be separated away to ensure a high degree of purity of the material. Despite the fact that the subsequently filtration process will separate most of these unwanted particles, it is always better to start from a purified dispersion in order to accelerate the filtering process and ensure a high quality end-product. The following methods are the most commonly used for purification purposes, they are briefly explained below.

Centrifugation

This was the method used during the preparation of our buckypapers and, inspite of being easy to handle and relatively quick to perform, this practice can be considered as part of the purification step. The suspension was centrifuged extensively (30 minutes) under 15.000 rpm by the use of a centrifugator "Centrifuge 5540" from Eppendorf. Bigger particles like amorphous carbon or the remainder big bundles of carbon nanotubes which were not broken up during sonication were deposited on bottom. All These undesired particles are separated by the effect of density divergence.

Oxidation

The oxidation is a good way to remove contaminants from the nanotubes. However, the main drawback of this technique is that, not only the impurities are oxidized but also partially the nanotubes. Fortunately, the oxidation of the particles is more important than for the nanotubes. This oxidation is mainly applied since foremost contamination comes from the metal catalyst particles which are largely reduced by oxidation. The quality of the process depends on various factors including the metal content, the oxidation time and the temperature which all play an important role during this procedure. Usually, one applies hydrogen peroxide (H2O2) or sulfuric acid (H2SO4) directly in a hot air stream (thermal oxidation) [25]. The high temperature applied also causes the decomposition of the amorphous carbon and the fullerenes.

Acid treatment

Acid treatment only has an influence on the metal catalyst. Nitric acid (HNO3) or Hydrogen chloride (HCl) are the chemicals used during this purification step. Nitric acid (HNO3) only affects the metal particles without modifying the structure of the carbon nanotubes whether hydrogen chloride can have a minimal impact on the CNT [28]. This treatment does not help in the separation of the other undesired components.

Magnetic treatment

Many publications claim that it is also possible to purify the material by effect of an electromagnetic field. In the process, the raw material is dispersed by sonication in a solution and the presence of a magnet splits the material into metallic particles and carbon nanotubes. This method seems to be suitable only for separating the metallic particles from the carbon nanotubes soot.

4.3 Buckypaper formation (Filtration process)

Later on, and once the dispersion is prepared, one can proceed with the filtration process by the use of a vacuum filter apparatus (see **Figure 4.4**). The lager size of the carbon nanotubes micelles allows for the separation of the impurities and helps in the formation of the buckypaper. This separation was done by filtration of the dispersion through a MCE membrane (**Figure 4.3**). This filter paper had pores of about 0,4 µm in diameter. A water pump was used to create the partial vacuum inside the flask. The sonicated solution was added into the funnel while the water pump system was activated. As a result, the carbon nanotubes bundles were left on the surface of the filter paper. The thicker the buckypaper becomes, the longer it takes to carry out the process. In order to produce larger buckypapers a longer time is therefore required. The average processing time for a piece of 12cm in diameter was 24 hours. When all the SDS solution had been filtered, the buckypaper was then rinsed with deionised water in order to remove further impurities and the remaining SDS molecules. The filter paper was taken out from the filtration apparatus and the buckypaper was carefully pealed off from the membrane. We let it dry in the air but it is also possible to dry it in an oven. Once dried, the buckypaper has a tendency to shrink slightly in size.

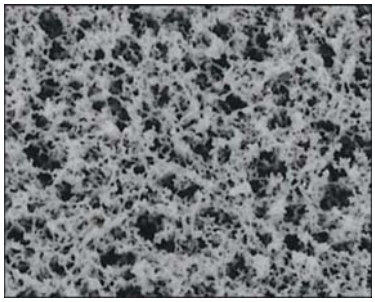

Figure 4.3: MCE membrane filter (0,40µm holes).

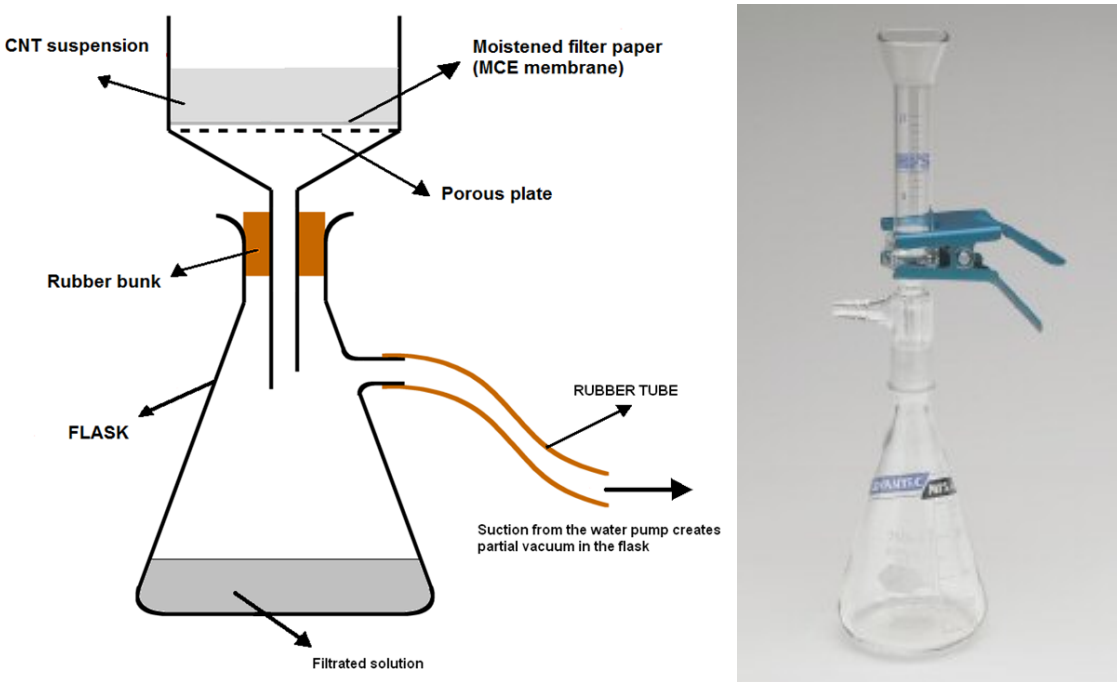

Figure 4.4: Apparatus for the preparation of the buckypaper (Schematic and picture).

Once the buckypaper was successively processed, due to SEM observations one can observe the structure of the buckypaper material (**Figure 4.5)**. Carbon nanotubes ropes are uniformly spread which makes up the nano-structured mat. Note there are three types of pores: large pores between the ropes, only visible in the SEM image, pores between the tubes and pores inside the tubes. These pores play an important role in the behaviour of the buckypaper.

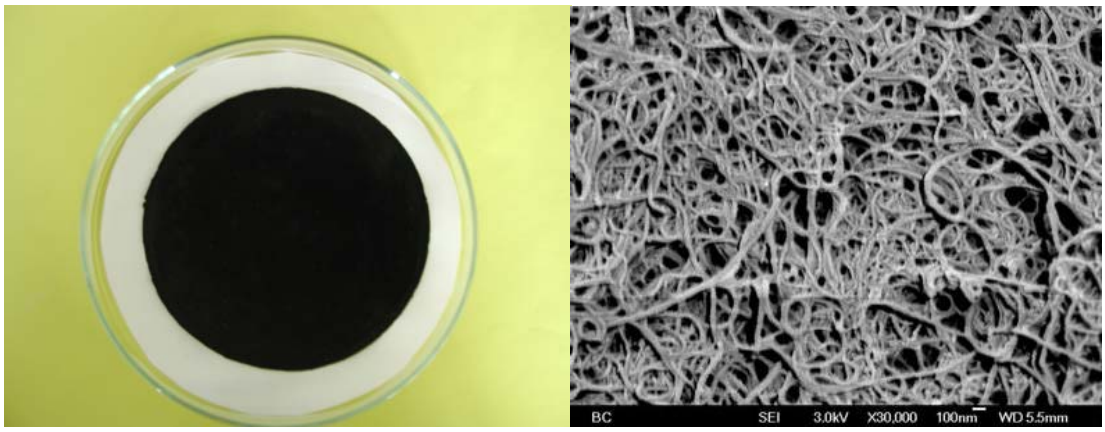

Figure 4.5: Final product and SEM picture of a buckypaper made out of purified SWNTs.

4.4 Results and discussions

In order to perform the conductivity measurements we cut small rectangular pieces of the different buckypapers. We measure the thickness (d) and the width (w), it is not necessary to figure out the length since the two probes of the measuring device are separated by 1mm.

Resistance or conductance measurements are generally made by just a two-point measurement method. However, when measuring very low values in the range of mili or micro ohm, the two point method is not adequate because resistance of the measuring components (lead resistance) becomes a significant factor. The four probe resistance measurement method eliminates this lead resistance. The principle of the 4-probe based measurements is showed in **Figure 4.6**. Two external current probes, C1 and C2, provides the current that circulates through the resistance under test while the other two internal potential probes, P1 and P2, provide a two-wire voltage measurement circuit that calculate the voltage drop across the resistance.

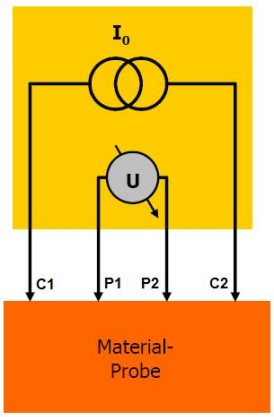

Figure 4.6: Representation of the 4-probe measurement method.

With the dimension of every sample and due to the electrical measurements one can uncover the conductivity of each material by the use of the following formula:

$$\text{Conductivity: } \delta[S/cm] = \frac{1}{R} = \frac{I[A]}{V[V]} \cdot \frac{l[mm]}{W[mm] \cdot d[mm]} \cdot 10$$

All the electrical measurements are exposed in **table 4.1.** The difference between single and multi wall carbon nanotubes is noticeable. According to these results, C-tubes seem to be the most conductive material within the single wall nanotubes sort. Furthermore, the advantages of single wall carbon nanotubes is quite evident; both of the two single wall materials used in this comparison are one order of magnitude more conductive than their multi wall competitors.

Intensity (mA)	Voltage (mV)					
	Awhanee	**C-tubes**	**Nanocyl**	**Baytubes**	**Elicarb sw**	**L.A. sw**
10	19,19	4,58	16,7	18,12	2,65	3,19
20	38,23	9,13	33,41	36,31	5,26	6,37
30	57,23	13,68	50,10	54,24	7,92	9,57
40	76,22	18,22	66,80	73,01	10,41	12,75
60	114,14	27,31	100,17	108.43	15,73	19,14
Conductivity (S/cm)	18,359	29,089	21,770	17,760	221,053	195,039

Table 4.1: Conductivity results of different raw materials.

In spite of the fact that single wall nanotubes lead to higher conductivity performances, it is not proven yet that they also provide better transparency values. Thus, we look for transparent conductive networks as a means to boost the transparency vs. conductivity ratio.
Elicarb single and multi wall carbon nanotubes are selected for this testing. Thomas Swan is the company producing these carbon nano-materials, references and concentration are detailed below:

- Single wall carbon nanotubes: - Product reference: PRO920
  - Batch reference: 61366/55
  - Concentration: 4,3% SWCNT
- Single wall carbon nanotubes: - Product reference: PRO920
  - Batch reference: 62510/56
  - Concentration: 3,7% SWCNT
- Multi wall carbon nanotubes: - Product reference: PRO936
  - Batch reference: K1790
  - Concentration: 14,3% MWCNT

For the preparation of the dispersion we follow the same procedure as in the preparation of the buckypaper. In this case, the concentration is 0.3mg/mL of wet cake material in 1% SDS solution. The dispersion is deposited on the substrate by spraying method with an air brush pistol (Harder & Steenbeck). This technique is simple and quick and allows us to

tune the transparency easily between 0% and 100%. During the process the substrate is placed over a hot plate (50ºC) to accelerate the drying of the small droplets on surface without melting the substrate. The substrate is a flexible transparent insulating foil of polycarbonate. Finally the samples are immersed into de-ionised water for 30 seconds to remove any trace of SDS and dried in air. Typical images of sprayed carbon nanotubes coatings are shown in **Figure 4.7** in order to demonstrate the homogeneity in larger scales. **Figure 4.8** shows the samples prepared for conductivity and transparency measurements.

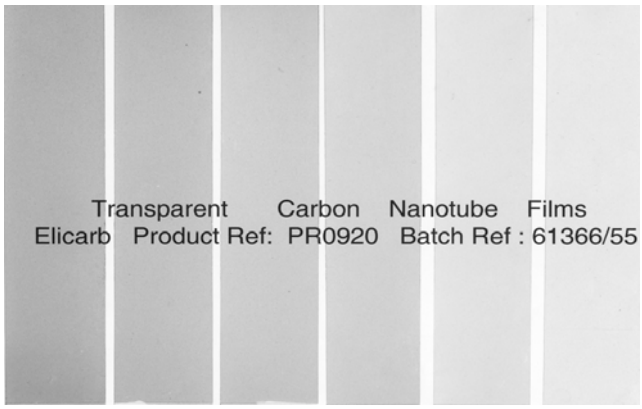

Figure 4.7: Samples of the transparent films on PET foils. Notice that the text lies behind the films.

Figure 4.8: Samples with silver contact electrodes for resistance measurements.

For the resistance/conductivity measurements is not possible to use the same 4-probe method already introduced, in this case the layers are very thin and it is extremely easy to scratch the surface and remove the conductive layer while measuring. That is the reason why silver contact electrodes are deposited on both end sides of the sample. Surface resistivity is then calculated in the following way:

$$R_s[\Omega/sq] = R[\Omega] \cdot \frac{l}{w}$$

The resistance is calculated by the use of a multi-meter. Transmittance measurements are recorded in a double beam spectrometer (Perkin Elmer, Lambda 2) between 190 and 1100 nm. Since surface resistivity and transparency change with the thickness of the coating, one has to look at the same transmittance to obtain a direct conductivity comparison. By this means coatings with different thicknesses are measured and plotted together. The results are summarised in **Figure 4.9** where the transmittance values are for wavelengths of 550nm. The difference between single and wall nanotubes is quite noticeable, both single wall nanotubes sorts show better transparency vs. resistance performance. Most likely this is due to a higher diameter of each multi wall carbon nanotube which increases the light absorption but not the conductivity.

It is known that individual nanotubes tolerate a high degree of mechanical stress such as bending and buckling. Deposited onto flexible substrates, the electrical properties of the network can be maintained also under bending. ITO will not show this flexibility and the foil break under torsion, even thought flexible ITO coatings on polymer have been reported [26] their flexibility is not comparable to the carbon nanotubes' based foils.

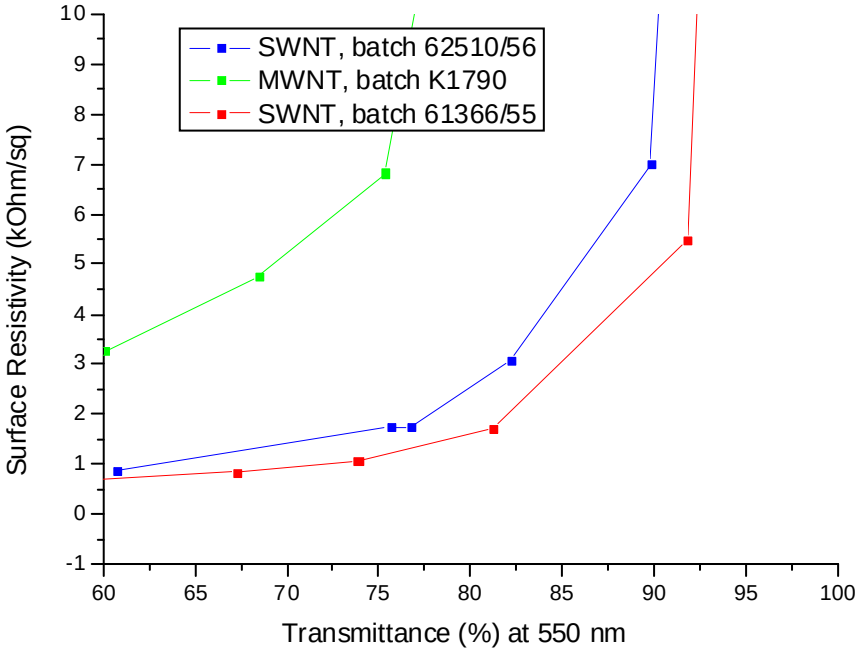

Figure 4.9: Surface resistivity as a function of transparency.

4.5 Conclusions

Both single wall and multi wall carbon nanotubes are interesting materials for conductive applications but for the transparent conductive networks developed in this project, single wall nanotubes seems to be more suitable. After testing with different carbon nanotubes sorts, single and multi wall tubes from diverse manufacturers, one can conclude that single wall carbon nanotubes are more conductive. Moreover, this enhanced conductivity allows one to obtain better transparency vs. conductivity ratio. One of the reasons for this behaviour is likely the high aspect ratio of single wall tubes compared with multi wall. The longer and the thinner the tubes are, the bigger the holes become within the tubes and the better light can pass through. Furthermore, it might not only be because of the shape of the tubes but also because of the electronic transport properties. As explained in chapter 2, single wall carbon nanotubes can be considered ballistic, so the resistivity of the networks should come mainly from the contacts within the tubes. Having said that, multi wall nanotubes, instead of being conductive can not be considered ballistic since the different shells in a tube can be metallic or semiconducting and that inter-shell interactions can affect the behaviour. From this point on, only single wall carbon nanotubes were decided to be used in further experiments.

Chapter 5

Substrate functionalisation, deposition methodology and CNT orientation

5.1 Introduction

The main step towards the manufacturing process of the transparent conductive coatings is to determine which deposition method enhances the transparency and the conductivity of the networks. Furthermore, due to the outstanding features of a single carbon nanotube, particularly regarding its electrical conductivity along the tube, one has also to determine if the orientation of the nanotubes over the substrate make sustainable improvements on the conductivity. Dip-coating, Adsorption, Spraying and a newly developed method by electric field exposure are the deposition techniques discussed within this chapter. Afterwards, which deposition method allows better orientation of the nanotubes over the lattice and its advantages in the transmittance and electrical properties are discussed. The goal was to determine which coating process reach better conductivity vs. transparency ratios.

As soon as carbon nanotubes are deposited over the substrate, good interfacial bonding between CNT and the substrate have to be guaranteed. CNT have to be attached easily during the deposition process and should remain stuck over the surface as long as possible. Firstly, we analyse different surface treatments and their benefits for each deposition method. We introduce Silane functionalization and PDDA polymer functionalisation and compare them to non-treated substrate. In this first study the observation and characterisation of the samples are carried out mainly by AFM microscopy.

5.2 Study of the substrate functionalisation

5.2.1 Substrate preparation previous to CNT coating

Previous to the CNT deposition on substrate, the samples have to be carefully cleaned and functionalized. The entire study was done using silicon oxide chips as it was assumed that similar results can be found with other surfaces. During the cleaning process, silicon oxide chips were chemically cleaned via 3 separate steps. Initially, in order to remove the photo-resistant on top, the chips were dipped into N-Methyl-2-pyrrolidone (NMP) for 15 minutes at 55ºC of temperature in the bath sonicator. Next, the chips were dipped into another beaker filled with acetone for 15 minutes at 55ºC of temperature in the bath sonicator. Lastly, we repeated the same modus operandi with Isopropanol. Finally, all the samples have been dried with Argon and kept in a plastic chip container. **Figure 5.1** display the surface of a silicon oxide chip after cleaning.

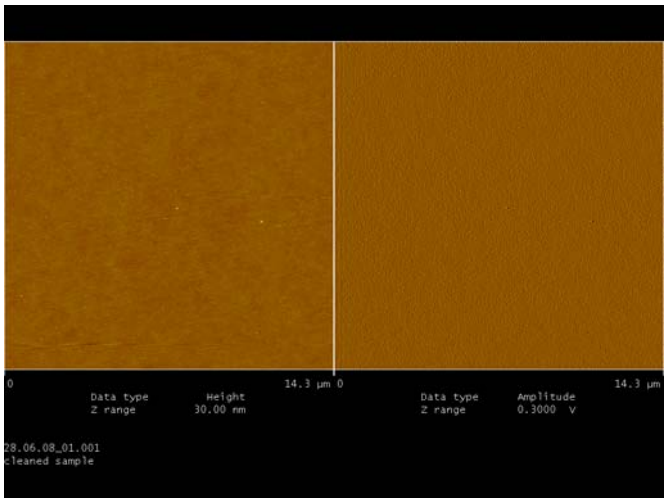

Figure 5.1: AFM capture of a cleaned silicon chip (scale: 4,3µm)

Once the chips were cleaned properly, we proceed with the functionalization of the substrate. During the silanisation process the samples were placed for 2 minutes in a beaker with 10 mL of H2O (de-ionised water) and 50 µL of (3-Aminopropyl-triethoxylane) and then rinsed in a beaker filled with de-ionised water for 1 min. During PDDA polymer treatment the samples were dipped into a mixture of PDDA polymer and water and then dried with argon flow. To determine the influence of the surface treatment we performed visual comparative tests using the three different deposition methods.

5.2.2 Effects of substrate functionalisation for adsorption deposition method

Morphology of the network after PPDA treatment of the substrate:

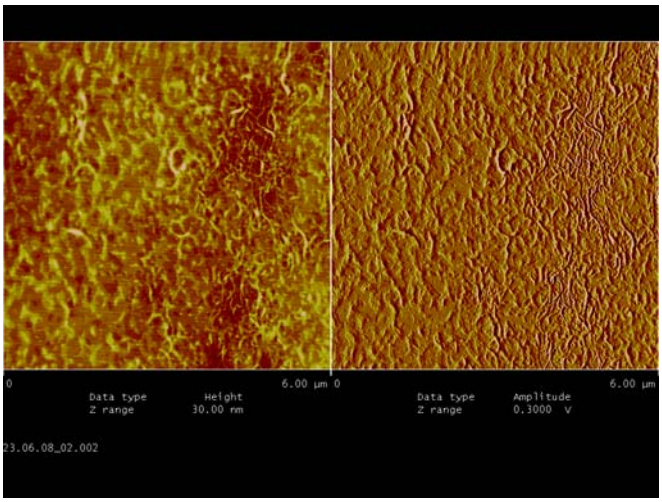

Figure 5.1: AFM picture of the sample after PDDA treatment (scale: 6µm).
Deposition method: Adsorption 30 drops. CNT material: HiPco nº1

Morphology of the network after Silane treatment of the substrate:

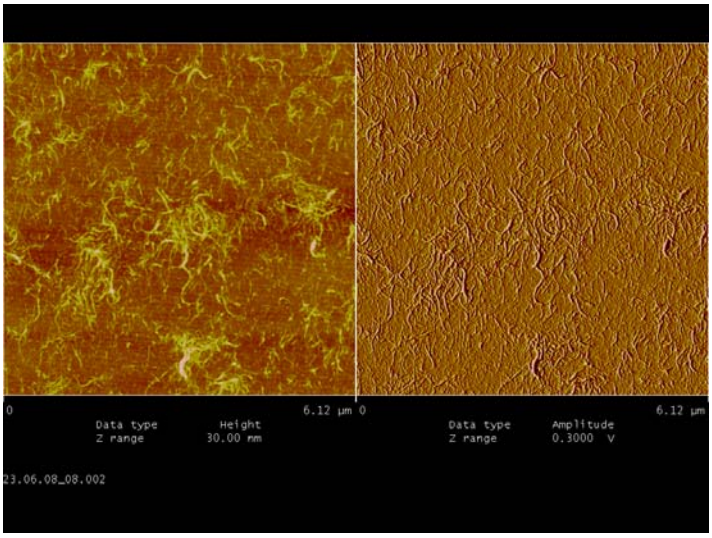

Figure 5.2: AFM picture of the sample after Silane treatment (scale: 6,12µm). Deposition method: Adsorption 40 drops. CNT material: HiPco nº1

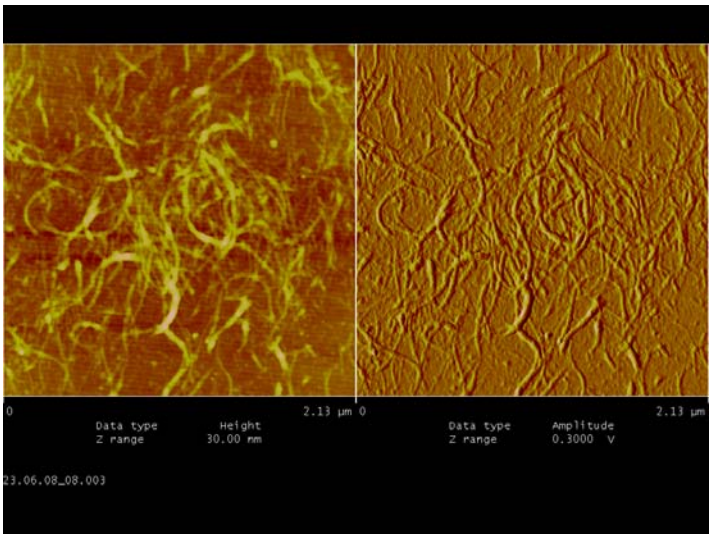

Figure 5.3: AFM picture of the sample after Silane treatment (scale: 2,13µm). Deposition method: Adsorption 40 drops. CNT material: HiPco nº1

Morphology of the network without treating the substrate:

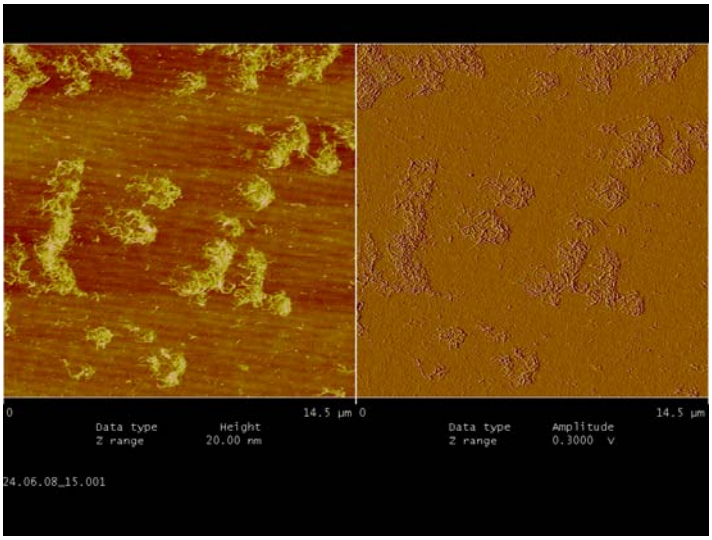

Figure 5.4: AFM picture of the non-treated sample (scale: 14,5µm).
Deposition method: Adsorption 40 drops. CNT material: HiPco nº1

5.2.3 Effects of substrate functionalisation for dip-coating deposition method

Morphology of the network after PPDA treatment of the substrate:

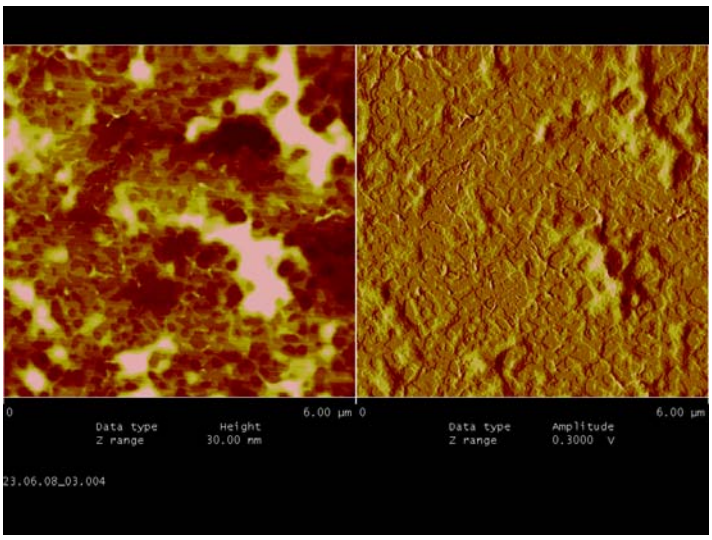

Figure 5.5: AFM picture of the sample after PDDA treatment (scale: 6,00µm).
Deposition method: Dip-coating 30 times x2 (program 5). CNT material: HiPco nº1

Morphology of the network after Silane treatment of the substrate:

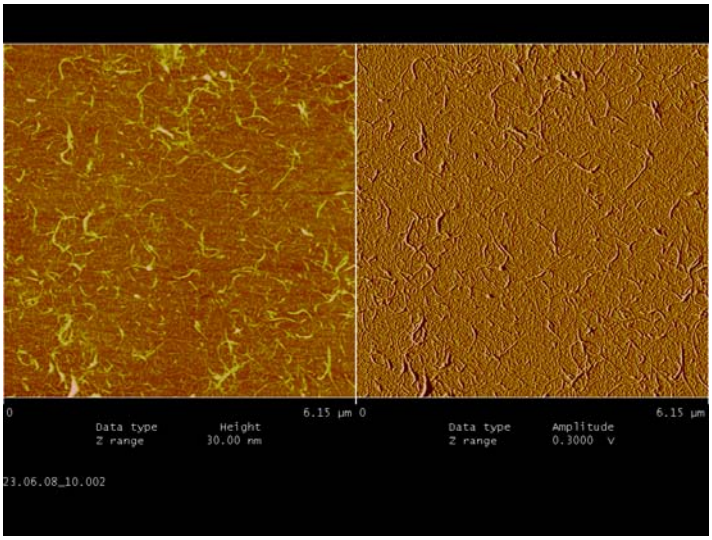

Figure 5.6: AFM picture of the sample after Silane treatment (scale: 6,15µm). Deposition method: Dip-coating 30 times x2 (program 5). CNT material: HiPco nº1.

Morphology of the network without treating the substrate:

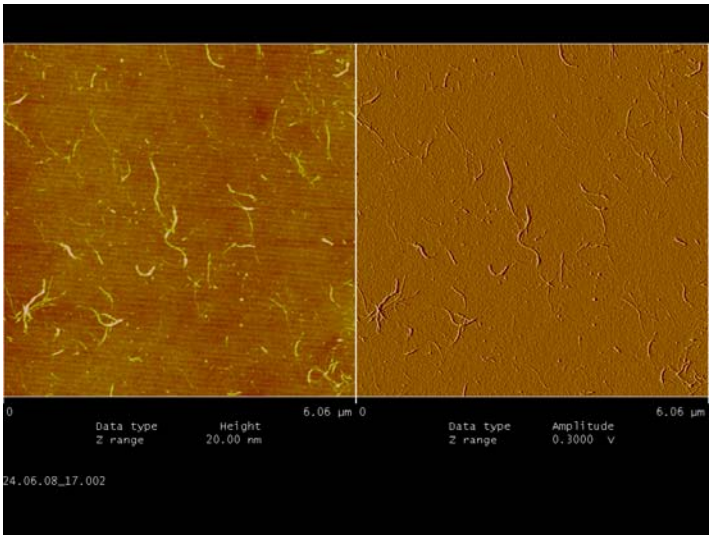

Figure 5.7: AFM picture of the non-treated sample (scale: 6,06µm). Deposition method: Dip-coating 30 times x2 (program 5). CNT material: HiPco nº1.

5.2.4 Effects of substrate functionalisation for spraying method

Morphology of the network after PPDA treatment of the substrate:

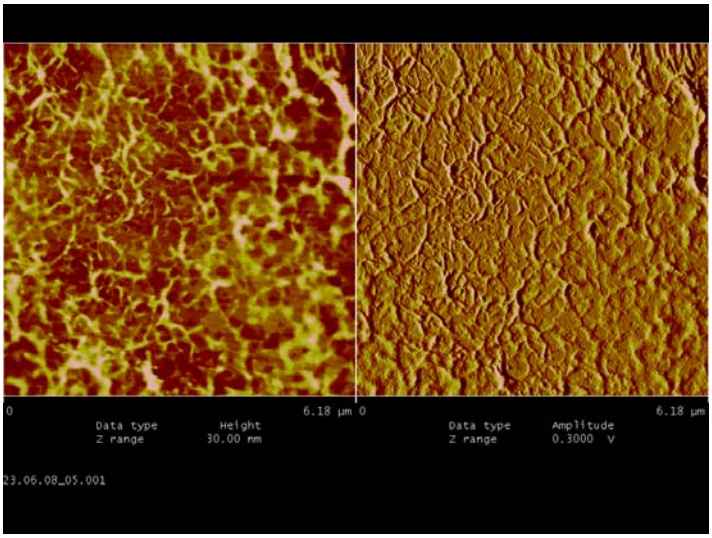

Figure 5.8: AFM picture of the sample after PDDA treatment (scale: 6,13µm). Deposition method: Spraying 1mL. CNT material: HiPco nº1

Morphology of the network after Silane treatment of the substrate:

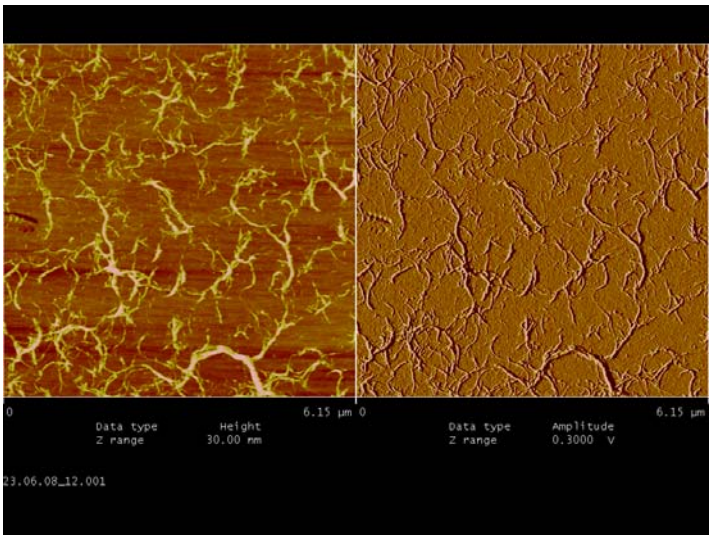

Figure 5.9: AFM picture of the sample after Silane treatment (scale: 6,15µm). Deposition method: Spraying 1 mL CNT material: HiPco nº1.

Morphology of the network without treating the substrate:

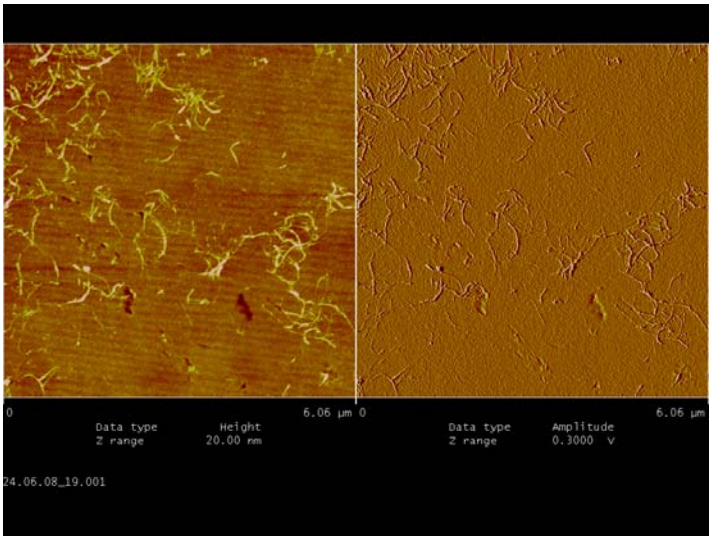

Figure 5.7: AFM picture of the non-treated sample (scale: 6,06µm).
Deposition method: Spraying 1 mL. CNT material: HiPco nº1.

5.2.5 Conclusion

After AFM observation of the samples, it was concluded that chemical modification of the solid substrates offer an excellent methodology for depositing carbon nanotubes on surface. For instance, since PDDA treatment in prone to keep on surface after CNT deposition, silane based modifications of the silicon oxide substrates appear to be ideal for helping the attachment of the CNT on solid substrates. In addition, the deposition procedure is enhanced since it takes less time to attach a large number of CNT over surface and, more importantly, the CNT networks are uniformly spread. PPDA treatment has a bigger influence on the morphology of the network while pictures show polymer traces after the CNT deposition which has a negative impact on the conductivity. In spite of accelerating the attachment of the CNT over the substrate compared with non-treated surface, PDDA treatment seems to be less convenient than silanisation. Since both chemicals, DAS silane and PDDA polymer, are transparent materials, the surface treatment do not have an influence in the transparency ratio of the samples.

5.3 Analysis of the different deposition techniques

Generally pre-requisites for obtaining CNT coatings with high optical qualities on glass or other transparent substrates are the cleanliness of the materials. It can be stated that the coating stage has to be carried out under clean-room conditions. Rather than do the cleaning step in clean room the substrates have been cleaned carefully following the process described in chapter 5.1.1 and the CNT dispersion has been centrifuged extensively trying to avoid any presence of dirtiness.

The UV-vis spectra were recorded in a double beam spectrometer (Perkin Elmer, Lambda 2) between 190 and 1100 nm. Conductivity measurements were carried out in four-probe configuration (Keithley 197 DMM) with pressed on contacts or by the use of chip carriers after evaporating 200 nm of gold+ chrome stripes over the network. These four gold+chrome surface stripes were later on bonded to the chip carrier using gold wires. A picture of the chip + chip carrier system can be found in **Figure 5.5**. AFM observation was carried out on a Nanoscope IIIa from Digital Instruments USA.

The special features and the performance of every coating method are summarized in the following sections.

5.3.1 Competing materials overview

Actually on the market, both ITO and polymers technology enjoy an excellent reputation in conductive transparent coating applications. As mentioned in the introduction, these materials are widely used in several industrial products ranging from electronics to materials science. With the aim of comparing the CNT networks performance one might identify the characteristics of these competing materials. Detailed below, a brief introduction of both materials can be found.

Indium Tin Oxide (ITO)

Indium oxide doped with tin oxide (ITO) is a transparent conducting material frequently used in thin coating form. ITO is commonly used in applications such as touch panels, plasma displays or solar cells. As showed in **Figure 5.1**, this material exhibits a high degree of transparency while preserving a suitable conductivity value [30]. For these outstanding optical and electronic properties, factors such as the deposition parameters and the starting material play an important role. For instance, the film must contain a high density of charge carriers to conduct, however, the higher the density of charge carriers, the lower the transparency becomes.

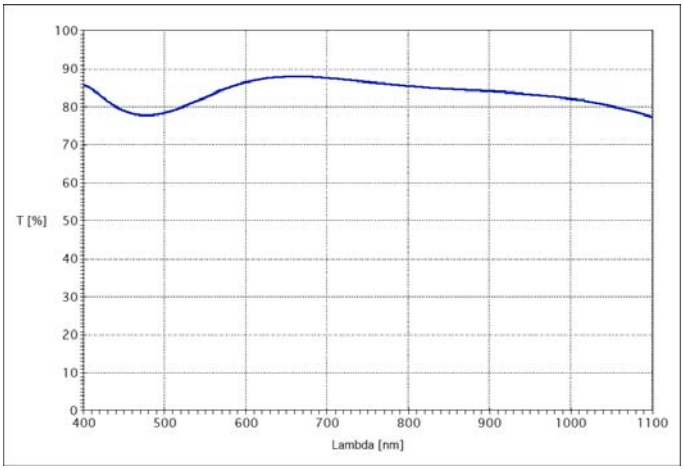

Figure 5.1: ITO transparency performance for a resistivity value of 8,5Ω/□ (transparency at 550nm: 82,76%)

As a coating, ITO is deposited on substrate by different methods such as electron beam evaporation or a range of sputtering techniques. A representation of the sputter deposition is illustrated in **Figure 5.2**. All the process is taking place in a vacuum chamber filled with argon gas. When sputtering in a vacuum chamber (recipient with a pressure of about 1-10 Pa), an electric field between the substrate to be coated (anode) and the cathode is applied. In this field electrons are accelerated and collide with the argon atoms floating around the chamber, this argon atoms are then ionised and move diffusively, reaching the substrate and condensing after undergoing a random walk.

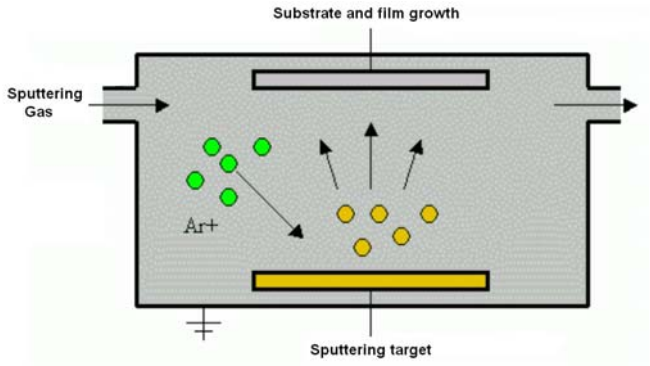

Figure 5.2: Schematics of the sputtering procedure.

In spite of its excellent performance (**Figure 5.2**), this technology has also some serious drawbacks: ITO coatings are not flexible, Indium element is pricey and the coating process is very expensive and only allows certain geometries. For instance, three dimensional surfaces are really difficult to coat uniformly.

PEDOT Polymer

Commonly used as conductive coating, this conducting polymer is already employed in several applications. Usually, most of the polymers are electrically insulating, however, some of them are electrically conductive due to its π-conjugated binding system. This binding system can be achieved by a system of double bonds, triple ties and aromatic rings. Others examples of such polymers, in addition to PEDOT (**Figure 5.3**) are Polyacetylen, Polyaniline and Polypyrrol.

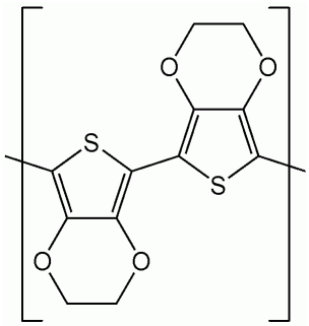

Figure 5.3: Molecular structure of PEDOT (Poly (3,4-ethylenedioxythiophene))

To deposit the polymer over the substrate different methods can be used such as spray coating, spin-coating or dip-coating. In chapter 6 there is a comparative performance study

of PEDOT polymers and Carbon nanotube based coatings in FM antenna applications. As with others technologies, polymers coatings also have some important drawbacks. With time or UV solar radiation the performance deteriorates significantly, the polymer chain of conjugated double bonds split and the conductivity drops.

Comparison

Detailed below one can find a comparison table with the main differences between these technologies.

	ITO coating	PEDOT coating	CNT coating
Conductivity	Excellent	Good	Good
Flexibility	No	Yes	Yes
Environmental stability	Yes	No	Yes

Table 5.1: Main properties of the different materials

ITO coatings obtain the best results in relation to electrical conductivity. On the other hand, despite having less electrical conductivity than its competitors, CNT based technology allows the coating of flexible substrates and has a great stability against environmental influences. This point is extremely important as long as transparent coatings is being implemented in industrial applications. For this, conductivity performance has to be ensured over a long period of time.

5.3.2 Adsorption deposition

Adsorption deposition is comparable with dip-coating deposition. In both methods, carbon nanotubes are adhered on a surface through the drying of the dispersion. During adsorption coating, one drop of dispersion is deposited on the surface and afterwards blown away by argon flow. One schematic view of the procedure can be found in **Figure 5.3**. The air flow direction is kept constant for every drop. The direction in which the gas is flowing gives the orientation of the carbon nanotubes. Silicon oxide chips (4.5 by 4.5 millimetres) have been used as substrate to measure conductivity performance and quartz glass substrates (with same dimensions) to measure the transparency.

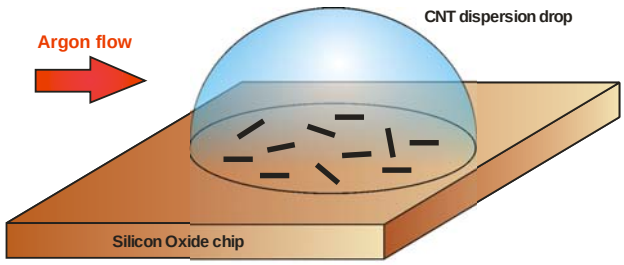

Figure 5.3: Adsorption deposition procedure on Silicon oxide chips.

Results and discussions

AFM pictures, as shown in **Figure 5.4**, illustrate the morphology of the CNT network after adsorption coating. After repeating the process for 40 drops in the deposition stage, the CNT concentration on surface is enough to reach the percolation threshold and allowed the electrons to flow along the surface.

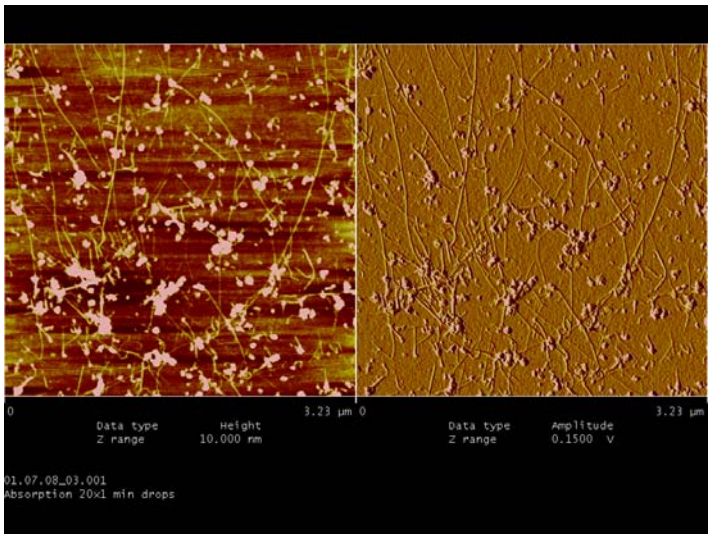

Figure 5.4: AFM image of a CNT network after adsorption deposition (40 drops, slow dry).

As showed in **Figure 5.4** the network seems to have certain anisotropy. The CNT are not randomly dispersed over the surface and appear to be oriented in the direction of the argon flow. To prove this visual remark, polarized Raman turned out to be a very helpful tool. As explained in chapter 3, one can characterise the orientation of the CNT network by analyzing the G-band intensities. Raman data is presented in **Figure 5.5**. In this plot, the received intensity was higher when the polarisation of the Raman laser was parallel to the Argon flow during the deposition stage. This confirms that the Argon flow leads the tubes to be oriented in the same direction.

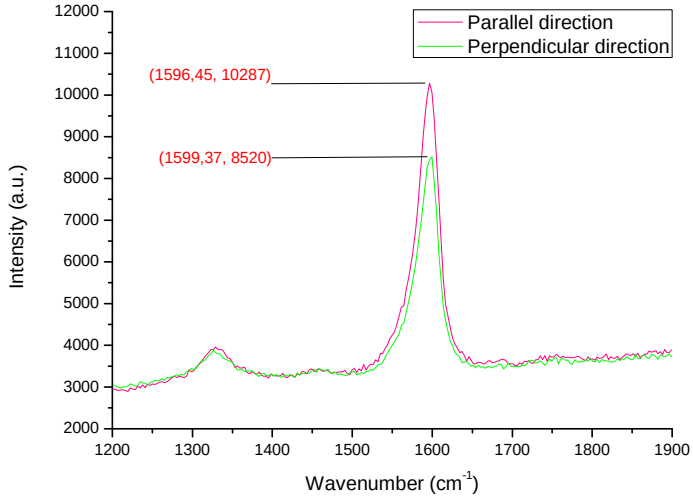

Figure 5.4: Polarised Raman spectra of both directions.

Due to the high aspect ratio of the carbon nanotubes, one may consider about the benefits of orienting the nanotubes for electrical conductivity. In order to check the difference in conductivity depending on the direction of the measurement, four gold stripes were evaporated over two identical samples (same distribution of the CNT), one sample has the stripes oriented perpendicularly to the Argon flowing direction and the other one in a parallel form. A picture of a sample with the four gold stripes evaporated on it can be found in **Figure 5.5** and **Figure 5.5 b**. Note in **Figure 5.5** that the chip sample was already embedded in a chip carrier ready to perform the conductivity measurements.

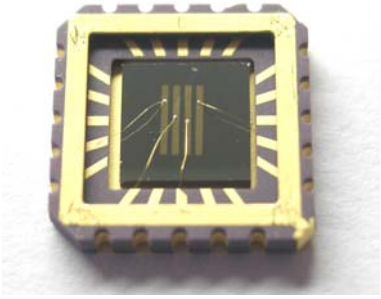

Figure 5.5: Sample configuration for temperature dependence and four-probe conductivity measurements.

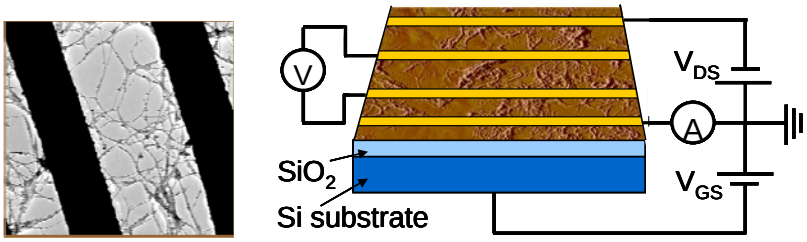

Figure 5.5 b: Image of the stripes lying over the CNT network and schematics of the 4-probe configuration.

Conductivity results are displayed in **Figure 5.6**. As expected, measurements proved that conductivity increased in the direction of the oriented CNT. One should take into account that "perpendicular orientation" means the stripes are standing perpendicularly to the direction of the CNTs. To check the influence of this orientation in the transparency, both samples were also evaluated by the use of the UV-vis spectrum analyzer. In **Figure 5.7** one can find the transparency performance of both samples. There is only one plot displayed in the graph since the spectrophotometer does not pick up any difference between oriented networks. Despite showing a big difference in conductivity the transparency values remain unchanged. We can conclude that adsorption deposition helps in orienting the CNT, which yield a better conductivity vs. transparency ratio of the resulting CNT network.

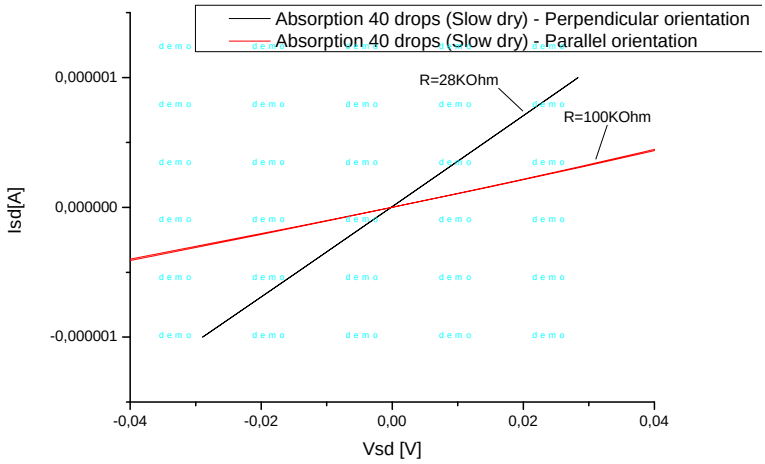

Figure 5.6: conductivity measurements of the adsorption sample (Parallel and Perpendicular directions)

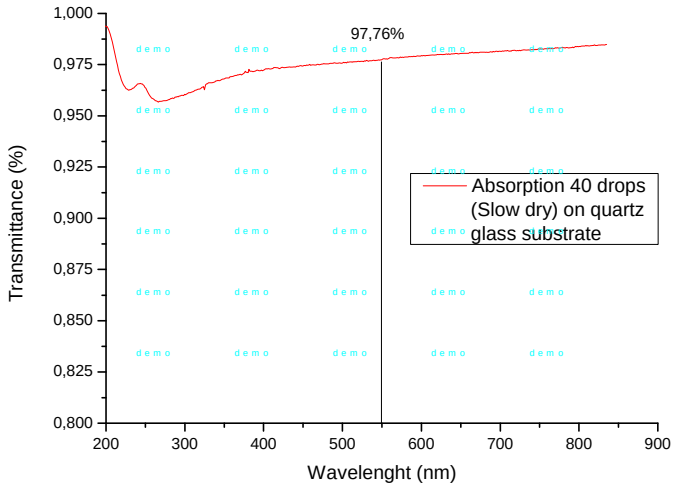

Figure 5.7: Transmittance measurements for adsorption samples

5.3.3 Spray deposition

The spray coating-technique is the simplest and quickest method for depositing CNT over surface. By the use of a commercial air brush pistol (from Harder & Steenbeck, Germany) one can easily tune the transparency of the samples from 0% to 100%. After preparation of the CNT dispersion, the suspension is then directly sprayed onto the substrates while keeping the substrate in a heating plate. The temperature must be around 100 ºC (depending on the substrate) to accelerate the drying of the small droplets on surface. This heating procedure became extremely helpful when spraying over big surfaces. One has to avoid bigger droplets formation to spread the carbon nanotubes as uniformly as possible. The big droplets decrease the conductivity vs. transparency ratio of the samples. After the deposition step, the samples were immersed into de-ionised water to remove SDS traces and dried with argon gas.
In **figure 5.8** one can see the running operation of this technique.

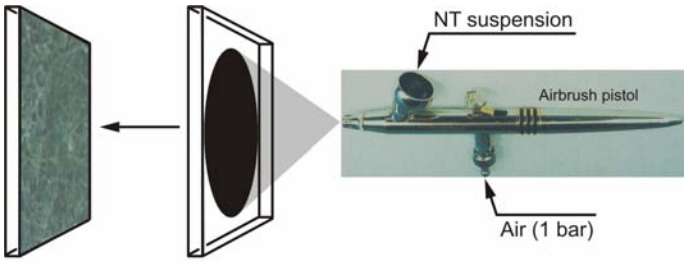

Figure 5.8: Spray deposition procedure.

Results and discussion

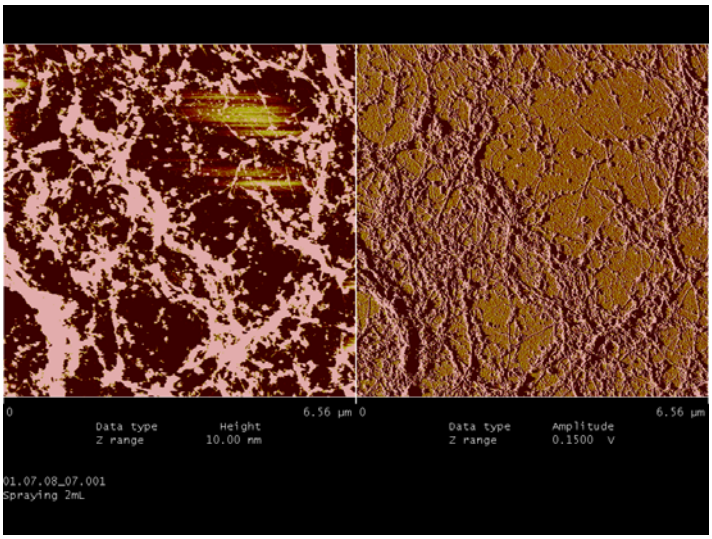

Figure 5.9: Morphology of the CNT network after spray coating deposition.

Typical images of sprayed CNT networks are shown in **Figure 5.9**. The coating is dense enough to ensure that the conductivity and the difference in density between samples is only a result of the number of sprayed layers. The resulting network is macroscopically

homogeneous, with this coating technique the CNT seems to be randomly dispersed and randomly oriented. Raman spectra, **Figure 5.10**, confirm this statement.

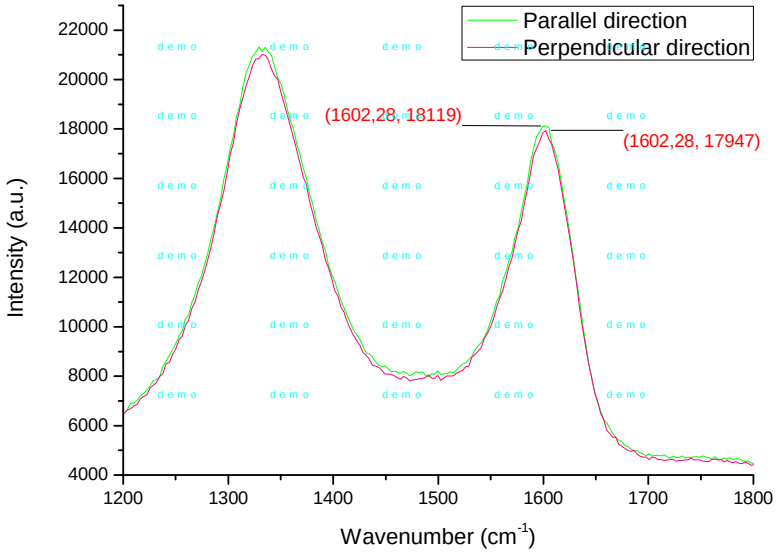

Figure 5.10: Raman spectra results for sprayed samples in both directions. Note that CNT used during the air brush attempt were from L.A. technique. These CNT were plenty of defects and impurities compared with ones from Thomas Swang.

Although the dispersion was extensively centrifuge, the network does not look as pure as for the others techniques, especially as dip-coating and adsorption techniques. In addition to the impurities coming from the CNT synthesis, like amorphous carbon or metallic catalyst, most of the contaminations came from the air brush. These contaminations cannot be avoided nevertheless they are small and have a very small aspect ratio compared to CNTs. Although they can lower significantly the transmittance they do not produce any consequences in the conductivity. Conductivity and transparency measurements of the sprayed samples are summarised in **Table 5.11**. Besides, in **Figure 5.12** one can observe the transparency behaviour depending on the wavelength from 200 to 900 nm.

Resistance (Ω/□)	**Transmittance (%) at λ=550nm**
40 620	95,61
5 470	91,76
1 730	81,26
1 060	73,86
850	67,31
600	55,53

Figure 5.11: Resistance vs. transparency values for spray coating deposition

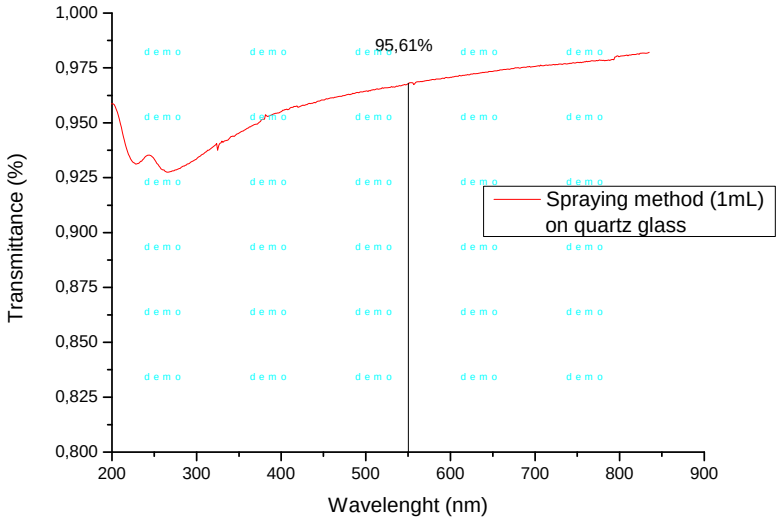

Figure 5.12: Transparency measurements of sprayed samples.

5.3.4 Electric field deposition

Electric field deposition is an easier and quicker way of coating transparent substrates with carbon nanotubes. Using two electrodes dipped into a CNT dispersion this deposition technique runs automatically when applying a voltage between them. The cathode can be all sorts of metal (Copper in our case) but the anode electrode should be a layer of aluminium deposited over a transparent substrate (quartz glass). **Figure 5.13** shows a square piece of quartz glass coated with a thin layer of aluminium (200 nm).

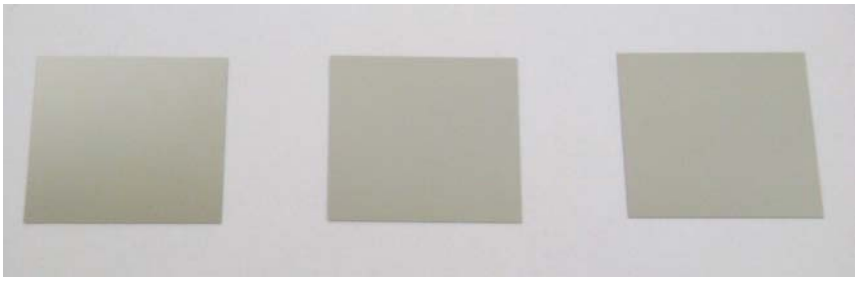

Figure 5.13: Aluminium coated quartz glass for electrode purposes.

In **Figure 5.14** one can find the schematic view of the devices used in the process: the power supply, the electrodes and the CNT+SDS dispersion. Despite the fact of being metallic or semi-conductive, carbon nanotube molecules are electrically neutral. Subsequently, through exposure to an electric field the CNT can be oriented as a dipole, but not moved towards the electrodes since the DC field between electrodes remains uniform.

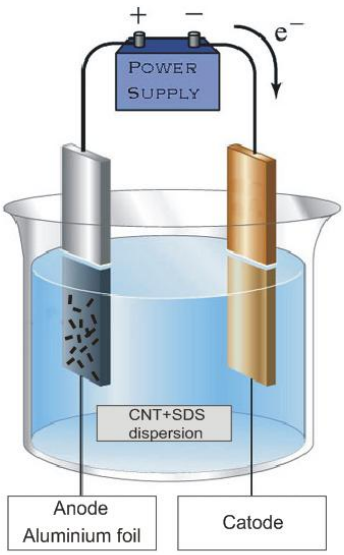

Figure 5.14: Schematics of the electric field deposition.

SDS plays an important role during the process as it assists in the motion of the CNT. Although the SDS molecule is also an electrically neutral molecule, once dissolved into water (de-ionised water) the Sodium cations Na+ are delocalised and the SDS molecule acquires a negative charge. This negatively charged cap end becomes the hydrophilic part of the molecule which interacts with the oxygen elements of the H2O molecule. The long CH3 chain (Hydrophobic part) remains electrically neutral and by Van der Waals interactions tends to bundle with CNT and others SDS molecules. This behaviour is known as micelle formation and it is shown in **Figure 5.15**.

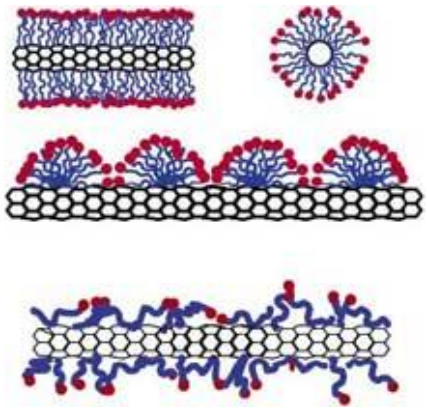

Figure 5.15: Schematic representation of the mechanisms by which SDS surfactant helps dispersing and moving the carbon nanotubes towards the anode electrode. From top to bottom: cylindrical micelle formation, hemi-micellar micelle formation and random adsorption of the SDS molecule
(Reprinted from [33])

The micelle formations (SDS + CNT) are negatively charged and are therefore attracted to the anode electrode. The deposition mechanism takes place until the aluminium on the substrate is completely oxidised and converted into aluminium oxide Al2O3 (alumina). Aluminium oxide is transparent but not conductive anymore. This feature makes the

process stop automatically when there is no more aluminium on surface. By choosing the thickness of the aluminium layer one can tune the concentration of CNT on surface. As result, a transparent and conductive layer based on CNT is deposited over the glass substrate. **Figure 5.16** shows the end result.

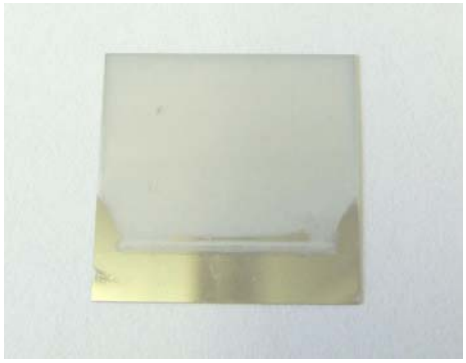

Figure 5.16: Transparent conductive coating based on CNT by electric field deposition

Results and discussions

AFM pictures, as shown in **Figure 5.17**, illustrate the morphology of the CNT network after applying the CNT coating by electric field deposition. With an initial layer of 200 nm of aluminium, the CNT concentration after depositon was enough to reach the percolation threshold and obtain a conductive layer.

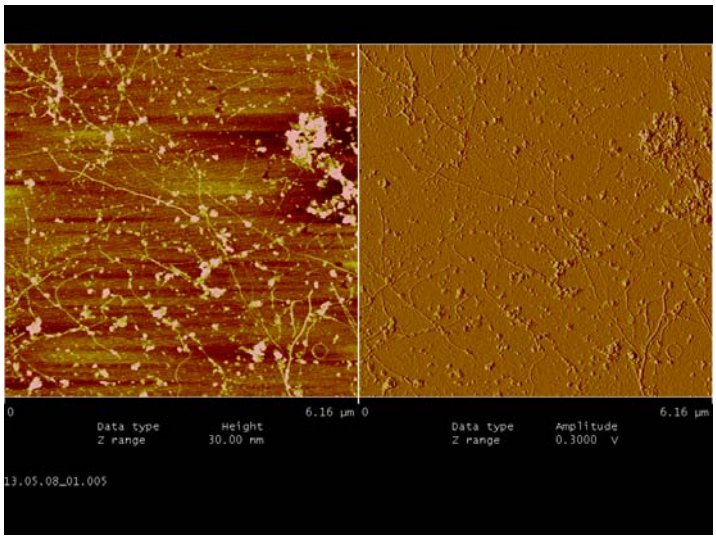

Figure 5.17: Morphology of the CNT network after Electric field deposition.

The resulting network appeared to be homogeneous and randomly oriented and the bundle formation was minor in contrast to the spraying deposition. Some dirtiness coming from the dispersion could be found on the surface as well as the resulting layer of aluminium oxide. Although necessary during the process, the aluminium oxide layer decreases the transparency of the samples. The high porosity of the aluminium oxide film tends to

scatter the light going through. Transparency measurements can be found in **Figure 5.18** and the conductivity vs. transparency characteristics can be found in **Figure 5.19**.

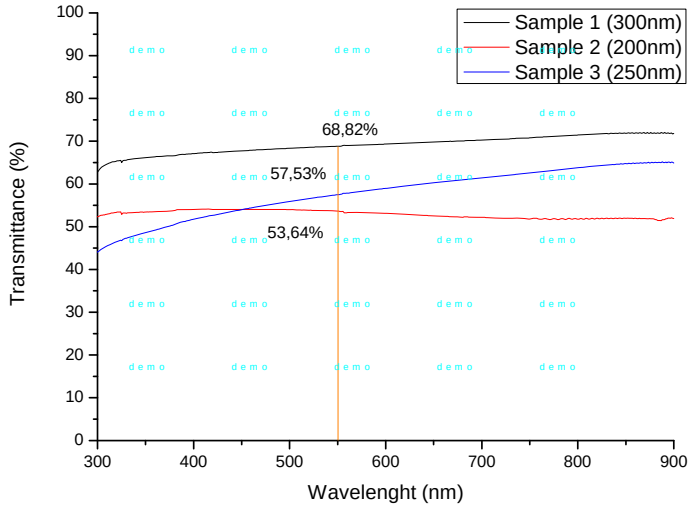

Figure 5.18: Transmittance measurements for electric field deposition with 3 different thicknesses of the aluminium layer.

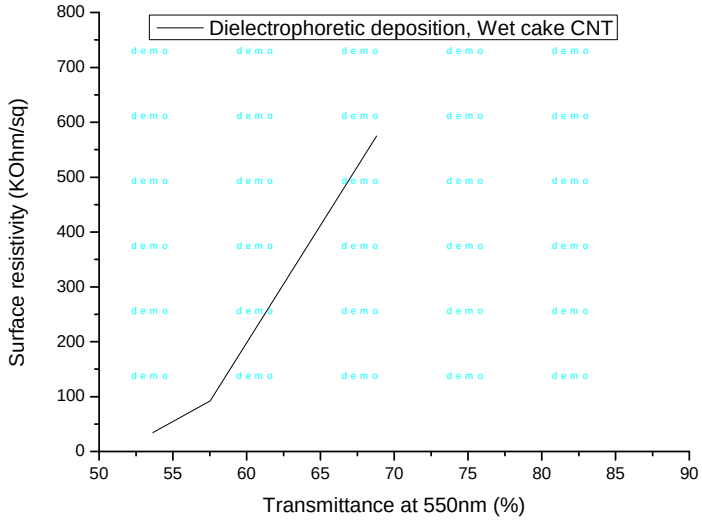

Figure 5.19: conductivity vs. transparency measurements for electric field deposition.

5.3.5 Dip-coating deposition

Dip-coating technique can be defined as a method where the substrate to be coated is immersed in a dispersion and then pulled out with a well-defined extraction speed. The coating thickness is mainly defined by the extraction speed, the solid content and the viscosity of the liquid. This coating thickness can be calculated by the Landau-Levich equation [32]:

$$h = 0{,}94 \cdot \frac{(\eta \cdot v)^{2/3}}{\gamma^{1/6} \cdot (\rho \cdot g)^{1/2}}$$

Where: h: coating thickness
η: viscosity
v: speed
γ: surface tension
ρ: liquid density
g: gravity

Usually, by choosing an appropriate viscosity, the coating thickness can be varied, but for CNT deposition we did not take these parameters into account. The substrates were coated several times in order to tune the concentration of CNT over the surface. The more times the substrate was dipped into the dispersion the more CNT were adhered on the surface. The schematic view of a dip coating process is shown in **figure 5.20**.

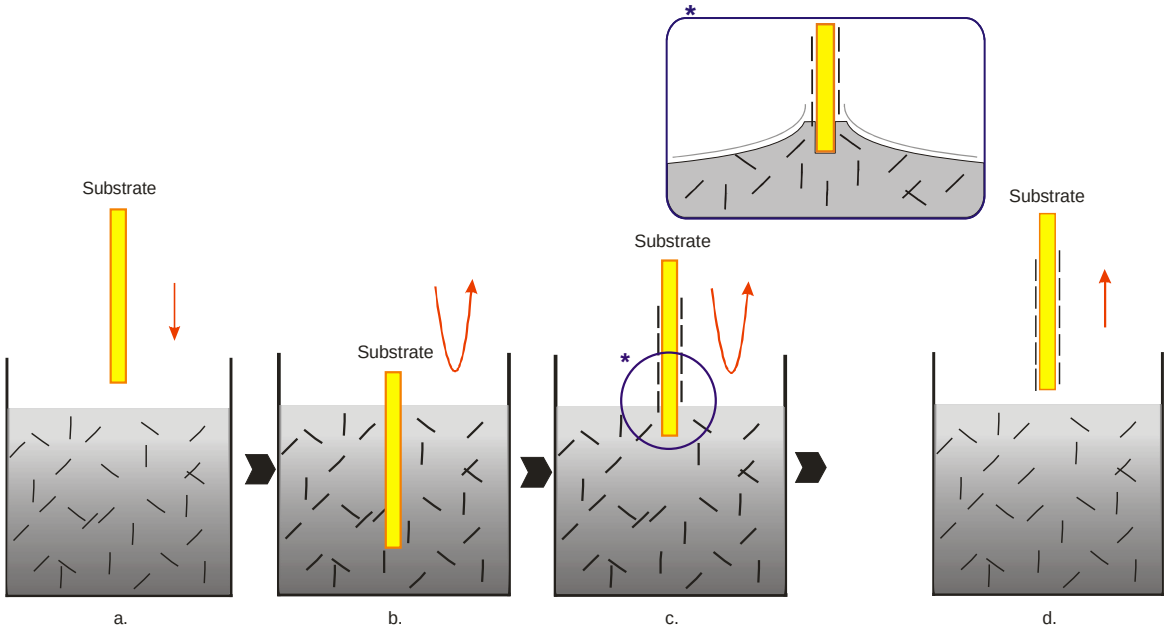

Figure 5.20: Main stages of the dip coating process: dipping of the substrate into the coating solution: b.) Dipping of the sample c.) Extraction of the sample and formation of the wet CNT layer d.) Drying of the CNT layer

Results and discussions

An AFM picture of the resulting network is presented in **Figure 5.21**. Later on, conductivity measurements confirmed the presence of a conductive CNT network over the substrate (**Figure 5.24**), which proved that CNT concentration was above the percolation threshold. Carbon nanotubes appeared uniformly spread on the surface but the orientation of the CNT seemed to favour the dipping direction. Raman spectra proved this assertion and also confirmed dip-coating as the best technique when seeking oriented networks. One

can find Raman data in **Figure 5.23**, where a higher difference between both directions comparing to the other deposition techniques is observable.

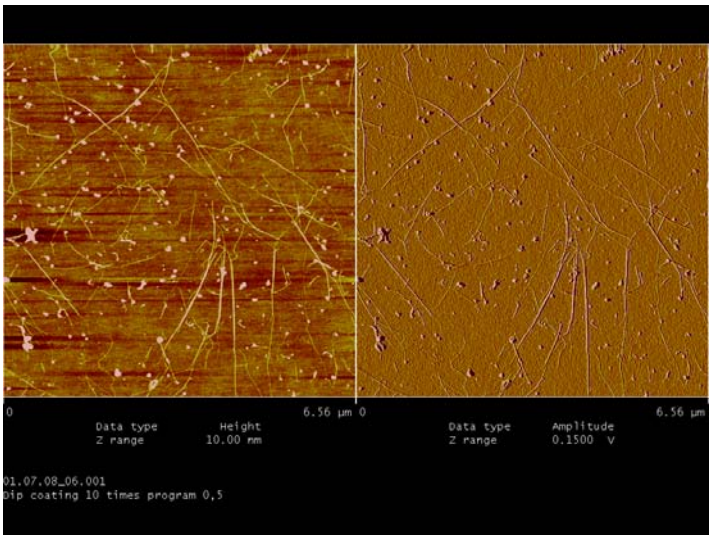

Figure 5.21: CNT network on Silicon oxide substrate after dip-coating procedure.

The dip-coated networks were free of impurities and the CNT bundle formation on the surface was not as critical as in the other deposition methods. At least, the CNT bundles on surface kept the high aspect ratio of the carbon nanotubes. From the morphology of the net one can expect good results in conductivity and transparency performance. Conductivity measurements are presented in **Figure 5.24** and transparency values in **Figure 5.25**. By modifying the pressure, humidity and speed one can improve the orientation of the CNT, but more importantly, the fundamental parameters were to dip the sample slowly and wait until the sample dries before the next dipping. By following these rules, one can reach great orientations as proved in **Figure 5.22**.

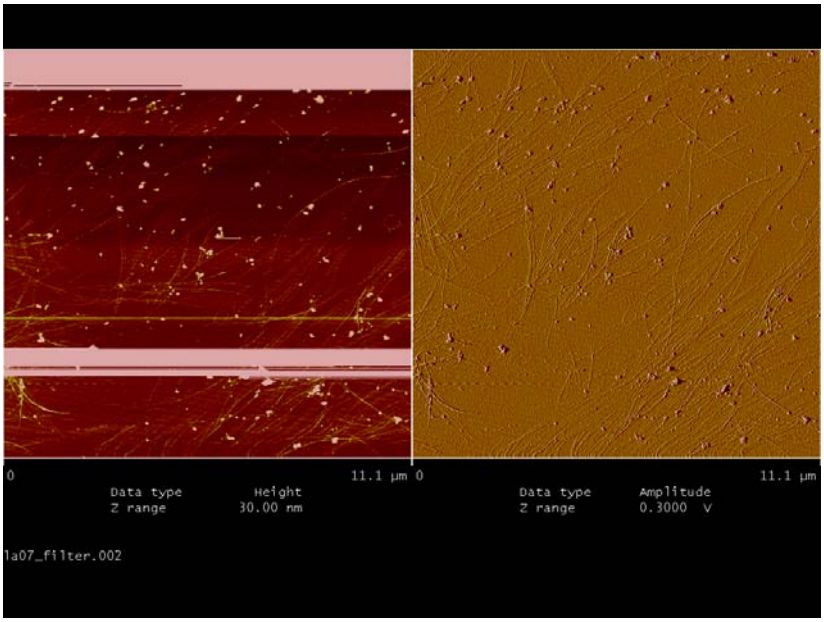

Figure 5.22: Image of a well oriented CNT network by dip-coating process.

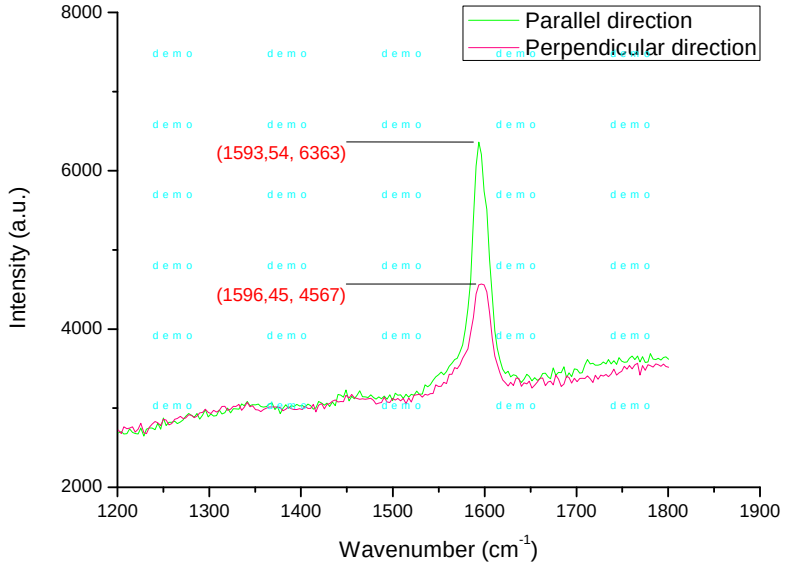

Figure 5.23: Polarised Raman spectra in both directions. Dip coating proved to be a suitable technique when looking for oriented CNT networks.

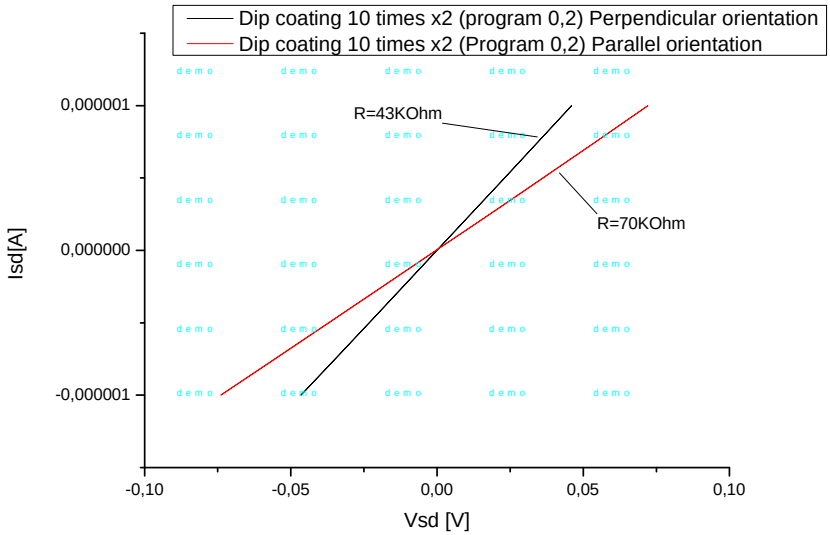

Figure 5.24: Conductivity performance in both directions. The orientation of the nanotubes clearly improves the conductivity of the samples.

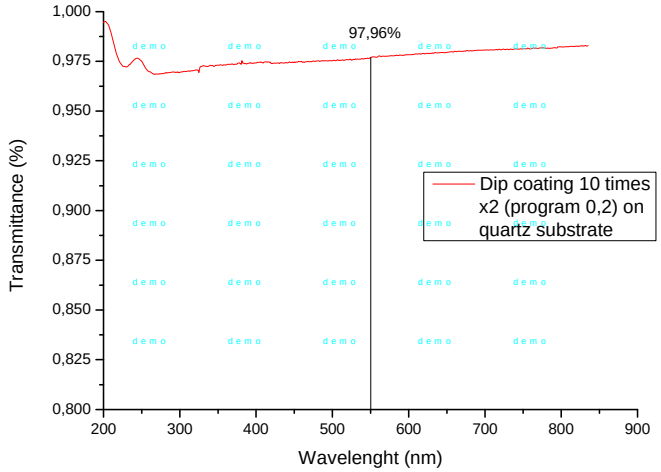

Figure 5.25: Transparency measurements of the dip coated samples. The values turned out to be extremely high when looking at the conductivity performance.

Study of the electronic transport properties of the dip-coated CNT network:

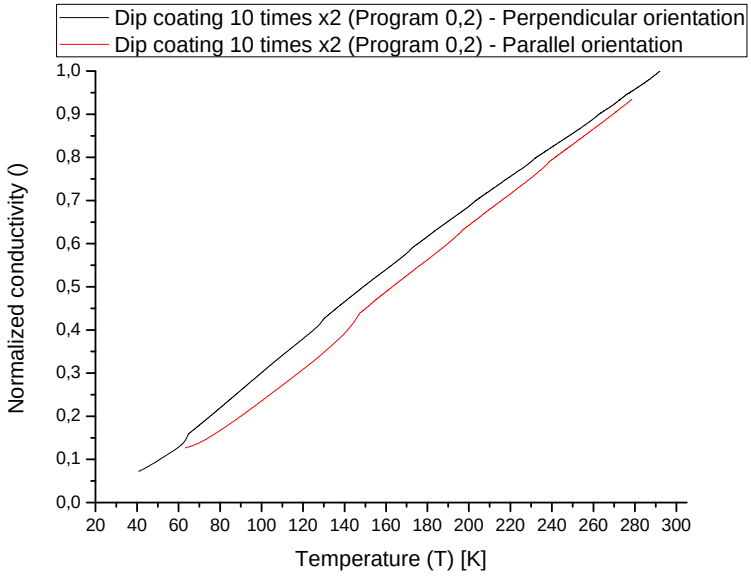

Figure 5.26: Temperature dependence of the electrical conductance of SWNT thin netwoks normalized to their room temperature (ln σ(T)/ σ(279K)).

As shown by in **Figure 5.26.1 Figure 5.26.2** and **Figure 5.26.3**, this thin networks show a behaviour closer to that for variable-range hopping (VRH) [37]:

$$\sigma(T) = \sigma_0 \exp\left[-\left(\frac{T_0}{T}\right)^{1/(1+d)}\right]$$

Where σ_0 and T_0 are constants and d is the dimensionality of the hopping conduction ($d = 1$ for our net). The CNT network were thin enough to make difficult a good metallic percolation paths through the sample [38]. The network appeared to behave as a semi-conducting 2-D network. One can see that the 2-D model suits better our conductivity measurements in the figures below.

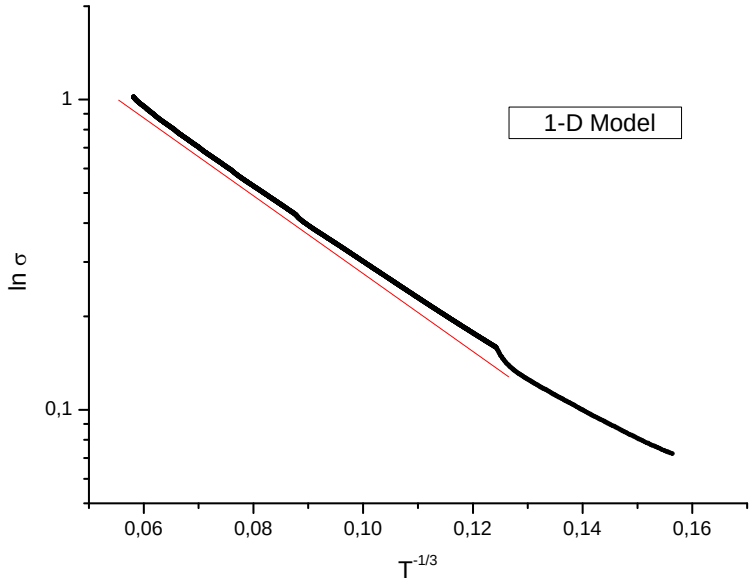

Figure 5.26.1: Adjustement for 1-Dimension network.

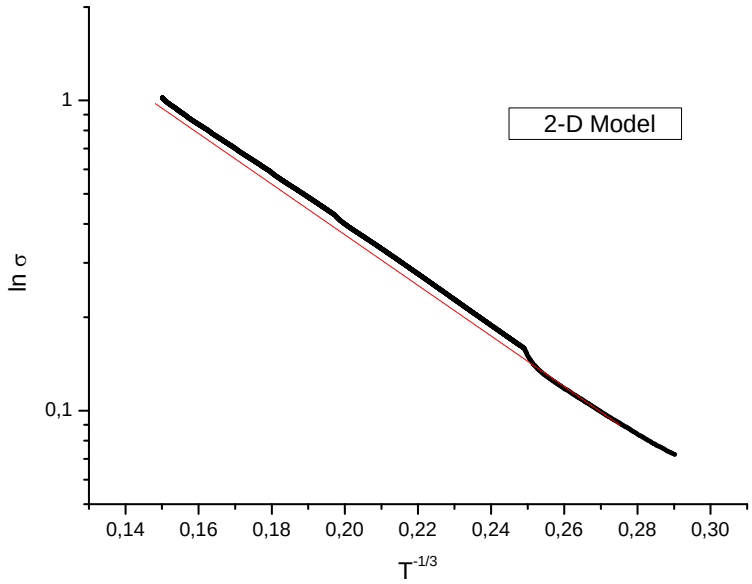

Figure 5.26.2: Adjustement for 2-Dimension network.

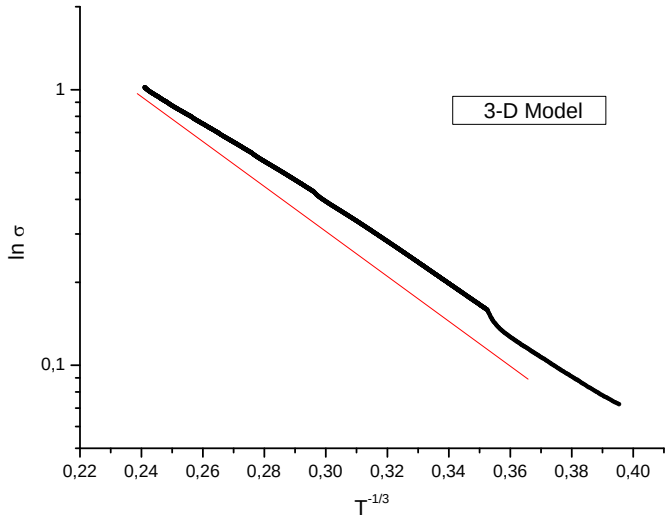

Figure 5.26.3: Adjustement for 3-Dimension network.

5.4 Conclusions

As proved during this section, the dip-coating treatment was the more efficient method for fabricating SWNT film of high electrical conductivity without a drastic drop in the optical transmittance. A comparative graph showing a general evaluation can be seen in **Figure 5.27**. As expected, adsorption deposition is close behind in performance as it is extremely similar to the dip-coating procedure. Indeed, adsorption deposition does not offer any advantage over dip-coating since even the orientation of the tubes over the substrate appears to be less oriented. Another important drawback is that this technique is an extremely high time-consuming procedure due to its drop-by-drop demeanour. These make adsorption deposition ineffective.

When compared with spray-coating, dip-coating shows better results as well. Considering the morphology of the network from the AFM pictures, this gain should be primarily due to more loose contacts in inter-tube and inter-bundle junctions of the spray-coated networks compared with the dipped ones. Base on this, the orientation of the tubes plays an important role as it avoids crossing-contacts between tubes. The orientation, as has been proven throughout this section, improves the conductivity without decreasing the transparency of the sample.

Although the electrical conductivity of the coats can be enhanced by increasing the number of dipping times, the dip-coating treatment with a large number of dipping times reduced the transmittance without corresponding improvements in electrical conductivity, indicating the patch-wise coating of the carbon nanotubes.

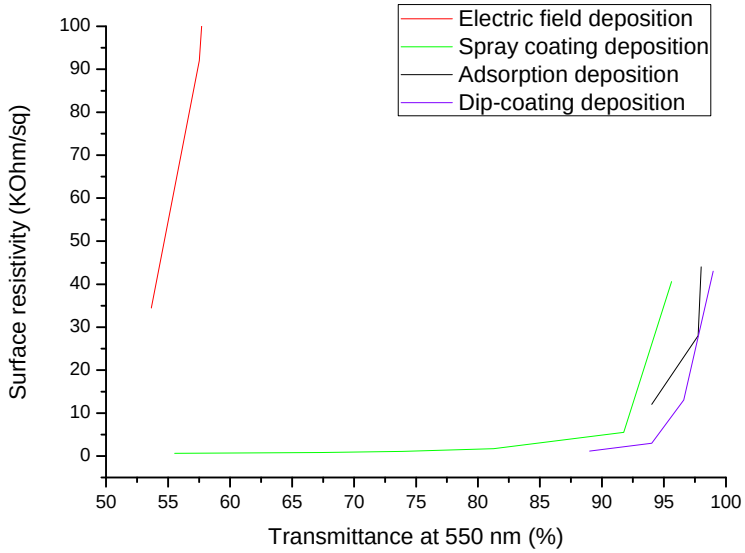

Figure 5.27: Comparison between all the deposition methods

In conclusion, spray coating can be considered the quickest and easiest route towards obtaining a reasonable transparent and conductive coating, while dip-coating is more suitable for applications requiring higher transparency vs. conductivity ratios, even when the contribution of the orientation of the nanotubes may be required.

Due to the values which have been achieved during this study it could be assumed that it would be possible to replace ITO technology in a few applications. Nevertheless, the performance of ITO is still far behind, which shows that further studies should be done in CNT technology.

Chapter 6

Some applications: printed antennas and electromagnetic shielding

6.1 FM antenna implementation

As it was previously mentioned, the outstanding properties of carbon nantotubes makes these molecules especially attractive for a number of technical applications. Transparent antennas based on CNT could be used in the automotive industry to replace the actual roof antennas. Antennas made out of these conductive transparent films could be directly deposited onto the windscreen or the lateral windows of the car, thus making them extremely easy to manufacture. Below, one can find the simulations of the antenna pattern design, the deposition processes and the performance measurements used during the study.

6.1.1 Antenna pattern design and simulation

The FM antenna should work in the frequency band ranging from 87 to 108 MHz, so it must have a flat frequency response within this range. To simulate and tune the antenna's dimensions properly, an E.M. field simulator software, such as Sonnet Professional Planar software from Sonnet Software, was used. This software models planar circuits within a metallic box, and can easily be used to examine the effect of substrate materials and different pattern designs. **Figure 6.1** shows the initial pattern design of the FM antenna.

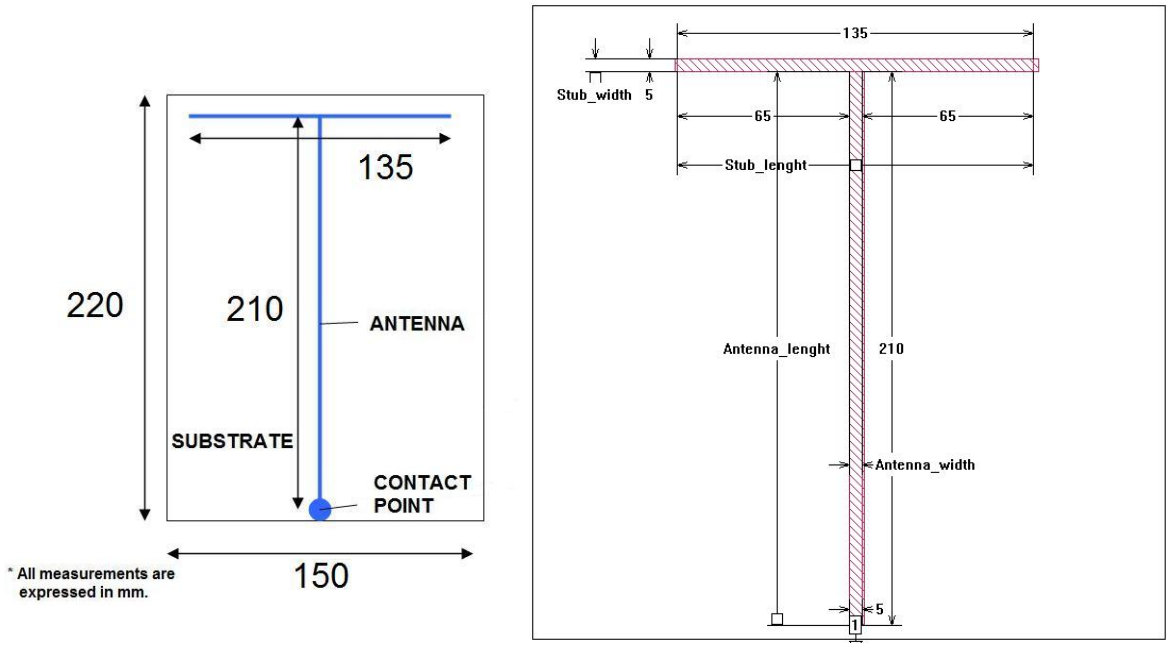

Figure 6.1: Initial pattern design of the FM antenna (a. schematics and b. Sonnet software drawing).

During this first approach, the antenna was regarded as a monopole with the contact point situated at the bottom (see **Figure 6.1**). Subsequently, the length of the antenna can be specified by the following dimensions:

$$L = \lambda / 4$$

After considering the frequency band (87-108MHz) the length of the antenna should be within 69,4 cm and 86 cm, soo too long to be located in the windscreen of the cars. To decrease this length, it was decided to place a 135 mm stub at the end of the antenna. Like one inductor placed near the contact point (at the beginning of the monopole), a capacitor situated at the back end of the antenna has the same electric effect, that is, to reduce the dimension of the antenna. This stub was nothing else that the implementation of the capacitor.

During the simulation step, we analyzed the reflection coefficient of the antenna (S11 parameter). It was expected to achieve low values with a flat response within the FM frequency band. **Figure 6.2** shows the simulation results.

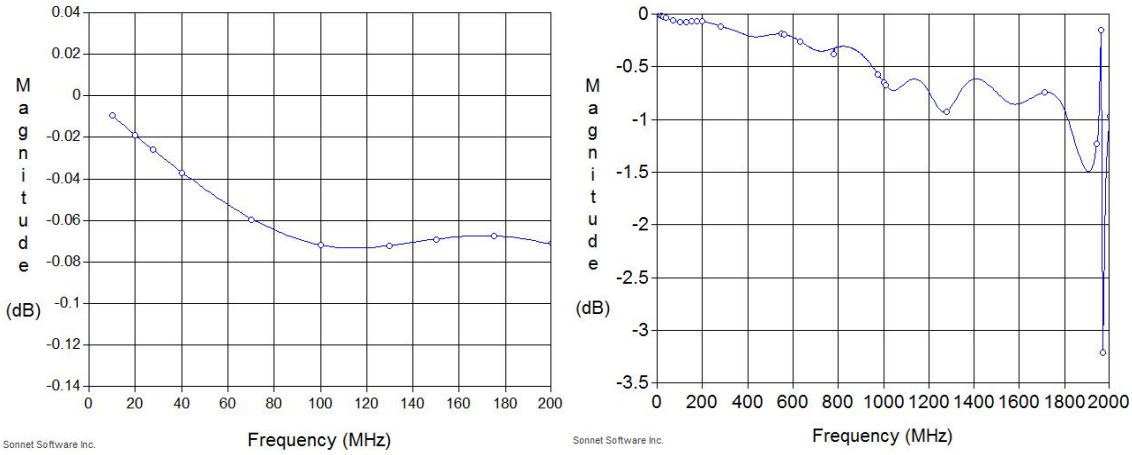

Figure 6.2: Reflection coefficient values (S11) for the initial pattern antenna design. The righ plot confirm that the antenna was radiating energy in higher frequencies. The dimensions were not tunned properly

As one can see, the results were disappointing, the reflection coefficient attain less than 0,06 dB of attenuation in the desired frequency range; the dimensions of the antenna were not well tuned for the specific frequency band. In spite of showing poor performance it was decided to follow this pattern design since the aim of the study was to prove the possibility of using CNT coating as a printed antenna. For this, CNT antennas will be compared with highly conductive silver paste antenna. Further antenna designs will be shown in section 6.2.3.

6.1.2 Coating methodology

All the samples were coated on normal glass substrates using spray coating, serigraphy and automatic film deposition procedures. These techniques have shown better

results than brush painting or other manual deposition methods. Drawdowns made by hand can show irregularities caused by variations in speed and pressure on the applicator tool, thereby the coating quality is compromised. **Figure 6.3** shows the automatic film deposition device from BYK-Gardner, which guarantees a stable downward force and linear speed of the film applicator, settable in 10 mm/s increments from 50 to 500 mm/s.

Figure 6.3: Automatic film applicator from BYK-Gardner company.

The Serigraphy method, also called screen printing, is illustrated in **Figure 6.4**. Throughout this technique the thickness of the coated film can not be controlled but the transparency of the film can be improved. Spray coating was already introduced in chapter 4, the running principle remains the same as for the small silicon oxide chips substrates. Through the use of these three different techniques repeatable and high quality results could be obtained.

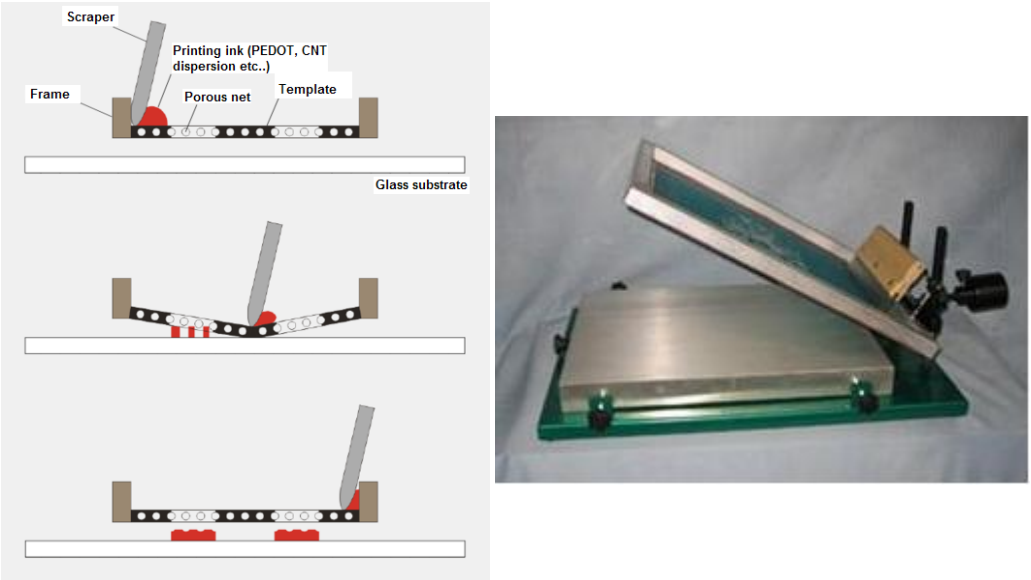

Figure 6.4: Schematics and picture of the coating process for the serigraphy deposition.

During this work diverse conductive materials were evaluated, PEDOT polymer (introduced in Chapter 5), single and multi-wall carbon nanotubes were faced together and compared with silver paste antenna. One should take into account that transparency was

not the most important parameter during this first attempt; our first challenge was to reach good antenna radiation performance level. An antenna sample, ready for the measurement stage is presented in **Figure 6.5**, shows how its transperancy can be checked by comparing it with the white background.

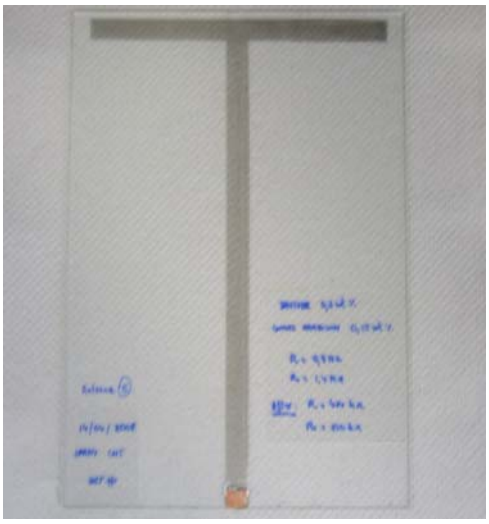

Figure 6.5: MWCNT (0,5 wt %) sprayed antenna example with a point to point resistance of ~400KΩ. Note that sample was not highly transparent ~70%.

Table 6.1 summarises all the combinations tried during the work. Not only different materials were tested but also different thickness of the layers. The deposition method applied has also been specified in the table. The point to point resistance is just measuring the resistance between the contact point and the top left edge of the antenna (R1) and between the contact point and the top righ edge (R2), this gives us information about the uniformity of the deposition.

ANTENNA NUMBER	MATERIAL	DEPOSITION METHOD	POINT TO POINT RESISTANCE	THICKNESS
1	Silver paste	Serigraphy	R1=14Ω R2=11Ω	< 1 mm
2	Silver paste	Serigraphy	R1=13,5Ω R2=16,3Ω	< 1 mm
3	Silver paste	Serigraphy	R1=13Ω R2=13Ω	< 1 mm
4	Silver paste	Manual brush painting	-	< 1 mm
5	0,3 wt % MW Baytubes + 0,15%wt Gummi Arabicum	Spraying	R1=405kΩ R2=515kΩ	< 1mm
6	0,3 wt % MW Baytubes	Serigraphy	-	< 1 mm
7	PEDOT polymer	Film applicator	-	0,1 mm
8	PEDOT polymer	Film applicator	-	0,14 mm
9	PEDOT polymer	Film applicator		0,5 mm
10	PEDOT polymer	Film applicator	-	1,3 mm
11	PEDOT polymer	Film applicator	-	0,14 mm
12	PEDOT polymer	Film applicator	R1=65kΩ R2=16Ω	1,5 mm
13	PEDOT polymer	Film applicator	-	1,2 mm

14	PEDOT polymer	Spraying	-	< 1 mm
15	0,25 wt% SW HiPco	Spraying	R1=2,5kΩ R2=3,3kΩ	< 1 mm

Table 6.1: List of the antennas used during the test.

6.1.3 Results and discussions

All the measurements were carried out using a network analyzer from Agilent Technologies (E5071C). This device was able to analyze frequencies from 9 KHz to 8,5 GHz. During the measurements all the antenna samples were repeatedly situated in the same position in order to have a similar surrounding environment. **Figure 6.6** shows the connections with the network analyzer and the position of the antenna. The antennas were placed over a metal plate acting as a ground plane, the antenna can be considered then as a dipole. During the measurements, and after trying with and without situating a metal ground plate under the antenna, we noticed that the performance was far better with it. This confirms that the dimensions of the antenna were not well designed.

Figure 6.6: Illustration of the test routine to measure the reflection coefficient (S11) of the antenna.

To contact the antenna, a short coaxial cable was used to reduce, as much as possible, the power losses in it. Only the most significant measurements are listed below (**Figure 6.7**), these plots are directly taken from the screen of the network analyzer. Appearing on the background of the screen there are the data plot of the silver paste antenna which can be used as a reference.

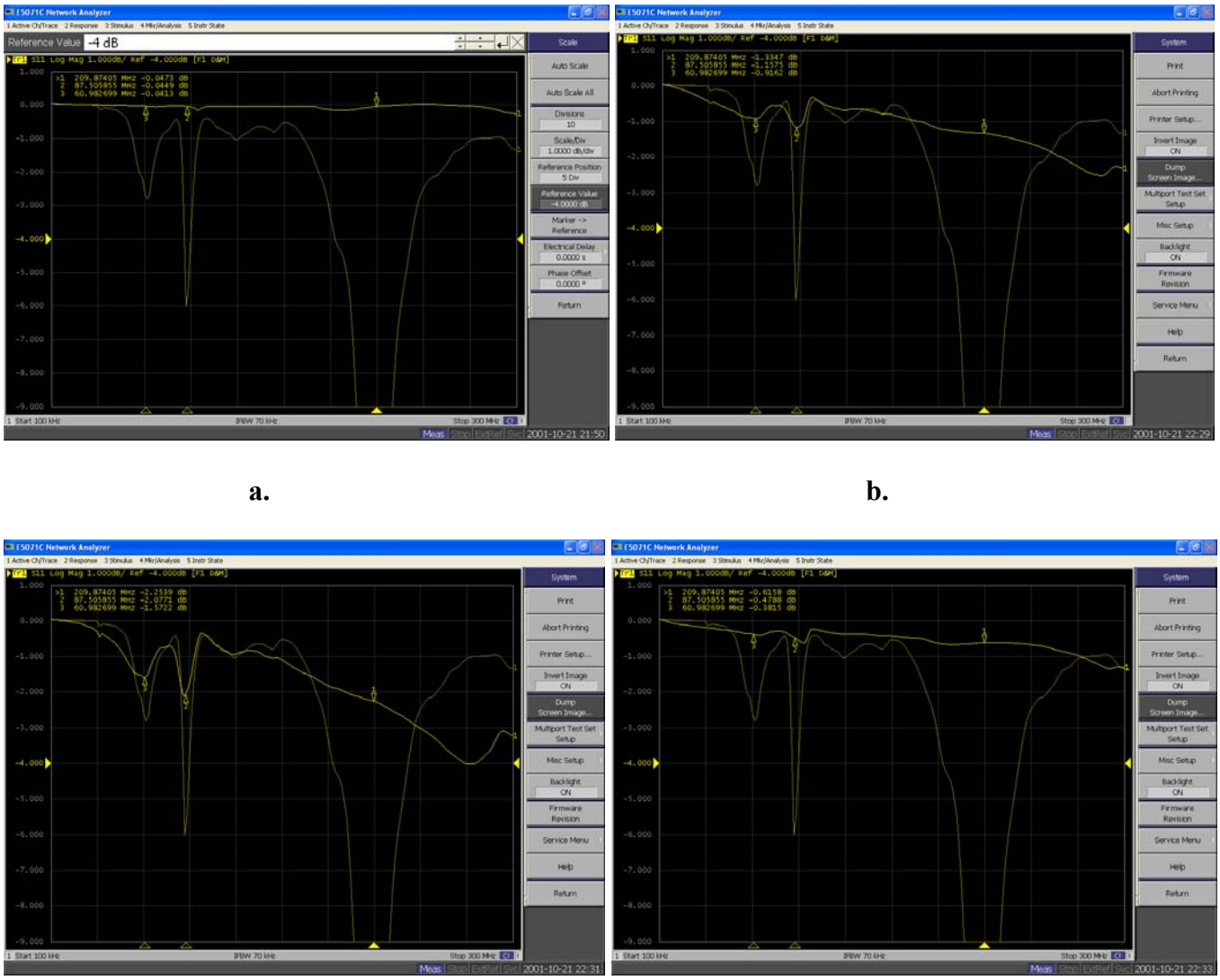

a. **b.**

c. **d.**

Figure 6.7: Comparative graphs for the reflection coefficient of every antenna. Note that the reflection coefficient of the silver paste antenna is plotted in every graph to be used as a reference
a. Antenna 5: MWNT Bay-tubes + Gummi Arabicum. Spray deposition
b. Antenna 12: PEDOT polymer. Film applicator
c. Antenna 14: PEDOT polymer . Spray deposition
d. Antenna 15: SWNT HiPco. Spray deposition

The antenna number 5, sprayed with a mixture of 0,3 wt % single wall CNT from Baytubes and 0,15 wt % of Gummi Arabicum, shows poor performance compared with the rest of the antennas. Antenna number 15, also sprayed with CNT but single wall from HiPco (CNT by High-Pressure CO Conversion method), prove to have an increased performance compared with the previous single wall antenna sample. Antenna number 12, with a 3,5 mm thick of material deposited with the Automatic Film applicator slightly improves the performance. The best values correspond to antenna number 14, which corresponds with the antenna sprayed with PEDOT polymer material. **Figure 6.8** present these results.

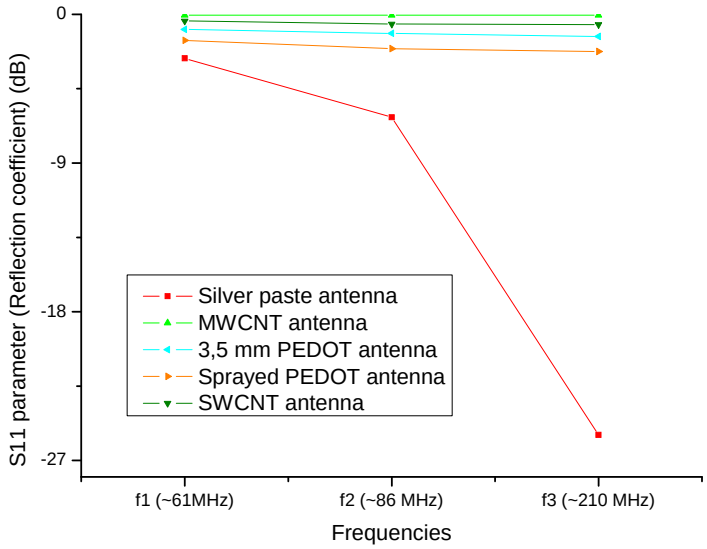

Figure 6.8: Final antenna comparison. Note that the antenna which performs better is the one with lower S11 value. The lower the S11 is, the more energy is radiating. Sprayed PEDOT antenna got better performance if we ignore the silver paste antenna (reference)

6.1.4 Further improvements

As discussed before and due to the fact that this printed antenna will not have the roof of the car acting as a metal ground (monopole antenna + metallic ground plane), it was decided to modify the shape of the antenna and convert it into a dipole structure. For this, the contact point should be shifted to the middle of the structure, ending up with a symmetrical geometry. The stub part will be kept as it was, just the dimension will be modified. All these stub structures should make the antenna smaller.
Apart from changing the antenna's dimensions, the antenna feed should be modified as well. Subsequently the antenna is fed from below with a coax probe attached to the middle of the antenna (Port 1). This is accomplished in Sonnet with an "ungrounded internal port", the connections between negative and positive poles to the antenna can be seen in **Figure 6.9**.

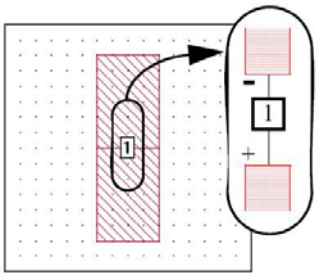

Figure 6.9: Illustration of the ungrounded internal port connection for the dipole antenna feed.

Furthemore, as soon as the antenna geometry is simulated inside a metallic box, one has to make sure the sidewalls are far enough from the radiating structure that the sidewalls have no affect. In addition, the top and bottom cover should be set to free space. After all these modifications and several simulation runs we came out with the pattern design presented in **Figure 6.10**.

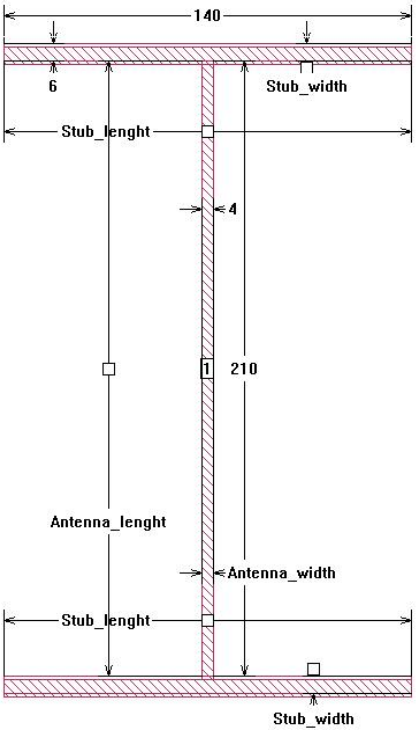

Figure 6.10: Sonnet representation of the dipole antenna.

The experimental results (simulations) are presented in **Figure 6.11**. Comparing with previous results (0,07 dB) the radiation performance has been improved by 4 dB aproximately. However, further improvements can be done by modifying the geometry and increasing the effective area of the antenna. This could yield lower S11 values and a flattened frequency response within the desired bandwith.

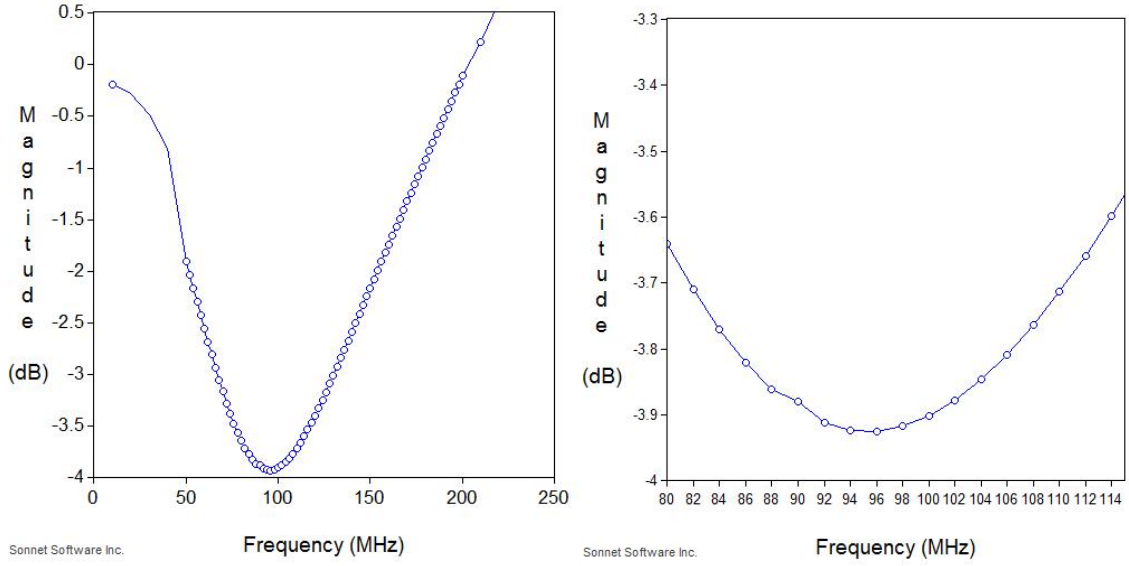

Figure 6.11: S11 parameter values for the dipole antenna.

6.2 Electromagnetic shielding.

The progressive increase in the use of electronic devices has led to the reduction in electromagnetic environmental pollution. Attenuation or shielding of electromagnetic waves, to protect electronic devices from failure, or to protect humans from harm, is an important task for today's engineers. Coatings based on carbon nanotubes offer attractive properties for this application, such as high electrical conductivity and widespread availability. For these specific purposes, electromagnetic shielding foils do not need to be transparent, hence the point is to obtain high conductive coatings by increasing the thickness of the layers. The main goal of our CNT foils is to attenuate EM waves as much as possible. During this section, different approaches were followed in order to get thicker CNT layers over the substrates. All the deposition procedures and their shielding performance will be described below.

6.2.1 Test setup and configuration

This section is written to report the shielding effectiveness of different CNT coatings using the ASTM 4935 standard, which is the standard test method for measuring the electromagnetic shielding effectiveness of planar materials. This test method does not exactly reproduce the electrical performance of the samples in all different applications but does allow evaluation of the differences between samples. One should take care in applying the absolute values obtained from these tests to other geometries or enclosure designs.

The ASTM measurement method is valid over a frequency range of 30MHz to 1,5GHz, thus any number of discrete frequencies may be selected within this range. In our case, the measurements will be performed in the frequencies ranging from 10 MHz to 510 MHz .

Before starting with the measure-ments some terminology should be introduced. Listed below are the definitions of the specific terms to this standard:

Dynamic range (DR): Difference between the maximum and the minimum signals measurable by the system.

Electrically thin: The thickness of the sample is much less ($<1/100$) than the electrical wavelength within the sample.

Far field: Region where electric field (E) and magnetic field (H) are orthogonal to each other and also to the direction of propagation of energy.

Near field: Region where E and H fields are not related by simple rules.

Shielding effectiveness (SE), also called electromagnetic field attenuation (EMFA): Received power ratio with and without the shielding material for the same incident power. It is usually expressed by the following equation:

$$SE = 10 \cdot \log \frac{P_1}{P_2} \qquad \text{(In decibels, dB)} \qquad (*)$$

Where: $P_1 =$ received power with the test specimen (shielding material)

$P_2 =$ received power with the reference specimen (without shielding material)

The reference and test specimens must be of the same material and thickness. Two specimens are considered to have identical thickness if the difference in the average thicknesses is less than 25 μm and the thickness variation within and between specimens is less than 5 percent of the average. In **Figure 6.2** both different specimens are demonstrated.

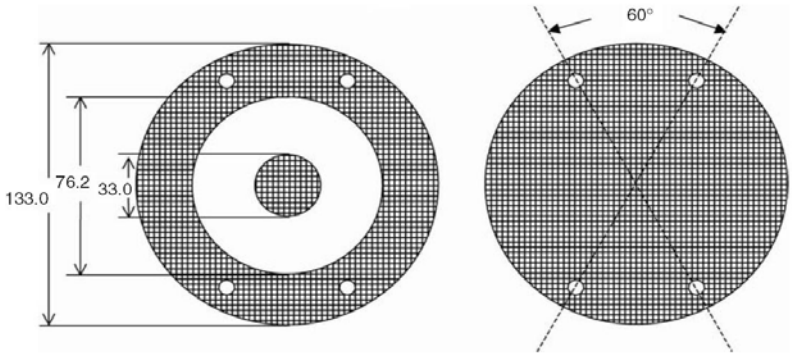

a. b.

Figure 6.2: Specific dimensions of reference (a.) and test specimens (b.) for shielding measurements (unit: mm).

The measurements of the electromagnetic attenuation (EMFA) were carried out with a home made transmission line cell (or specimen holder), according to the standard ASTM 4935, and connected to a spectrum analyzer (Hewlett-Packard 8591A). **Figure 6.3** shows this basic apparatus. Apart from the specimen holder and the spectrum analyzer, coaxial cables with a characteristic impedance of 50 Ω were used to connect everything together.

Note that during these measurements only the range between 10 MHz and 510 MHz (far-field) was scanned.

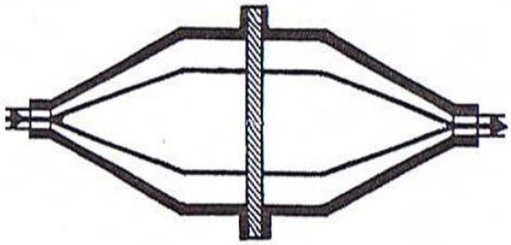

Figure 6.3: Picture and schema of a transmission line chamber (or specimen holder) according to the standar ASTM D 4935. The chamber has an external shell diameter of 84mm.

The measurement procedure was as follow: two pieces of the reference specimen were placed in the middle of the transmission line chamber taking care that the disk for the centre conductor was aligned correctly. Then, while using this reference specimen, the received power (P2) was measured. Next, the reference sample was replaced with the load sample and the received power (P1) was measured again. The EMFA of the material can be calculated by the relation (*)

6.2.2 Coating procedures and electromagnetic attenuation results

Painted foils

Initially to get an idea about the possibilities of the carbon nanotubes coatings as an electromagnetic trap, a layer of carbon nanotubes plus sulfonated polyphosphazene paste (SPP) was deposited on a 0,5 mm thick polycarbonate film by the use of a painting brush. The SWCNT/SPP paste was prepared following next procedure:

1. 5 mg of SWNT plus 0,02g of SPP ware dispersed into 50 mL of de-ionised water and then sonicated during 6 hours.
2. After the sonication process, the black solution was concentrated to 2mL by the use of an evaporator.

The resulting coating were extremely thin and irregular over the substrate, that is why the measurements merely showed any EMFA effect. Nevertheless, it is possible to reach a maximum EMFA value of 1,4 dB by putting six samples together. All six samples attain 3 mm thickness (maximum following the standard). The measurements of these first samples are demonstrated in **Figure 6.4**

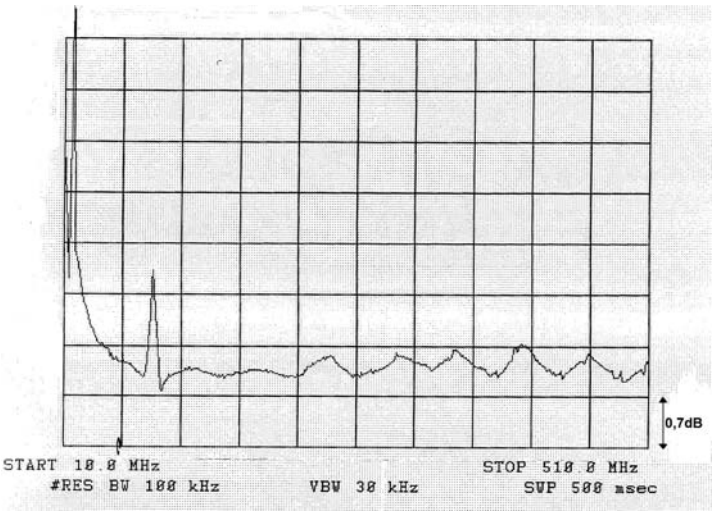

Figure 6.4: EMFA results for a group of six SWCNT/SPP samples.
1,4 dB of EMFA. Note that we were systematically taking the maximum value.

Sprayed foils

Further on, it was decided to use muti wall carbon nanotubes, in particular C-tubes, instead of single wall ones. C-tubes (see Chapter 4) showed the higher conductivity values among others multi wall carbon nanotube sources. Furthermore, multi wall tubes are substantially cheaper than SWCNT, thus they allow for the use of bigger amounts of material. During the deposition step, polycarbonate foils were intensively sprayed on both sides by the use of a commercial air brush. 250 mg of C-tubes material was dispersed into 1% SDS solution and deposited over the substrate. Every samples was sprayed with 250 mg of MWCNT material approximately. When measuring, two sample together reached a maximum EMFA value of 15 dB. When placing four samples together 22 dB of EMFA were achieved. The thickness of the four samples together was 1,74 mm, so there was still 1,26 mm to improve the performance. **Figure 6.5** shows these results.

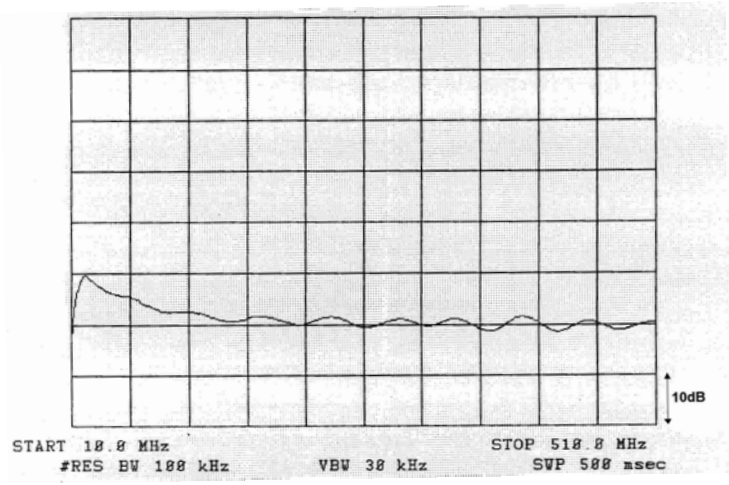

Figure 6.5: EMFA results of four sprayed MWNT samples with 1,74 mm of thickness.
22dB of EMFA was obtained.

In spite the improvement in EMFA performance, it was concluded that spraying deposition method was not suitable for this kind of purposes. This method is too time consuming when thicker layers are needed. In attempts to overcome these problems, it was decided to use foils directly made of buckypapers.

Bucky paper foils

During this new stage, not only the deposition method has been changed but also the CNT material itself. It was decided to replace the multi wall nanotubes with single wall tubes from laser ablation technique With these changes one can expect to reach better attenuation performance. As mentioned before, buckypapers seem to be a more reasonable approach since it is exclusively made of carbon nanotubes. In regards to the spray coated samples, most of the thickness comes from the polycarbonate substrate, which is not conductive, so it makes no contribution to electromagnetic absorption. The construction of buckypapers was already introduced in Chapter 3, and in the EMFA test the same procedure was followed. **Figure 6.6** shows the EMSA measurements for a single 113 μm thick backypaper sample.

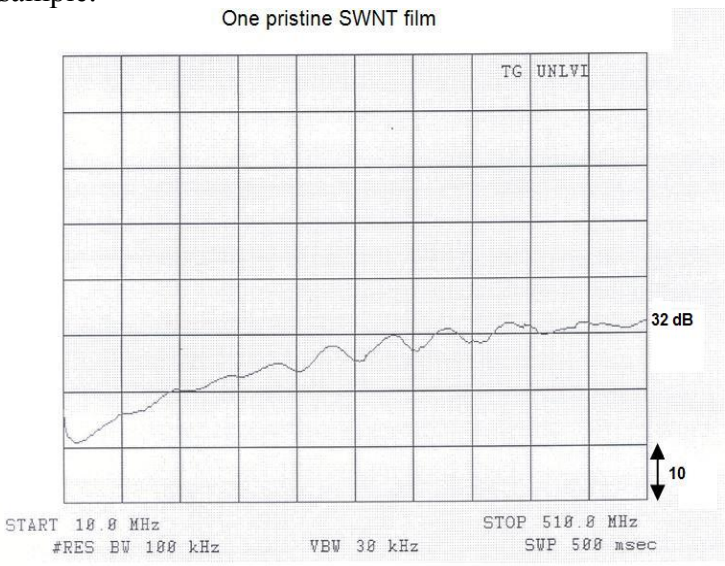

Figure 6.6: EMFA results of a single SWCNT buckypaper foil (113μm). 32dB of EMFA was reached.

The results show an improvement in the EM shielding comparing to previous measurements. One single buckypaper was able to attain 32 dB of EMFA. The next step was to put the foils together until 3 mm of thickness was reached, 3 mm corresponds to the maximum thickness when following the ASTM 4935 standard. Seven samples were put together, which gives a thickness of about 2,78 mm. **Figure 6.7** shows the measurements.

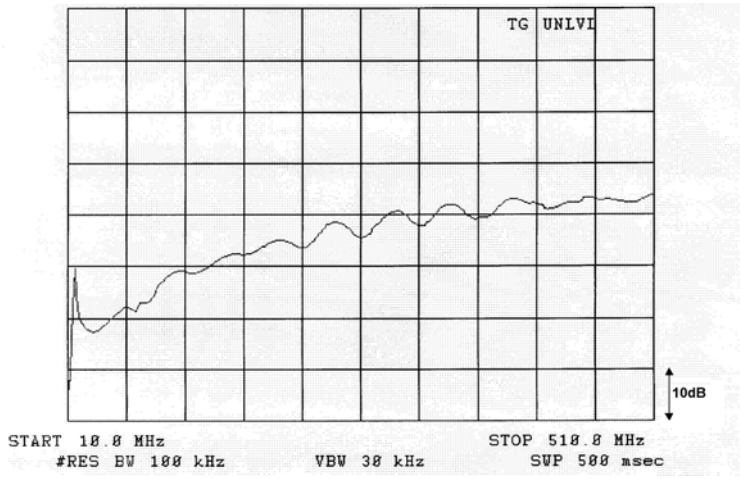

Figure 6.7: EMFA results after placing seven foils all together (2,78 mm). 45 dB EMFA was obtained.

As expected, the EM attenuation was improved and the samples allowed 45 dB of attenuation. Afterwards, in an attempt to increase the performance without changing the CNT source nor the thickness, it was decided to separate every conductive film from each other. A thin layer of insulating polycarbonate was placed in between each sample so a sandwich structure was constructed. This polycarbonate film was thinner than the ones used previously as a substrate. We expected that highly planar parallel layers might improve the efficiency of the attenuation. The results seem to have an influence in the shielding as **Figure 6.8** demonstrates. The measurements were close to 50 dB of attenuation (49 dB), which represents 4 dB more by simply separating the foils by a PC layer. The seven samples with the eight PC separating layers were, all together, of about 3 mm thick.

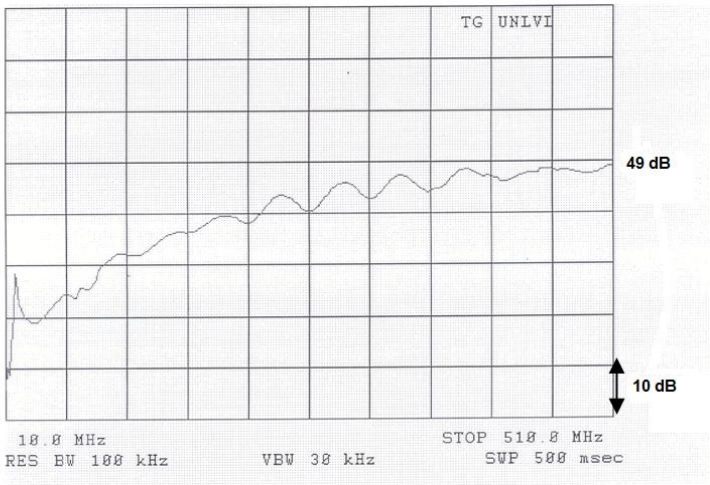

Figure 6.8: Seven pristine SWNT films alternated with eight polycarbonate foils (3 mm). 49 dB of EMFA.

6.2.3. Theoretical calculations and comparison between coating procedures

The conductivity of the material and the electromagnetic shielding are related by:

$$a = 20\log(1 + Z_0 \cdot d \cdot \sigma/2)$$

Where a is the attenuation, d is the thickness of the sample, σ its electrical conductivity and Z_0 the intrinsic impedance of the air. With $\mu_r = \varepsilon_r = 1$, $\varepsilon_0 = 8{,}85 \cdot 10^{-12}\, F/m$ and $\mu_0 = 1{,}26 \cdot 10^{-6}\, H/m$ Z_0 can be calculated according to:

$$Z_0 = \sqrt{\frac{\mu_0 \cdot \mu_r}{\varepsilon_0 \cdot \varepsilon_r}} = 377\Omega$$

By this relation it is possible to determine which is the required conductivity to obtain the desired electromagnetic attenuation (80dB). **Figure 6.9** represents the theoretical EMFA values for different thicknesses using the relation above. The justification for the validity of this equation implies the fact that one can consider conducting foils as *electrically thin* [34][35][36]. Also in **Figure 6.9,** one can observe the theoretical electromagnetic shielding performance of the different CNT. These calculations came from the conductivity measurements done in chapter 4, where both C-tubes and LA nanotubes were analyzed.

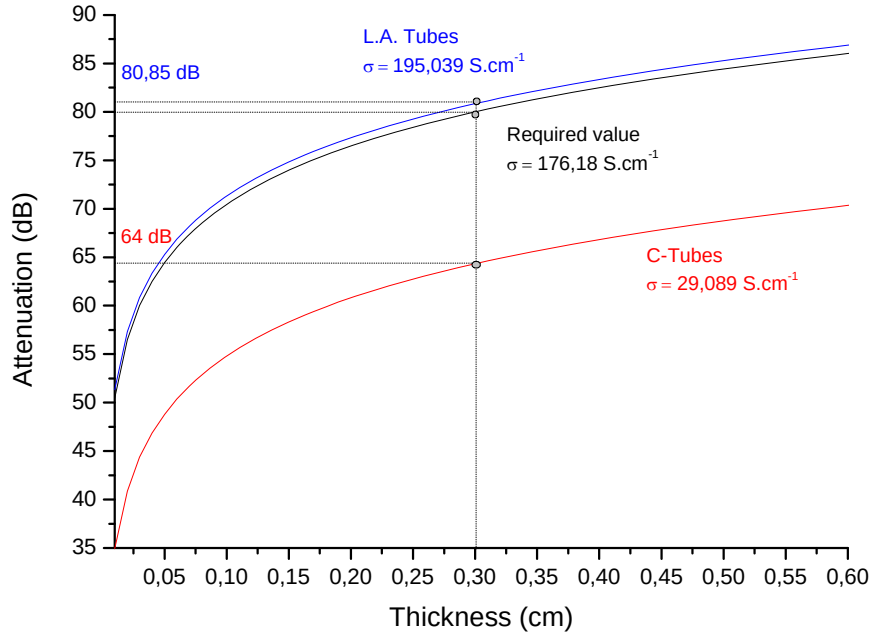

Figure 6.9: Theoretical EM attenuation vs. thickness for different isotropic materials based on CNT. Black curve shows the theoretically required conductivity to get 80 dB of EMFA with 3mm of thickness. Red and blue plots were based on conductivity measurements from C-tubes and L.A. tubes, these investigations were done in chapter 4. Note that measured valuesdiffer from the theoretical calculations.

The theoretical calculations do not really match with the experimental measurements, this is mainly due to the presence of the substrate. The polycarbonate substrate is an insulating material which is contributing to the thickness of the sample without having any shielding effect. Yet even when this thickness is subtracted from the relation, experimental and theoretical calculations are not in agreement. Another explanation for this behaviour is that buckypapers foils do not have uniform conductivity and thickness, and more importantly, some samples presented cracks and irregularities over the surface.

In spite of being applicable only for isotropic materials, one can use this relation to compare the shielding performance of the laminated and non-laminated samples. Due to slight differences in the thickness of the produced disc, the results of the measurements should not be compared with each other at this point.. Therefore, all results were additionally normalized to a disk thickness equal to d = 3mm by applying the equation before. **Figure 6.10** shows the comparative results. Note that laminated sample shows a higher "fictitious" conductivity value due to the lamination process.

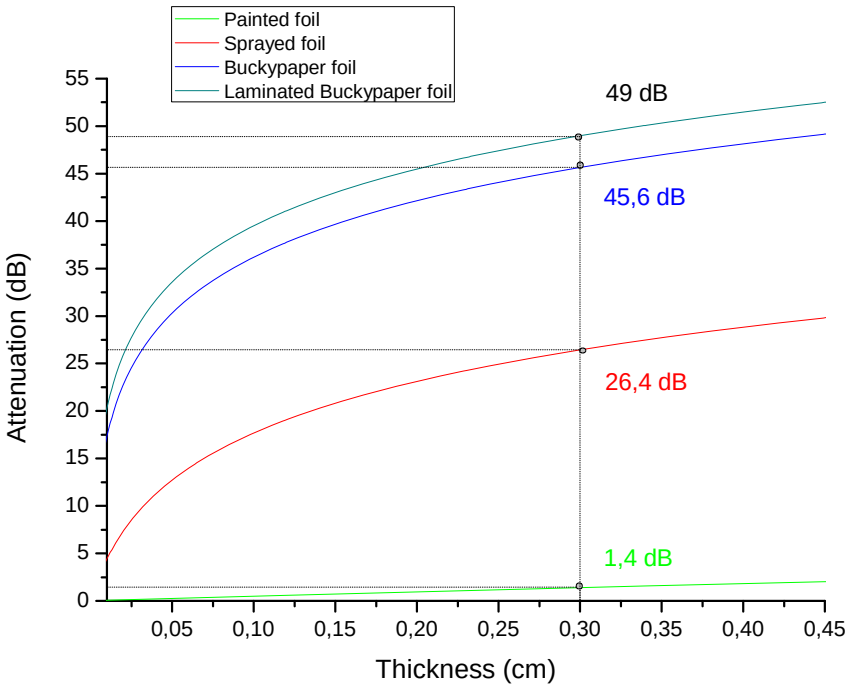

Figure 6.10: Comparison between coating procedures.

As a result from our comparison, it can be concluded that buckypaper foils made of highly conductive single wall carbon nanotubes increase shielding effectiveness. Furthermore, the lamination process also appears to be beneficial. This lamination forces the electromagnetic wave to go through the interface between two different media several times so that the wave is attenuated due to reflections. For further improvements one could try to use more conductive SWCNT and increase the number of foils in the lamination process.

6.3 Conclusions

As a conclusion we can say that carbon nanotubes can be usefull in printed antennas or electromagnetic shielding as well as in many others areas. Although the results show suitable performance, future efforts should focus on improving the pattern design of the antenna. Simulations with Sonnet software revealed the importance of a well tunned antenna structure. Moreover, these preliminary results confirm the importance of a highly conductive CNT material. To obtain better CNT, further improvements have to be done in the growing or purification processes.

Conductive polymers, even though they showed better results in the antenna comparison, can not be considered a real substitute for ITO. Polymers degraded when exposed to light and with the passing of time and these makes them unsuitable for industrial purposes.

General conclusions

Our initial work is based on previous investigations of transparent carbon nanotube coatings studied by M. Kaempgen [39] amongst others. We tried to improve the performance of the networks by experimenting with all the different deposition methods and a result we ended up with a new deposition technique by applying an electric field between two electrodes immersed in a CNT dispersion. We were interested in the deposition step since it appeared to be a reasonable way of improving the performance of the networks. In addition, after observing of the samples, we investigated the impact of the orientation of the CNT over the substrate. As it was proved in Chapter 5, this orientation has an impact in the conductivity and yield to better electrical conductance in one direction. The work mainly consisted in mastering the dip coating deposition technique to get optimal values in the orientation of the CNT. To study the orientation properties I learnt characterization techniques such as Atomic Force microscopy (in its tapping mode), Raman spectroscopy and the basics of Scanning Tunneling Microscopy and X-Ray photoespectroscopy to be usefull as they were the usual tools used to characterise the CNT bulk material. As well, I gained information about the procedures involved in the preparation of the samples (cleaning, functionalisation, deposition, wire bonding).

Figure 6.11: Transparent film speakers made of CNT.
Picture from Filsco company.

After several months we finally got the first results necessary to compare each deposition method and to prove the benefits of orienting the CNT. The results were very promising and, eventhough the performance of ITO material were far ahead, we were able to improve the orientation CNT over the substrates.

As it was commented in the introduction, carbon nanotubes are very appealling for their potential use in transparent conductive coatings. Compared with its competitors, CNT are extremely stable in time and are easely accesible. In spite of showing slightly inferior performance than Indium Tin Oxide and even though being far from getting completely transparent conductive networks, we can anyhow confirm that for some applications the performance obtained were adequate enough. Printed antennas are one of the examples and, more importantly, there are several companies who have started developing new products based on CNT technology. **Figure 7.1** and **Figure 7.2** show a transparent film speaker and a TV screen using CNT as transparent electrodes. This confirms that CNT technology can find its own gap in the market.

Figure 6.12: First TV screen using CNT material as transparent electrode.

As a final remark, this work opens a door to others new applications and state of the art Information Systems as its range of applications goes from electronics and telecommunications to physics or material science.

Annex

Some of the work in this thesis was presented by Viera Skakalova at SPIE conference on Optics and Photonics in San Diego on the 10-15 August 2008 ("Electrical properties of random carbon nanotubes networks") during the time I was working on it.

Additionally, some parts of this thesis will appear in the journal "Contributions to Science" as a publication: "Transparent and flexible electrodes and sensors based on carbon nanotube thin films". The last section about electromagnetic shielding is still in progress to be published in a specialized magazine.

Bibliography

[1] S. Iijima, *Helical microtubules of graphitic carbon*. Nature 354, 56 (1991).

[2] R.E. Smalley, D.T. Colbert. *Perspectives of Fullerene Nanotechnology.* p.3-10, Kluwer Academic Publishers (2002).

[3] R. Bacon. "*Growth, Structure and Properties of Graphite Whiskers*." J. Appl. Phys. 31 283 (1960).

[4] S. Iijima, T. Ichihashi. "Single-shell carbon nanotubes of 1-nm diameter." Nature 363 603 (1993).

[5] D.S. Bethune et al. "Cobalt-catalysed growth of carbon nanotubes with single-atomic-layer walls." Nature 363 605 (1993).

[6] A. Thess, R. Lee, P. Nikolaev, H. Dai, P. Petit, J. Robert, C. Xu, Y.H. Lee, S.G. Kim, A.G. Rinzler, D.T. Colbert, G.E. Scuseria, D. Tom_anek, J.E. Fischer, R.E. Smalley. "Crystalline Ropes of Metallic Carbon Nanotubes." Science 273 483 (1996).

[7] R. Saito, G. Dresselhaus, M.S. Dresselhaus, Physical *Properties of Carbon Nanotubes*, Imperial College Press, London (1999).

[8] S. B. Sinnot et al., *Chem.Phys.Lett.* 315, 25-30 (1999).

[9] Zhao, X., et al., Bull. Res. Inst. Meijo Univ. (1996) 1, 7

[10] T. W. Ebbesen and P. M. Ajayan, Nature 358, 220-222 (1992).

[11] M.S. Dresselhaus, G. Dresselhaus, and P. Avouris. Carbon Nanotubes: Synthesis, Structure, Properties and Applications, volume 80. Springer-Verlag, 2001.

[12] E. Joselevich, C.M. Lieber. "Vectorial Growth of Metallic and Semicon-ducting Single-Wall Carbon Nanotubes." Nano. Lett. 2 1137 (2002).

[13] K.H. Lee, J.M. Cho, W. Sigmund. "Control of growth orientation for carbon nanotubes." Appl. Phys. Lett. 82 448 (2003).

[14] L. Zhang, Y. Tan, Daniel E. Resasco. „Oriented Growth and Subsequent Handling of Vertical Single-walled Carbon Nanotube Forest Characterized by Electron and Probe Microscopy", Microsc Microanal 13(suppl. 2)2007

[15] Guo, T., Nikolaev, P., Thess, A., Colbert, D. T., and Smalley, R. E. Catalytic growth of single-walled nanotubes by laser vaporization. Chemical Physics Letters 243(1,2), 49-54. 1995.

[16] R.E. Smalley et al. "Growth mechanisms for single-wall carbon nanotubes in a laser-ablation process." Appl. Phys. A 72 573 (2001).

[17] Bandow, S., et al., Phys. Rev. Lett. (1998) 80 (17), 3779

[18] Kataura, H., et al., Carbon (2000) 38 (11-12), 1691

[19]. Kataura, H., et al., Jpn. J. Appl. Phys. (1998) 37, L616

[20] K. Terabe, T. Hasegawa, T. Nakayama, M. Aono, Nature, 433, 47 (2005).

[21] Yasuda, Ayumu, Kawase, Noboru, and Mizutani, Wataru. Carbon-Nanotube. Formation Mechanism Based on in Situ TEM Observations. Journal of Physical Chemistry B 106(51), 13294-13298. 2002.

[22] J.C. Kearns, R.L. Shambaugh, J.Appl. Polym. Sci., 86, 2079 (2002)

[23] M.S. Dresselhaus, P. Avouris, Introduction to Carbon materials research, Carbon Nanotubes, Topics in Applied Physics, vol. 80, pp. 1-9 (2001).

[24]M.S. Dresselhaus, G. Dresselhaus, and P. Avouris. *Carbon Nanotubes: Synthesis, Structure, Properties and Applications*, volume 80. Springer-Verlag, 2001.

[25] H. Riedel, „Analyse und Optimierung von Carbon Nanotubes für deren Einsatz in aktuatorische Systeme“, Diplomarbeit, Universität Ulm, 2006

[26] H. Kataura, Y. Kumazawa, N. Kojima, Y. Maniwa, I. Umezu, S. Masubuchi, S. Kazama, X. Zhao, Y. Ando, Y. Ohtsuka, S. Suzuki, Y. Achiba, *Proceedings of the International Winter School on Electronic Properties of Novel Materials (IWEPNM99)* edited by H. Kuzmany, M. Mehring, and J. Fink, (American Institute of Physics, Woodbury, NY, 1999).

[28] Z.Yu, L. E. Brus, *J. of Phys. Chem. B*, **105**, 6831(2001).

[29] Cappella, B. & Dietler, G. Force-distance curves by atomic force microscopy Surf. Sci. Rep. 34, 1-104 (1999).

[30] http://www.pgo-online.com/de/katalog/ito.html

[31] Problems of conductive polymers as thermole

[32] L. D. Landau, B. G. Levich, Acta Physiochim, U.R.S.S., 17 (1942) 42-54

[33] Small-Angle Neutron Scattering from Surfactant-Assisted Aqueous Dispersions of Carbon Nanotubes

[34] K.H. Moebius, Kunststoffe 78 (1988) 345.

[35] P.F. Wilson, M.T. Ma, J.W. Adams, IEEE Trans. Electromagn. Compatibility 30 (1988) 239.

[36] U. Leute, Kunststoffe und EMV, Expert Verlag, Renningen, 2006.

[37] N. F. Mott and E. A. Davis, Electronic processes in Non-Crystalline Materials, 2nd ed. (Clarendon, Oxford, 1979).

[38] Electronic transport in carbon nanotubes: from individual nanotubes to thin and thick networks. V. Skakalova, A.B. Kaiser, Y.S. Woo, S. Roth.

[39] Transparent carbon nanotube coatings. M. Kaempgen, G.S. Duesberg, S. Roth